

# **Laser-based surface functionalisation: advances in durability and 3D processing**



**Antonio García Girón**

A thesis submitted to the University of Birmingham  
for the degree of Doctor of Philosophy

November 2019

Department of Mechanical Engineering  
School of Engineering  
University of Birmingham

UNIVERSITY OF  
BIRMINGHAM

**University of Birmingham Research Archive**

**e-theses repository**

This unpublished thesis/dissertation is copyright of the author and/or third parties. The intellectual property rights of the author or third parties in respect of this work are as defined by The Copyright Designs and Patents Act 1988 or as modified by any successor legislation.

Any use made of information contained in this thesis/dissertation must be in accordance with that legislation and must be properly acknowledged. Further distribution or reproduction in any format is prohibited without the permission of the copyright holder.

# Abstract

Surface functionalization is gaining interests for industry and research due to the new attractive properties that can be “imprinted” on metal components, e.g. bacteria repellence or hydrophobicity among others. Considering the available alternative technologies to achieve such functional responses, direct laser writing is gaining a popularity due to its cost-effectiveness, selectivity and relatively short processing time. It allows surface properties to be modified or tuned by patterning and texturing at micron or submicron scales. However, laser surface functionalization has some limitations, too, such as the durability of the produced topographies and hence of their functionality, and also capabilities to apply it on free-form surfaces. In this context, the focus of the research presented in this thesis is on addressing these open issues. In particular, a combination of plasma surface alloying and laser patterning is proposed in order to increase hardness of produced functional surfaces, and thus to increase their wear resistance and durability. It was found that alloyed surfaces could retain their hardness after laser functionalization, and their wear resistance was increased. Furthermore, the impact of wear direction and wear cycles on functional response and topography dimensions was studied. Also, a method to study the effects of the process disturbances in patterning 3D surfaces is proposed, especially on resulting topographies and their functional responses. Correlations between process disturbances, areal surface parameters, resulting topography dimensions and functional response were found. All together, the research advances the knowledge in laser surface patterning and addresses key constraints for the broader use of this technology by industry.

# Acknowledgments

In the first pages of my thesis I would like to express my most sincere gratitude to the people who made it possible, who believed in my skills and who supported and encouraged me during the last 4 years. Thanks to my supervisor, Prof. Stefan Dimov, for giving me this opportunity and for his inestimable guidance and advice during all the PhD. I would also like to thank to my second supervisor, Dr Karl Dearn, to my colleagues from the Micro Manufacturing group and the University of Birmingham.

My gratitude to the European Commission and all the Laser4Fun consortium members. To the Early Stage Researchers in the L4F project, my colleagues and friends, who made this research really enjoyable and whose professionalism is beyond price. In particular, I would like to thank the ESR who went to Birmingham with me, Dr Jean-Michel Romano, for all the good moments we had together, for the thousand hours we spent in the lab, for his never ending support and help, and specially for being my friend. I would like to express my deepest gratitude to Fran, Virginia, Andrés and my colleagues from B/S/H/ for making this possible and for their faith on me.

I would like to thank my friends, for their encouragement and for making my life much better. To Alberto, a soulmate and the best flatmate I will have. To Nacho, who is the first friend I ever had and the most loyal person I ever knew. To Carlos, for having always a smile in his face and wise words to comfort my soul. To Javi, and the many exciting adventures we lived together in Birmingham, Vesta or Zaragoza. To Peluko and Monty, because no matter the distance, they were always with me.

I want to express my sincere gratitude to José Ignacio Peña and Daniel Sola, who were my mentors during my first steps in a laboratory, who helped me to write my first journal paper, and the first ones to think I could ever do a PhD.

The last one and deepest gratitude is for my family, Mamá, Papá, Tío, Tía, Amelia, Luis and my girlfriend María: *“Muchas gracias por vuestro amor y apoyo incondicional, por estar siempre a mi lado y por creer en mí en cada momento, por empujarme siempre hacia adelante y ayudarme a no rendirme, por ser mi luz en los momentos más oscuros y mi mayor alegría en los momentos felices”*.

Finally, I want to dedicate the thesis to Afif Batal, my best friend and most inspiring colleague. Because your friendship was the best part of the last years, and with you by my side Birmingham was sunny and warm even in the darkest winter day.

# Table of contents

	Page
Abstract .....	i
Acknowledgments .....	ii
Table of contents .....	iv
List of tables.....	viii
List of figures .....	x
Nomenclature.....	xvi
List of publications and presentations .....	xx
<b>General introduction</b>	
<b>Chapter 1</b> .....	- 1 -
1.1 Motivation.....	- 2 -
1.2 Research aim and objectives .....	- 6 -
1.3 Thesis organization .....	- 8 -
<b>Literature review</b>	
<b>Chapter 2</b> .....	- 10 -
2.1 Nature as source of inspiration .....	- 11 -
2.2 Surface functionalization techniques .....	- 14 -
2.3 Fundamentals of wettability .....	- 20 -
2.3.1 Wetting states .....	- 20 -
2.3.2 Measurement techniques .....	- 23 -

2.4 Introduction to LASER technology.....	- 26 -
2.4.1 Basic principles .....	- 26 -
2.4.2 Beam delivery .....	- 29 -
2.5 Laser surface functionalization.....	- 32 -
2.5.1 Patterning strategies .....	- 32 -
2.5.2 Applications for laser patterned surfaces .....	- 35 -
2.5.3 Durability of laser patterned surfaces.....	- 43 -
<b>Combined surface hardening and laser patterning approach for functionalising stainless steel surfaces</b>	
<b>Chapter 3</b> .....	- 46 -
3.1 Introduction .....	- 50 -
3.2 Materials and Methods.....	- 54 -
3.2.1 Sample preparation .....	- 54 -
3.2.2 Laser processing .....	- 55 -
3.2.3 Characterization techniques.....	- 57 -
3.3 Results and discussion .....	- 58 -
3.3.1 Ablation threshold .....	- 58 -
3.3.2 Microstructure analysis .....	- 59 -
3.3.3 Chemical analysis.....	- 64 -
3.3.4 Wettability .....	- 66 -
3.3.5 Hardness .....	- 68 -
3.3.6 Abrasion test.....	- 71 -

3.4	Conclusions .....	- 72 -
<b>Durability and wear resistance of laser-textured hardened stainless steel surfaces with hydrophobic properties</b>		
<b>Chapter 4</b> .....		<b>- 74 -</b>
4.1	Introduction .....	- 78 -
4.2	Materials and methods.....	- 83 -
4.2.1	Sample preparation .....	- 83 -
4.2.2	Laser processing .....	- 84 -
4.2.3	Hydrophobic coating .....	- 85 -
4.2.4	Abrasion test.....	- 85 -
4.2.5	Characterization methods .....	- 87 -
4.3	Results and discussion .....	- 88 -
4.3.1	Surface analysis .....	- 88 -
4.3.2	Wettability .....	- 94 -
4.3.3	Chemical analysis.....	- 97 -
4.3.4	Durability of coated samples.....	- 102 -
4.4	Conclusions .....	- 104 -
4.5	Supporting information .....	- 107 -
<b>Experimental investigation of processing disturbances in laser surface patterning</b>		
<b>Chapter 5</b> .....		<b>- 112 -</b>
5.1	Introduction .....	- 116 -
5.2	Methods and Experiments.....	- 121 -

5.2.1	Methodology .....	- 121 -
5.2.2	Experiments.....	- 125 -
5.3	Results and discussion .....	- 129 -
5.3.1	Effects on surface topography.....	- 130 -
5.3.2	Effects on surface profiles .....	- 132 -
5.3.2.1	FOD effects .....	- 132 -
5.3.2.2	BIA effects .....	- 134 -
5.3.3	Effects on areal surface parameters.....	- 136 -
5.3.4	Effects on functional response .....	- 138 -
5.3.5	Correlations between disturbances, areal parameters and functional response .....	- 140 -
5.3.6	Patterning of 3-D surfaces .....	- 142 -
5.4	Conclusions .....	- 143 -
<b>Contribution to knowledge and future research</b>		
<b>Chapter 6</b> .....		- 147 -
6.1	Contributions .....	- 148 -
6.2	Future research .....	- 153 -
List of references .....		- 155 -

## List of tables

	Page
<b>Chapter 2</b>	
<b>Table 2.1.</b> <i>Surface modification techniques</i> .....	54
<b>Chapter 3</b>	
<b>Table 3.1.</b> Ablation thresholds of as-received, carburised and nitrided samples obtained with pulse durations of 220 ns and 15 ns.....	54
<b>Table 3.2.</b> Normalised chemical composition in weight (%) of stainless steel and plasma treated samples without (the reference one) and after laser patterning with 220 ns and 15 ns pulse durations.....	60
<b>Chapter 4</b>	
<b>Table 4.1.</b> The total reductions (R) after 300 parallel and perpendicular abrasion cycles.....	85
<b>Table 4.2.</b> Surface compositions at the four investigated states on as-received and carburised stainless steel samples. ....	95
<b>Chapter 5</b>	
<b>Table 5.1.</b> Laser processing parameters.....	131

**Table 5.2.** Pearson coefficients together with P-values for the investigated correlations between disturbances, areal parameters and contact angles. ....131

# List of figures

Page

## Chapter 1

**Fig 1.1.** A laser patterned free form surface (GF Machining Solutions website) .....4

**Fig 1.2.** The effects of beam incident angle and off-focus laser processing on resulting patterns: (a) a channel as part of a patterned surface produced at focus and laser beam normal to the surface; (b) the same channel but after off-focus patterning; (c) the same channel produced with a beam incidence angle of  $40^\circ$ .....5

## Chapter 2

**Fig 2.1.** Images of gecko skin (a-b) [3] and gecko foot (c-d) [4] .....11

**Fig 2.2.** Springtail and detail of the skin. The hierarchical structure of the skin is formed by dual scale patterns, with different sizes [5] .....12

**Fig 2.3.** Example of lotus leaf covered with dust (a) and cleaned after water drops drag the dust (b). SEM image of the surface topography of the lotus leaf (c) [6].....13

**Fig 2.4.** Combination of chemical etching and surface coating to produce hydrophobic surfaces [18].....15

**Fig 2.5.** Pillar like structures with overhangs at the top edge fabricated by combination of photolithography and consecutive wet etchings [20] .....16

**Fig 2.6.** As received glass surface (a), and glass surface after sandblasting (b) [22] .....17

**Fig 2.7.** Combination of laser patterning (a, b) and plastic injection moulding (c, d) to produce hydrophobic surfaces on polypropylene [23].....18

**Fig 2.8.** Sketch of a liquid drop on a surface and its Young's angle ( $\theta$ ).....19

<b>Fig 2.9.</b> Sketch of rough surfaces in Wenzel wetting state (a) and Cassie-Baxter wetting state (b).....	21
<b>Fig 2.10.</b> Theta Lite optical goniometer from Biolin Scientific (a) and example of a contact angle measurement (b).....	22
<b>Fig 2.11.</b> Sketches of (a) sliding angle measurement [38] and (b) advancing/receding angle measurement (Biolin Scientific Website). .....	23
<b>Fig 2.12.</b> Sketch an atom in a low energy state (a) and the possible radiative processes: absorption (b), spontaneous emission (c) and stimulated emission (d) .....	25
<b>Fig 2.13.</b> Sketch of a basic laser source. ....	27
<b>Fig 2.14.</b> Differences between short (a) and ultrashort (b) pulses [45] .....	28
<b>Fig 2.15.</b> Sketch of the laser beam propagation through a focusing lens, with a focal distance $f$ . $w_0$ is the minimum spot diameter at focus. $Z_r$ is the Rayleigh length and $\theta_D$ is the divergence of the beam.....	29
<b>Fig 2.16.</b> SEM images of patterns performed with (a) nanosecond DLW [48], (b) femtosecond DLW [49], (c) DLIP [50] and (d) triangular LIPSS [51] .....	31
<b>Fig 2.17.</b> Example of a steel surface after an ice rain test, where the dark area was laser patterned [80] .....	34
<b>Fig 2.18.</b> Examples of anti-bacterial patterns: (a) pillars, (b) circular holes and (c) channels [83] .....	35
<b>Fig 2.19.</b> Examples of cell cultures: (a) non-irradiated surface and (b-c) irradiated surfaces [92] .....	36
<b>Fig 2.20.</b> Examples of aesthetical patterns: (a-b) Surfaces covered with LIPSS showing light scattering effect [95]. (c) Image formed by combination of multiple oxidised single spot [55]. (d) Example of a Gabor zone plate lens for sensing applications [100]. .....	37

<b>Fig 2.21.</b> Sketch of a moving specimen ring patterned with dimples to reduce friction [111].....	38
<b>Fig 2.22.</b> Hydrophobic channel-like (a) and cell-like (b) patterns [48].....	39
<b>Fig 2.23.</b> Images of a DC KlöcknerLonon40 kVA plasma furnace used for low temperature plasma surface alloying (University of Birmingham).....	42

### Chapter 3

<b>Fig 3.1.</b> Mass concentration of the plasma carburised (a) and nitrided (b) samples vs the depth from the surface.....	50
<b>Fig 3.2.</b> 3D topography of a cell-like pattern (a) and 3D topography of a channel like pattern (b), on an area of 323x323 $\mu\text{m}$ ; (c) cross-section of the 3D patterns, showing the height of redeposited material (H) and depth of ablation (D).....	55
<b>Fig 3.3.</b> Ablation depths (D) and heights of bulges (H) for as-received and plasma treated samples.....	56
<b>Fig 3.4.</b> SEM micrographs of stainless steel and plasma treated samples patterned with 15 and 220 ns pulses. Cracks produced on the nitrided surfaces are pointed out with white arrows.....	58
<b>Fig 3.5.</b> (a) Stabilized CA of laser patterned and reference surfaces. The dashed red line indicates the transition from hydrophobic to super-hydrophobic (CA higher than $150^\circ$ ). (b) Sliding angles for the plasma carburised and nitrided samples after laser patterning. (c) Examples of water drops bouncing on plasma carburised stainless steel before (Ref_C) and after laser patterning.....	62
<b>Fig 3.6.</b> Cross-sections of the plasma nitrided samples after laser patterning with 220 ns (a) and 15 ns (b) pulses.....	64

**Fig 3.7.** Cross sections of the channels produced with 220 ns (a) and 15 ns (b) pulse durations on plasma carburised samples with nano indentations at different depth from the processed surface.....65

**Fig 3.8.** The topography and cross-sections of stainless steel (a) and plasma carburised (b) samples with channel-like patterns produced with 15 ns laser, before and after the abrasion test.....67

## **Chapter 4**

**Fig 4.1.** (a) a sketch of the Elcometer 1720 Abrasion and Washability Tester. (b) the relative orientation between the two abrasion directions and channel-like patterns...79

**Fig 4.2.** 3D images of patterns produced with pulse durations of 15 ns (a) and 220 ns (e); topographical profiles resulting after irradiation with 15 ns (b) and 220 ns (f) pulses before and after the wear tests (300 abrasion cycles); SEM images of the topographies produced with 15 ns and 220 ns before (c & g) and after (d & h) the wear tests, respectively.....82

**Fig 4.3.** Topography and bulges' evolutions after abrasion cycles: (a) the depth changes of the channels produced with 15 ns pulses after 100, 200 and 300 cycles; (b) the height changes of the bulges generated with 220 ns pulses after 100, 200 and 300 cycles.....84

**Fig 4.4.** SCAs of the reference and patterned samples after 10 days stabilization.....88

**Fig 4.5.** SCA evolution after 100, 200 and 300 parallel (a) and perpendicular (b) abrasion cycles.....89

**Fig 4.6.** Deconvolution of the carbon (C 1s) and oxygen (O 1s) regions of as-received and plasma carburised samples patterned with 220 ns laser pulses.....91

**Fig 4.7.** SCA evolution after 100, 200 and 300 wear cycles on uncoated and coated carburised samples patterned with 220 ns pulses, as well as the reference coated un-patterned surface.....96

**Figure S4.1.** 3D images of the samples produced with 15 ns pulses on both, as-received and carburised stainless steel, before, during and after the wear tests.....101

**Figure S4.2.** 3D images of the samples produced with 220 ns pulses on both, as-received and carburised stainless steel, before, during and after the wear tests.....102

**Figure S4.3.** Side and front views of the drop shape before and after parallel abrasion, showing the drop spreading along the channel direction, for sample 220C.....103

**Figure S4.4.** XPS surveys for both, as-received and carburised stainless steel, before and after laser patterning with 220 and 15 ns of pulse durations.....104

## Chapter 5

**Fig 5.1.** The laser processing setup (a) employed to produce channel-like patterns on: b) 3-D and c) planar surfaces.....111

**Fig 5.2.** Representative examples of profiles for the three sets of samples produced with: a) varying channel distance, b) FOD, c) BIA and d) the different surface parameters measured on profiles of the samples produced with BIA deviations. The black dashed lines represent the reference sample produced at focus with 100  $\mu\text{m}$  distance between lines and BIAS of 0 while the coloured solid lines represent the patterns' profiles.....114

**Fig 5.3.** SEM micrographs of channels on a reference sample produced with 100  $\mu\text{m}$  distance between them and without FOD and BIA deviations in a) and b) with x750 and x130 magnifications, respectively. SEM micrographs of channels on samples produced

with: c) an increased distance between them to 150  $\mu\text{m}$ , d) FOD of 1 mm, and e-f) BIA of 40°.....120

**Fig 5.4.** Surface profile parameters of samples produced with increasing FOD, i.e.: a) bulges' height, H; b) channels depth, D; c) channels width, W; and d-e) their deviations from the reference profile.....123

**Fig 5.5.** Surface profile parameters of samples produced with varying BIA, i.e.: a) bulges' heights (H); b) channels' depth (D); c) channels' width (W), d) walls tapering angles ( $\theta$ ); and e-h) their deviations from the reference profile.....125

**Fig 5.6.** Areal surface parameters: a-c) area ratios,  $A_r$ ; and d-f) arithmetical mean heights,  $S_a$ , for the set of samples produced with the three processing disturbances, i.e. channel distance, FOD and BIA, respectively.....127

**Fig 5.7.** Contact angles, CA, for the set of samples produced with the three processing disturbances, i.e. a) channel distance, b) FOD and c) BIA, respectively.....129

# Nomenclature

Nomenclature	Definition	Chapters
3D	Three-dimensional space	2, 3, 4, 5, 6
Ar	True to projected area ratio	5
BIA	Beam incident angle	5, 6
C	Carburised stainless steel	4
CA	Static contact angle	2, 3, 5
CAD	Computer aided design	2
CAM	Computer-aided manufacturing	5
Ce( $\tau$ )	Nomenclature for pillar like samples, followed by pulse duration ( $\tau$ )	3
Ch	Channel	5
Ch( $\tau$ )	Nomenclature for channel like samples, followed by pulse duration ( $\tau$ )	3
CW laser	Continuous wave laser	2
D	Ablation depth	3, 5
Dev [%]	Calculated deviations	5
DL	Diameter of the beam before the lens	2
DLIP	Direct laser interference patterning	2
DLW	Direct laser writing	2, 4
DOF	Theoretical depth of focus	2, 5
E	Energy per line	3
E <sub>1</sub>	Low energy state	2
E <sub>2</sub>	High energy state	2
EDX	Energy dispersive X-Ray	3

Ep	Pulse energy	2, 3
F	Focal distance	2
f	Pulse frequency	2, 3
f <sub>1</sub>	Area fraction of solid in contact with liquid	4
f <sub>2</sub>	Area fraction of air in contact with liquid	4
FOD	Focal offset distance	5, 6
FV	Focus variation	3
GDOES	Glow-discharge optical emission spectroscopy	3, 4
H	Height of the solidified material	3
H <sub>1</sub> & H <sub>2</sub>	Height of the bulges	5
IGES file	Initial Graphics Exchange Specification file	2
ISO	International Organization for Standardization	4
LED	Light-emitting diode	2
LIPSS	Laser induced periodic surface structures	2, 4
LMM platform	Laser micro-machining platform	5
LV	Liquid-vapour interface	3
M <sup>2</sup>	Beam quality factor	2, 5
Measured	Values measured with a focus variation microscope	5
N	Atomic population	2
N <sub>0</sub> , N <sub>1</sub> , N <sub>2</sub> ...	Normal of the planes	5
N1	Atomic population with electrons in low energy state	2
N2	Atomic population with excited species	2
P	Average power	2, 3
P <sub>0</sub>	Incident photon	2
P <sub>D</sub>	Pulse distance	3
P <sub>i</sub>	Photon released by spontaneous emission or stimulated emission	2

Pp	Peak power	2
r	Ratio between actual area and projected area	2, 4
R	Rolling angle	3
R (%)	Reduction of the patterns after abrasion	4
Ref	Reference value	5
S(CB)	Solid area fraction in contact with the liquid (Cassie-Baxter regime)	2
S	Laser scanning speed	3
Sa	Arithmetic mean height of the surface	5
SCA	Static contact angle	4
SEM	Scanning electron microscope	3, 4, 5
SL	Solid-liquid interface	3
SS	Stainless steel	4
SV	Solid-vapour interface	3
UV light	Ultraviolet light	2
W	Width of channels	5
X <sub>f</sub>	Final value of channel depth or bulge height after abrasion	4
X <sub>i</sub>	Initial value of channel depth or bulge height	4
XPS	X-Ray photoelectron spectroscopy	4, 6
ZR	Rayleigh length	2
$\alpha$	Deviation of BIA	5
$\alpha_0, \alpha_1, \alpha_2...$	Relative angles between normal and laser beam	5
$\gamma_{LV}$	Liquid-vapour surface tension	2
$\gamma_{SL}$	Solid-liquid surface tension	2
$\gamma_{SV}$	Solid-vapour surface tension	2
$\Delta l$	Nominal distance between channels	5
$\Delta l'$	Actual distance between channels	5

$\theta$	Effective contact angle	2, 4
$\theta_1$ & $\theta_2$	Tapering angles	5
$\theta_{CB}$	Cassie-Baxter contact angle	2, 3
$\theta_D$	Divergence of the beam	2
$\theta_w$	Wenzel contact angle	2
$\lambda$	Wavelength of the laser light	2, 3, 5
$\sigma_{ij}$	Surface tension between interfaces	3
$\sigma_{LV}$	Surface tension between liquid and vapour interfaces	4
$\sigma_{SL}$	Surface tension between solid and liquid interfaces	4
$\sigma_{SV}$	Surface tension between solid and vapour interfaces	4
$\tau$	Pulse duration	2
$\varphi$	Solid-water area fraction	3
$\varphi_0$	Pulse fluence	2
$\omega_0$	Beam radius at focus	2, 5

## List of publications and presentations

The following publications and conference talks presented part of the job carried out during the thesis, as well as other research task related with the Laser4Fun project.

### Journal paper publications

- **Garcia-Giron A., Romano J.-M., Liang Y., Dashtbozorg B., Dong H., Penchev P. and Dimov S.S.**, Combined surface hardening and laser patterning approach for functionalising stainless steel surfaces, *Applied Surface Science* 439 (2018) 516-524, doi:10.1016/J.APSUSC.2018.01.012
- **Garcia-Giron A., Romano J.-M., Batal A., Dashtbozorg B., Dong H., Martinez Solanas E., Urrutia Angos D., Walker M., Penchev P. and Dimov S.S.**, Durability and wear resistance of laser-textured hardened stainless steel surfaces with hydrophobic properties, *Langmuir* (2019) 35, 5353-5363, doi:10.1021/acs.langmuir.9b00398
- **Garcia-Giron A., Romano J.-M., Batal A., Michatek A., Penchev P. and Dimov S.S.**, Experimental investigation of processing disturbances in laser surface patterning, *Optics and Lasers in Engineering* (2019), (Accepted, under edition process), doi:10.1016/j.optlaseng.2019.105900

## Conference presentations

- ILAS 2017 5th UK Industrial Laser Symposium, (Grantham, UK), 22-23 March 2017
- 39th International MATADOR Conference on Advanced Manufacturing, (University of Manchester, Manchester, UK), 5-7 July 2017
- World Congress on Micro and Nano Manufacturing 2018 (Portorož, Slovenia), 18-20 September 2018
- 19th International Symposium on Laser Precision Microfabrication, (Edinburgh, UK), 25-28 June 2018

## Other presentations

- 5th International Summer School on Trends and new developments in Laser Technology, Fraunhofer IWS, Dresden, Germany (2016)
- Summer School on Advanced Laser Processing 2017, University of Twente, Enschede, Netherlands (2017)
- Poster session within the EU-H2020 Laser4Fun workshop, Zaragoza, Spain (2017)
- Summer School on Laser Micro/Nanostructuring and Surface Tribology, CNR IFN and Politecnico di Bari, Bari, Italy (2018)

## Proceeding papers

- **Garcia-Giron A.**, Romano J.-M., Liang Y., Dashtbozorg B., Dong H., Penchev P., Dimov S.S. Combined Surface Hardening and Laser Patterning for Producing Wear Resistant Hydrophobic Surfaces, Proceedings of 2nd World Congress on Micro and Nano Manufacturing (WCMNM) (2018) - Surface Functionalization, 75-78, doi:10.3850/978-981-11-2728-1\_16

## Other publications as co-author

- Romano J.-M., Helbig R., Fraggelakis F., **Garcia-Giron A.**, Werner C., Kling R., Dimov S.S. Springtail-inspired triangular laser-induced surface textures on metals using MHz ultrashort pulses, Journal of Micro and Nano Manufacturing (2019), 7(2), 024504, doi:10.1115/1.4043417.
- Romano J.-M., Ahmed R., **Garcia-Giron A.**, Penchev P., Butt H., Delléa O., Sikosana M., Helbig R., Werner C., Dimov S.S. Subwavelength Direct Laser Nanopatterning via Microparticle Arrays for Functionalizing Metallic Surfaces, Journal of Micro and Nano Manufacturing (2019) 7(1), 010901, doi:10.1115/1.4042964.
- Romano J.-M., Gulcur M., **Garcia-Giron A.**, Martinez-Solanas E., Whiteside B.R., Dimov S.S. Mechanical durability of hydrophobic surfaces fabricated by injection moulding of laser-induced textures, Applied Surface Science (2019), 476, 850-860, doi:10.1016/j.apsusc.2019.01.162.

- *Romano J.-M., **Garcia-Giron A.**, Penchev P., Dimov S.S.* Triangular laser-induced submicron textures for functionalising stainless steel surfaces, *Applied Surface Science* (2019), 440, 162–169, doi:10.1016/j.apsusc.2018.01.086.
- *Joshi G.S., Dashtbozorg B., Romano J.-M., **Garcia-Giron A.**, Gaudio C., Dong H., Dimov S.S., Ancona A., Carbone G.* Experimental investigation of the tribological and wettability properties of laser-textured martensitic steel surfaces, *Proceedings of the 19th International Symposium on Laser Precision Microfabrication (LPM)* (2018), JLMN-18-049, 1-5.
- *Cardoso J.T., **Garcia-Giron A.**, Romano J.-M., Huerta-Murillo D., Jagdheesh R., Walker M., Dimov S.S., Ocaña J.L.* Influence of ambient conditions on the evolution of wettability properties of IR-, ns- laser textured aluminum alloy, *RSC Advances* (2017), 7, 39617, doi:10.1039/C7RA07421B.
- *Huerta-Murillo D., **García-Giron A.**, Romano J.-M., Cardoso J.T., Cordovilla F., Walker M., Dimov S.S., Ocaña J.L.* Wettability modification of laser-fabricated hierarchical surface structures in Ti-6Al-4V titanium alloy, *Applied Surface Science* (2019), 463, 838-846, doi:10.1016/j.apsusc.2018.09.012.
- *Romano J.-M., Ahmed R., **Garcia-Giron A.**, Penchev P., Delléa O., Dimov S.S.* Towards large area submicron surface texturing by femtosecond laser irradiation of microparticle arrays, *Proceedings of 2nd World Congress on Micro and Nano Manufacturing (WCMNM)* (2018) - Himalaia H2020 project session, 309-312, doi:10.3850/978-981-11-2728-1\_10.
- *Romano J.-M., **Garcia-Giron A.**, Penchev P., Dimov S.S.* Triangular self-organized surface textures produced by femtosecond laser irradiation on stainless steel and titanium alloy, *Proceedings of 2nd World Congress on Micro and Nano*

- Manufacturing (WCMNM) (2018) - Laser Processing I, 103-106, doi:10.3850/978-981-11-2728-1\_09.
- *Romano J.-M., **Garcia-Giron A.**, Penchev P., Gulcur M., Whiteside B.R., Dimov S.S.* Lotus-leaf inspired surfaces: hydrophobicity evolution of replicas due to mechanical cleaning and tool wear, Proceedings of 3rd World Congress on Micro and Nano Manufacturing (WCMNM) (2019), (Accepted).
  - *Batal A., Michalek A., **Garcia-Giron A.**, Nasrollahi V., Penchev. P, Sammons R., Dimov S.S.* Effect of laser processing conditions on wettability and proliferation of Saos-2 cells on CoCrMo alloy surfaces, Advanced Optical Technologies, (Accepted).
  - *Romano J.-M., Fantova-Sarasa J., Concheso C., Gulcur M., Dashtbozorg B., **Garcia-Giron A.**, Penchev P., Dong H., Whiteside B.R., Dimov S.S.* Effects of tool wear on hydrophobic polymer surfaces replicated using plasma treated and laser-textured stainless steel inserts, Tribology – Materials, Surfaces & Interfaces (Submitted).
  - *Dashtbozorg B., Li X.Y., Romano J.-M., **Garcia-Giron A.**, Sammons R.L., Dimov S.S., Dong H.* Response of Metastable S-Phase Layer formed on AISI 316L to Ultrashort Pulsed Laser Texturing, Applied Surface Science (Submitted)
  - *Vercillo V., Tonnichia S., Romano J.-M., **Garcia-Giron A.**, Aguilar-Morales A., Alamri S., Dimov S.S., Lasagni A.F., Bonaccorso E.* Design Rules for Laser Patterned Icephobic Metallic Surfaces for Aeronautic Applications (In preparation)

- *Dashtbozorg B., Romano J.-M., **Garcia-Giron A.**, Li X.Y., Sammons R.L., Dimov S.S., Dong H.* Low Temperature Plasma Nitriding and Pulsed Laser Patterning for Durable Textured Surfaces (In preparation)

# **Chapter 1**

---

## **General introduction**

---

## 1.1 Motivation

Surface functionalization is of great interest to industry and research due to the attractive properties that can be “imprinted” on almost any material and thus applied in many application areas. Especially, additional functionalities can be selectively imbedded into surfaces, e.g. hydrophobicity, ice detachment, bacteria repellence, friction reduction or cell growing enhancement, among others. Considering the range of surface properties of interest to industry, wetting is particularly attractive, as it is generally interrelated and underpins several applications, i.e. self-cleaning, liquid transportation, micro-fluidics or drag reduction.

Surface properties depend on both, chemistry and surface topographies, and the common ways to achieve them is by employing chemical coatings, modifying the surface roughness or introducing surface patterns. Chemical etching or sandblasting are techniques widely used to modify and increase the surface roughness, whereas photolithography, electron beam lithography, polymer replication or laser patterning are applied to create surface patterns at micro and nano scales or multiscale ones.

Laser micro processing is a non-contact method that does not require an extensive surface preparation, use of chemicals or other consumables. Furthermore, the wastes, gases and debris produced during the process can be considered negligible and can be evacuated from the laser-material interaction area with fume extractors. Thus, it can be regarded as an environmentally friendly technology. Moreover, there are constant advances in high dynamics scan heads and laser sources that are reducing processing

times while increasing process yields and thus to make laser patterning a promising and very attractive option for many applications, e.g. drag reduction in aeronautics, self-cleaning for home appliances or bacteria repellence for medical tools, among others. But, at the same time, there are open issues in making laser patterning a viable option for surface functionalization and thus for its broader use by industry. In particular, there are some shortcomings that have to be addressed before it is widely deployed in industrial processes, e.g. the durability of the produced patterns or the processing of free form surfaces.

The performance of functionalised/engineered surfaces depends on whether the surface patterns, roughness or chemical coatings remain unaltered during the lifespans of products. Wear and scratches can impact and deteriorate their functional responses, progressively, and thus to degrade their designed properties to states when it is necessary to recondition surface topographies or coatings, or even to replace components and in some cases even the whole product. Thus, it is important to address the issues relating to durability of the functionalised surfaces in order to make them more wear resistant.

Increasing the surface hardness of the substrate materials can increase the durability of the patterns, and thus to increase the lifespan of given surface properties. There are technologies available that with a minimal impact on cost can increase significantly the hardness of substrate surfaces, e.g. one of these promising technologies is plasma surface alloying that can be applied on a wide range of metallic materials and can be easily up scaled. The process involves an atomic diffusion into the surface to a given

depth, usually a few microns, which leads to surface compression, and hence to higher hardness. Then, a dual effect can be achieved by combining plasma surface alloying with laser patterning to achieve synergistic effects on engineered surfaces. However, the impact of the laser irradiation on plasma treated substrates is still unstudied.

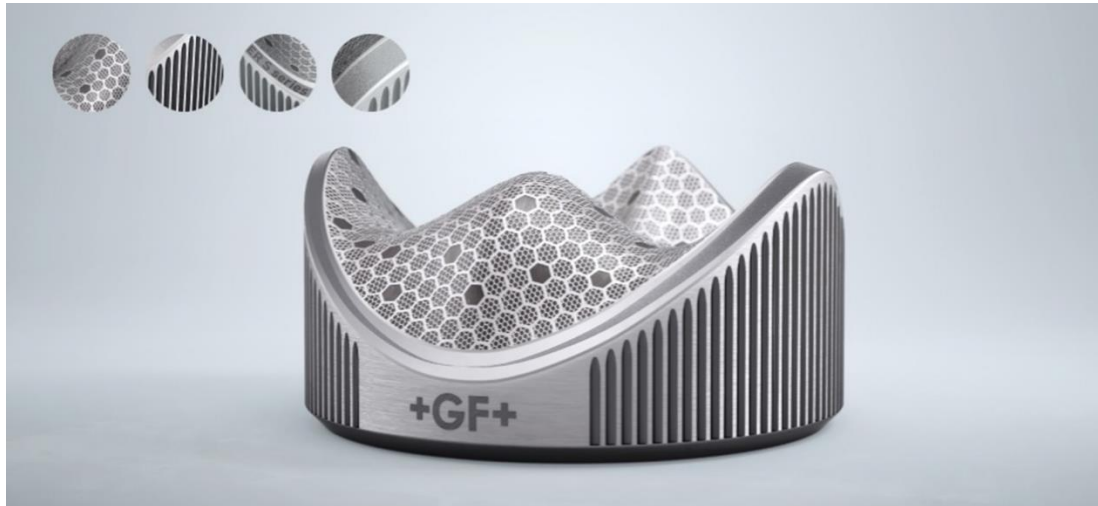


**Fig 1.1.** A laser patterned free form surface (GF Machining Solutions website). [1]

Another important issue in achieving a broader use of laser patterning as a solution for surface functionalisation is the processing of free form surfaces as shown in Fig. 1.1. This is a challenging task that usually requires 3D surfaces to be partitioned into fields and each of them to be patterned separately in order to treat relatively large areas. In particular, the beam delivery sub-systems of lasers processing setups have limitations in regards to their working volumes, e.g. the processing volumes are determined by 3D scan heads in combination with used focusing lenses. In addition, every laser processing setup has a specific depth of focus within which it can be considered that the patterning process is in control or the variations of the resulting surface topographies are acceptable. However, if the laser processing is done outside the respective depth of

focus, the effects on resulting patterns are significant as depicted in Fig. 1.2a-b. The beam spot size increases in the laser-material interaction area and as a consequence of this the processing conditions deviate substantially from those achievable in focus.

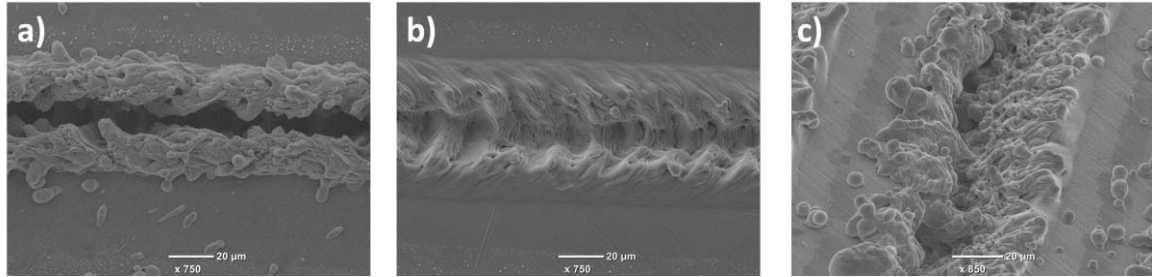


**Fig 1.2.** *The effects of beam incident angle and off-focus laser processing on resulting patterns: (a) a channel as part of a patterned surface produced at focus and laser beam normal to the surface; (b) the same channel but after off-focus patterning; (c) the same channel produced with a beam incidence angle of 40°.*

Furthermore, the processing conditions can be affected by the beam incident angles due to changes in light absorption and surface reflectance. In addition, this can alter the resulting patterns on surfaces, due to their geometrical distortions when they are produced on 3D surfaces. Besides, the dynamics on any molten material in the laser-material interaction area can differ when curved surface are processed because this can influence the material evacuation and recasts' formation, and thus lead to significantly distorted topographies as shown in Fig. 1.2a and Fig. 1.2c.

All aforementioned effects can be present when laser processing free form surfaces and as a result the produced patterns can be altered and also their functional response. Therefore, they should be considered as processing disturbances and therefore should

be studied systematically in order to minimise their impact on resulting patterns with their respective functionalities. Especially, such investigations can inform the process design and allow an “adaptive” partitioning when processing 3D surfaces.

## **1.2 Research aim and objectives**

The aim of this research is to broaden the industrial use of laser patterning for surface functionalization, especially the creation of hydrophobic surfaces, by addressing its limitations in regards to the durability of produced functional topographies and also in patterning 3D surfaces. The first is addressed by investigating synergistic effects when combining plasma surface alloying and laser patterning to produce hydrophobic patterns with increased durability and wear resistance. Wear resistance is related with the surface hardness, and the combination of both, plasma surface alloying and laser patterning can result in more durable functional surfaces. However, plasma surface alloying produces metastable phases, and is necessary to investigate whether the nanosecond laser patterning, as a thermal treatment, can affect to the stability of the alloyed surface and retain the hardness. Furthermore, it is required to study the correlation between wear cycles and functional response, topography erosion and chemical composition of the functional surfaces in order to understand their relationship with the wear resistance.

At the same time to investigate the limitations in patterning 3D surfaces, a methodology is proposed to study the negative effects of key processing disturbances and use the results in developing “adaptive” surface partitioning approaches and thus to minimise them. Laser patterning has some limitations when processing freeform surfaces, as an

optical device its processing field is on the focal plane, and this is drawback for industry. The common approach is to divide 3D surfaces into smaller discrete marking fields and process them separately. However, in each marking field there are points out of focus and with different angles of incidence, and these disturbances can affect the final pattern created in the processed surface, and thus, the functional response. The impact of the processing disturbances on the obtained topographies and their functional response must be investigated in order to reduce deviations from the desired functionality.

The aims of this research will be achieved through the following objectives:

- i) *To develop a manufacturing process that combines synergistically the capabilities of plasma surface alloying and laser patterning to fabricate wear resistant hydrophobic surfaces.* Carbon and nitrogen-based gases will be used to alloy stainless steel surfaces and then to pattern them with 15 and 220 nanosecond laser pulses. Channel and pillar-like structures will be studied. The effects of laser-material interactions will be investigated in regards to the resulting surface functionality, hardness, delamination of the hardened layer, compositional and microstructural changes.
- ii) *To investigate the wear resistance and durability of plasma alloyed and laser patterned hydrophobic surfaces.* An abrasion test will be proposed to study the wear resistance of the patterned surfaces together with their functional response. The abrasion effects on surface topographies and functionality, and chemical composition of the patterned surfaces will be investigated.

iii) *To investigate the effects of key processing disturbances present in laser patterning 3D surfaces and study their impact on the resulting surface topography and functionality.* The three disturbances that will be investigated are focal offset distance and beam incident angle variations and patterns' geometrical distortions. A methodology to investigate their effects on resulting surface patterns and functionality will be proposed. In particular, a method will be developed to study the effects of these three processing disturbances on resulting patterns and their functional responses, i.e. their hydrophobic properties, and use the results for developing "adaptive" surface partitioning approaches that can minimise their negative effects.

### **1.3 Thesis organization**

This thesis is organized in 6 chapters.

**Chapter 1** provides a general introduction, where the motivation, research aim and objectives, and the thesis organization are presented.

**Chapter 2** reviews the state-of-the-art in the research relevant fields, i.e. in surface functionalization, basic laser principles and surface characterisation.

The research carried out and the contributions to knowledge claimed in this thesis are presented in Chapters 3 to 5.

**Chapter 3** describes the proposed synergistic approach in combining plasma surface alloying and laser patterning to produce hydrophobic surfaces with higher durability.

Samples are produced and analysed, in terms of resulting wettability, hardness, delamination of the hardened layer, compositional and microstructural changes, and abrasion resistance.

**Chapter 4** presents an investigation into the wear resistance and durability of plasma alloyed and laser patterned hydrophobic surfaces. The abrasion effects on surface topographies and functionality, and chemical composition of the patterned surfaces are investigated.

**Chapter 5** describes a methodology for investigating the effects of key processing disturbances in patterning 3D surfaces, especially their impact on the resulting topographies and their functionality. It is explained how the results of such systematic research can be used in developing “adaptive” surface partitioning approaches and thus to minimise the negative effects of investigated processing disturbances. In addition, a process monitoring approach is proposed based on areal roughness parameters.

**Chapter 6** summarises the contributions to knowledge and main conclusions of the conducted research. In addition, future research directions are discussed.

## **Chapter 2**

---

### **Literature review**

---

This chapter offers a summary on bio-inspired applications and surface functionalization techniques. In particular, wetting properties and laser technology fundamentals are introduced.

## **2.1 Nature as source of inspiration**

Since the very early steps of mankind, humans observed their surroundings and tried to learn from nature. For example, they discovered that fire was not only a frightening and dangerous phenomenon, but also something useful that could be used to process their food, stay warm during the winter, illuminate during the dark nights and scare away wild animals or enemies. Nature is a broad source of inspiration and it is very usual for scientist to look at it and try to copy features from plants or animals, this is called bio-inspiration [2]. As evolution went on, animal species were equipped with special characteristics that allowed them to survive. These characteristics were not only bigger claws or stronger hawks, but also small features in their skin, legs or wings, to cite a few, that allowed them to hide better, swim faster, or even protect them from the natural elements. A good example of this kind of animals with enhanced characteristics is the gecko, a specie of lizard, and the singularity of the geckoes lies in their skin and feet [3–5]. The skin of the geckoes is composed by scales of some microns covered by submicron sized hairs (Fig. 2.1). This dual scale structures are hydrophobic, showing low particle adhesion and self-cleaning properties, and thus protecting the geckoes from contaminants. Furthermore, the submicron hairs show good antibacterial behaviour, protecting the gecko from potential diseases. The feet of the gecko are of great interest

as well, as they are covered by hierarchical structures, giving them a large surface of adhesion, which allows them to climb smooth and rough vertical walls.

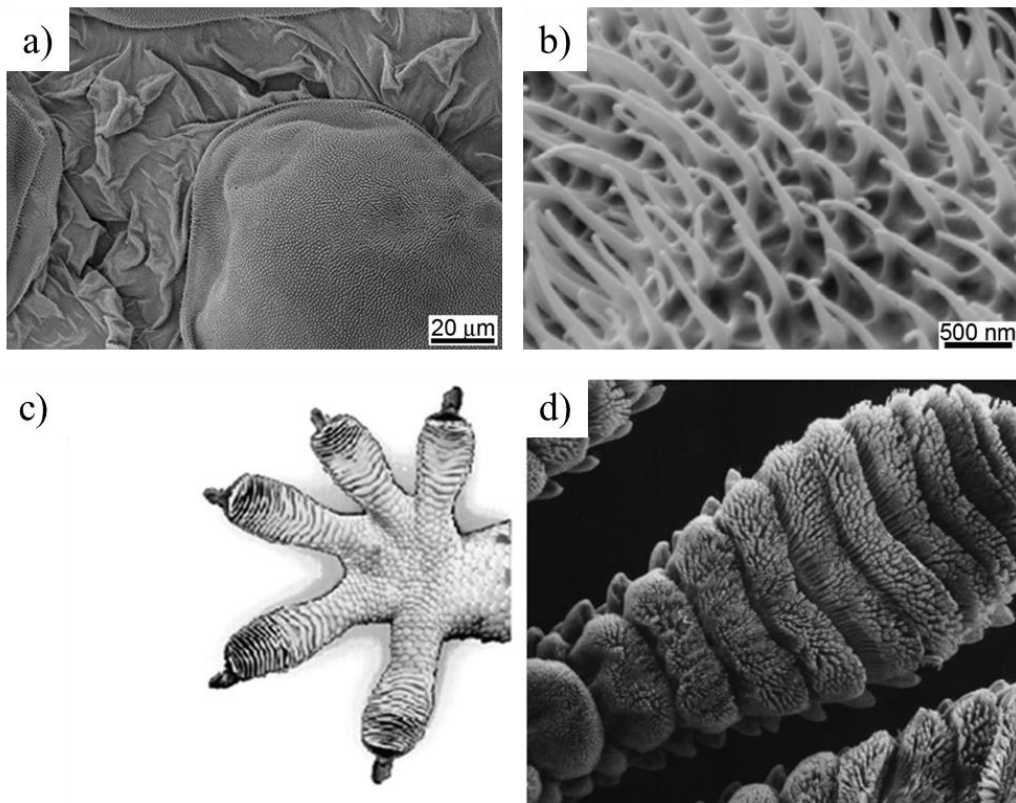


**Fig 2.1.** Images of gecko skin (a-b) [4] and gecko foot (c-d) [5].

Another interesting animal is the springtail. The skin of the springtails has a hierarchical topography, with different sizes of features (Fig. 2.2). This structure makes the springtail cuticle omniphobic, i.e. it does not only repel water, but also oils or another liquids, and it works even when the springtail is fully immersed into water [6].

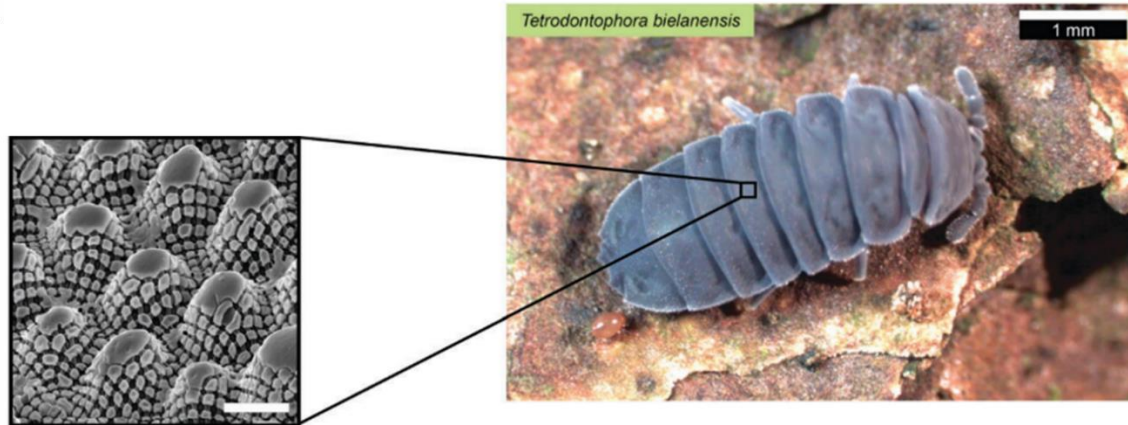


**Fig 2.2.** Springtail and detail of the skin. The hierarchical structure of the skin is formed by dual scale patterns, with different sizes [6].

In the case of the Kingdom plantae, some examples can be found all around the world, and the most renowned and interesting one is the lotus (*N-nucifera*). Lotus leaves are so hydrophobic that water drops roll off their surface, dragging all the particles or contaminants present, and giving the plant a self-cleaning effect, as can be observed in Fig. 2.3 [7]. This phenomenon is produced by a combination of surface topography and chemistry. From one side, the surface topography of the lotus leaf is formed by pillar-like microstructures covered by smaller submicron features, i.e. a dual scale topography, as in the cases of the gecko or the springtail. On the other hand, the surface of the lotus leaves is covered with epicuticular wax crystalloids, composed by, for example, hydrocarbons, that are non-polar [8]. The combination of the hierarchical structures and the non-polarity makes the lotus leaves extremely hydrophobic, with self-cleaning properties and drops rolling off the surface, and it is not surprising that scientists often refer to this kind of water repellence as the lotus effect.

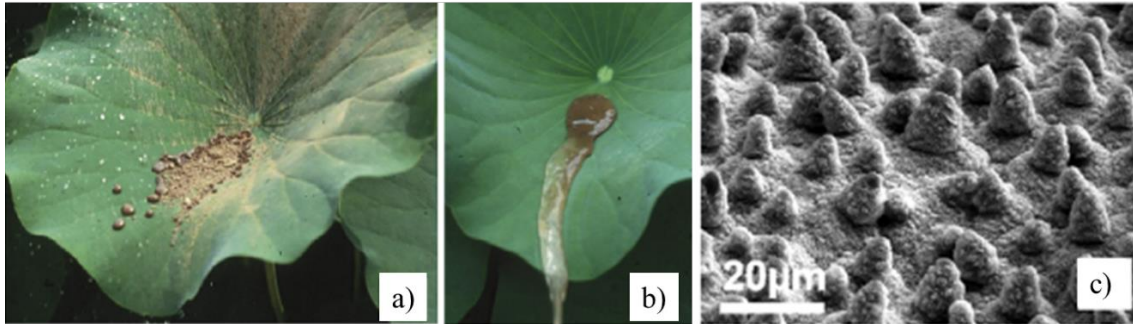


**Fig 2.3.** Example of lotus leaf covered with dust (a) and cleaned after water drops drag the dust (b). SEM image of the surface topography of the lotus leaf (c) [7].

The abovementioned cases are only a few examples of the broad spectrum of living beings with special characteristics, in particular, with hydrophobic and self-cleaning properties, as it is the main focus of this research. There are much more cases, and also some other different effects, as for example, the colorization in some butterfly wings [9], or the drag reduction effect of the shark skin, that minimizes the friction with water [10]. All of the previously mentioned characteristics are caused by the presence of hierarchical surface topographies with different sizes and shapes and served as inspiration for scientist to develop new techniques to manufacture materials with enhanced functionalities.

## 2.2 Surface functionalization techniques

Surface functionalization is gaining interest in many fields in industry and research. It adds new properties to already existing products or materials, as hydrophobicity [11], bacteria repellence [12], reduction of friction coefficient [13], or anti-icing properties [14], for example. There are three main approaches to change surface properties of a material, the first one, to change the chemistry, for example adding a chemical coating

to the surface [15]; the second one, to change the surface topography [16], in order to mimic the topographies present in nature, as the lotus leaf, mentioned before; and the third one, a combination of both, chemical coating and surface topography [17]. There are many techniques to modify surface properties and some of them are presented in Table 2.1. and introduced below:

	Investment	Consumables	Min. pattern size	Wastes	Flexibility	Pattern control	Maintenance
Surface coatings	\$\$	Yes	N.A.	High	N.A.	N.A.	Medium
Chemical etching	\$\$	Yes	1-100 $\mu\text{m}$	High	Low	No	High
Photolithography	\$\$\$	Yes	100 nm	Medium	High	Yes	High
EBL	\$\$\$	Yes	100 nm	Medium	High	Yes	High
Sandblasting	\$	Yes	50-100 $\mu\text{m}$	High	Low	No	Medium
Polymer replication	\$\$	Yes	1-100 $\mu\text{m}$	No	Low	Yes	High
Laser	\$\$	No	250 nm	No	High	Yes	Low

**Table 2.1.** Surface modification techniques.

- Surface coatings: the substrate is covered with a thin layer of another material with different properties; thus, mechanical attributes of the bulk material do not change, but the surface has different characteristics. Coatings can be applied for several purposes, from aesthetics to thermal isolation, wear resistance, anti-fouling, hydrophobicity and so on. In the case of hydrophobic coatings, several chemicals can be applied to reduce the surface energy if the substrate, as organo-triethoxysilanes, fluoroalkylsilane, alkoxysilane, fluorinated silane or fluorocarbon compounds, along with others [18].

- Chemical etching: a strong acid is used to attack the surface and induce a surface oxidation and thus, an increase in the roughness. For example, Want et al. combined chemical etching and coating to produce super hydrophobic surfaces [19]. As observed in Fig. 2.4, first, the surface was attacked with the etching solution, and an oxide layer was formed. Then, an ultrasound bath was used to remove part of the oxides, obtaining a rough surface. Finally, a non-polar layer was applied, obtaining a hydrophobic surface.

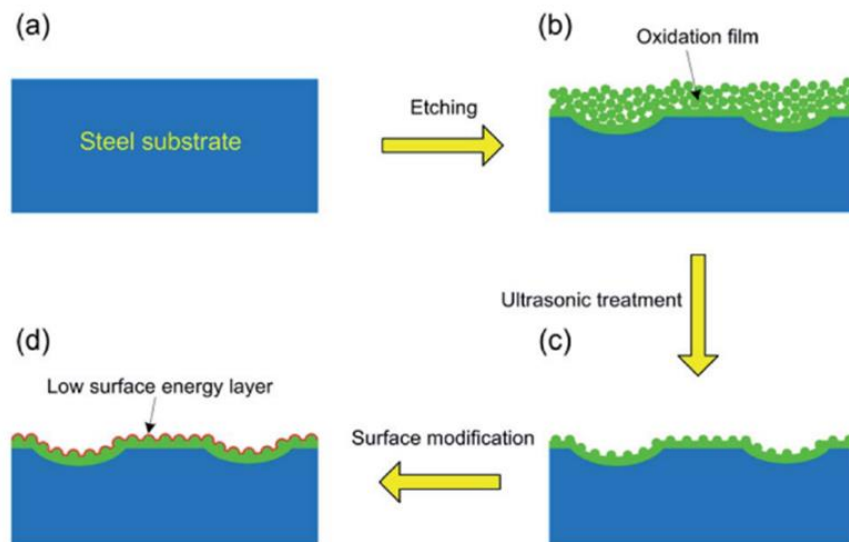


**Fig 2.4.** Combination of chemical etching and surface coating to produce hydrophobic surfaces [19].

- Photolithography: this technique allows the selective material transference from a donor photomask to a photosensitive wafer, by irradiating it with UV light. This technique was successfully used by Suzuki et al. to apply selectively hydrophobic coatings to a surface, creating a channel-like pattern which was used to change the direction of the drops rolling out of the surface [20]. Photolithography can

be combined with other techniques, for example, with wet etching, to produce pillar-like structures with overhangs, as the ones observed in Fig. 2.5 [21].

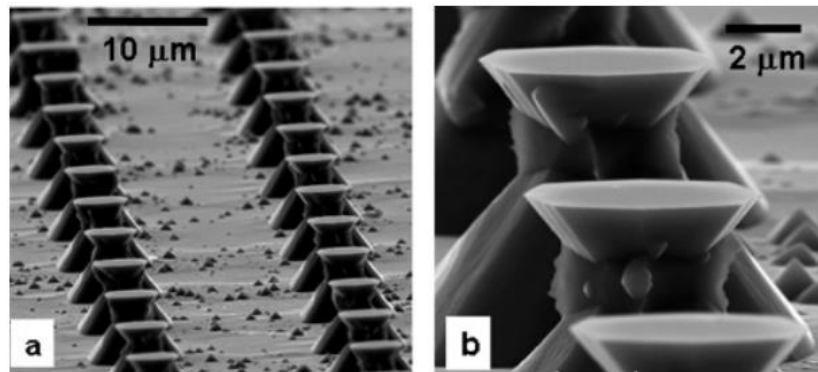


**Fig 2.5.** Pillar like structures with overhangs at the top edge fabricated by combination of photolithography and consecutive wet etchings [21].

- Electron-beam lithography (EBL): the concept is very similar to the photolithography. The substrate is covered with an electron sensitive film and an electron beam is used to scan the surface and perform a defined pattern. The scanned part has a different solubility than the initial substrate, and after cleaning the surface with a solvent, the defined pattern remains. For example, Li et al. produced micro bowl structures using electron-beam lithography, and after coating them with fluorocarbon they exhibited high hydrophobic adhesive properties [22].
- Sandblasting: it is another method to induce an increase in surface roughness, in this case, a torrent of a fluid, usually compressed air, containing abrasive particles is blown towards the substrate, eroding the surface. The increase in roughness can be combined with a chemical coating to obtain hydrophobic

surfaces [23]. Fig. 2.6 shows a glass surface before and after the sandblasting, it can be observed an increase in the roughness.

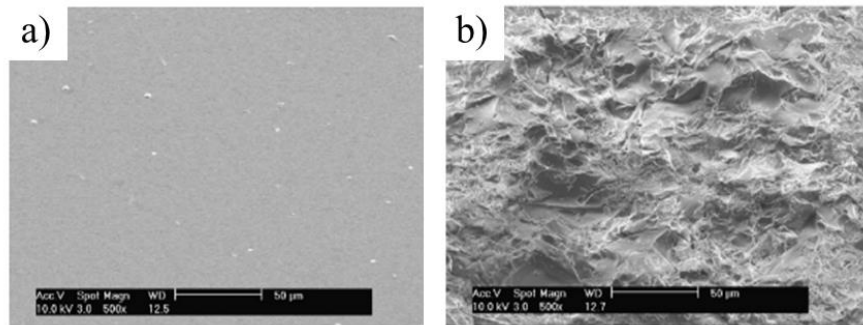


**Fig 2.6.** *As received glass surface (a), and glass surface after sandblasting (b) [23].*

- Polymer replication: the negative of a defined topography can be patterned on a metallic master and replicated in the final part by means of plastic injection. Romano et al. created patterns with different sizes and shapes in masters for injection moulding, and successfully transferred them to polymers, studying the wetting properties of the obtained surfaces [24]. The process is shown in Fig. 2.7. First, a femtosecond laser source (Fig. 2.7b) was used to create the negative of the targeted topography in stainless steel inserts to introduce them into plastic injection moulds (Fig. 2.7a). Then, the inserts were placed into the moulds and the molten plastic injected at 230°C (Fig. 2.7c). A piston is used to press the molten plastic before it cools down, in order to allow the plastic to flow into the micron scale patterns. When the plastic part is solidified, an ejector nozzle pushes it and helps to detach it from the mould. Finally, the plastic part with the designed pattern is obtained (Fig. 2.7d).

- Laser patterning: laser technology is one of the most interesting technologies for surface functionalization. It is fast, accurate and efficient. It does not require the use of chemicals and as a non-contact tool it does not require the use of consumables either. Furthermore, it can be used in a wide range of materials, and for many applications, as laser cutting, drilling, welding or surface patterning.

Fundamentals of laser technology will be introduced in Section 2.4, and examples of surface functionalization by means of laser patterning techniques will be discussed in Section 2.5.

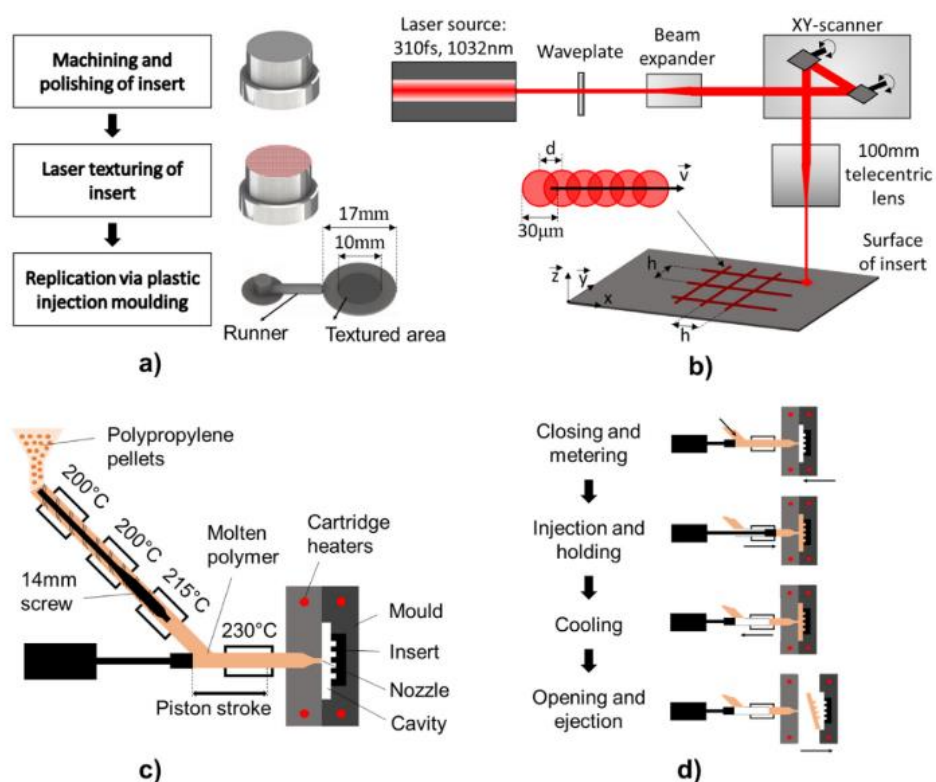


**Fig 2.7.** Combination of laser patterning (a, b) and plastic injection moulding (c, d) to produce hydrophobic surfaces on polypropylene [24].

## 2.3 Fundamentals of wettability

### 2.3.1 Wetting states

The term wettability refers to the way a surface behaves in contact with a liquid, whether if it spreads or stays in shape of drops. The first studies of wettability were published in 1805 by Thomas Young. In order to quantify the wettability of surfaces, Young described the static contact angle (also known as Young's angle) between a drop and a surface as the tangential angle between the three phases, i.e. liquid, air and solid [25], as depicted in Fig. 2.8. The static contact angle (CA) can be calculated as follows:

$$\cos \theta = \frac{\gamma_{SV} - \gamma_{SL}}{\gamma_{LV}} \quad (2.1)$$

Where  $\theta$  is the angle between drop and solid in equilibrium, and  $\gamma_{SV}$ ,  $\gamma_{SL}$  and  $\gamma_{LV}$ , are the surface tensions between solid-vapor, solid-liquid and liquid-vapor phases, respectively. Surface tensions are associated with the composition of the three phases involved, and if the atmospheric conditions are unchanged, their values are constant. It is worth noting that for a given surface and liquid, an increase on the temperature leads to a change in the contact angle, as the surface tensions depend on the temperature conditions [26].

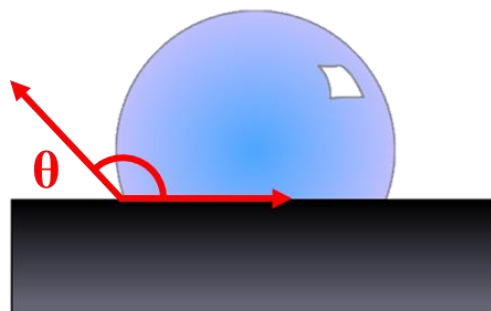


**Fig 2.8.** Sketch of a liquid drop on a surface and its Young's angle ( $\theta$ ).

The contact angle gives information about the wettability of the surface. Conventionally, a surface with CA higher than 90° is considered hydrophobic, and when CA is smaller than 90° is hydrophilic [27]. Furthermore, a surface with CA higher than 150° and with small sliding angles is considered superhydrophobic [28,29].

However, flat and smooth surfaces are ideal and in reality, every existing surface has some degree of roughness, which influences the wettability.

Two different wetting states can be possible in rough surfaces, i.e. Wenzel [30] and Cassie-Baxter [31] states. In the first one, the liquid is fully wetting the surface (See Fig. 2.9a), whereas in the other, air pockets are trapped between solid and liquid, forming a liquid-solid-air interface characterized with high contact angles (See Fig. 2.9b).

In the case of a Wenzel wetting state, the apparent contact angle can be measured using the following equation:

$$\cos \theta_W = r \cos \theta \quad (2.2)$$

Where  $\theta$  is the contact angle for a smooth surface, as described by Young in Eq. 2.1, and  $r$  is the ratio between the actual area and the projected area, being always bigger than 1. Analysing Eq. 2.2, it can be deduced that rough surfaces amplify the wetting states, i.e. hydrophilic surfaces will be more hydrophilic with smaller contact angles, and hydrophobic surfaces will be more hydrophobic, with higher contact angles.

The Cassie-Baxter state describes a situation where air is trapped between the drop and the surface, and thus, the contact area can be divided in liquid-solid and liquid-air interfaces [29,32]. The apparent contact angle in a Cassie-Baxter wetting state can be calculated as follows:

$$\cos \theta_{CB} = S \cos \theta + (S - 1) \quad (2.3)$$

Where  $\theta$  is the Young's angle discussed in Eq. 2.2, and it only depends on the surface tensions of the three interphases in contact, i.e. liquid, solid and air, and thus, their chemical properties. And  $S$  is a surface factor representing the solid area fraction in contact with the liquid, and it depends on the surface roughness.  $S$  can take values from 0 to 1, where 0 would mean that the drop is completely in contact with air, and 1 that the surface is totally wet, and thus, the liquid would be completely in contact with the surface, without air trapped, as shown in as in Fig. 2.9a. It can be calculated that large volumes of air trapped will always lead to small values of  $S$ , and thus high contact angles. Is worth noting that both, Wenzel and Cassie-Baxter wetting states can offer high contact angles, as can be calculated from Eq. 2.2 and Eq. 2.3, however, the main difference is the full wetting or the presence of air trapped, respectively. In the case of Wenzel wetting states, even if there is a high contact angle, the drop is touching the bottom of the surface and pinned with the roughness, and thus, drops will not roll off the surface. However, Cassie-Baxter wetting states have air trapped and the drop is not pinned on the surface, resulting a contact between drop and surface with freedom of movement, that allows the drop to roll off. Cassie-Baxter wetting state is linked with super-hydrophobicity and thus, with properties as self-cleaning or antifouling.

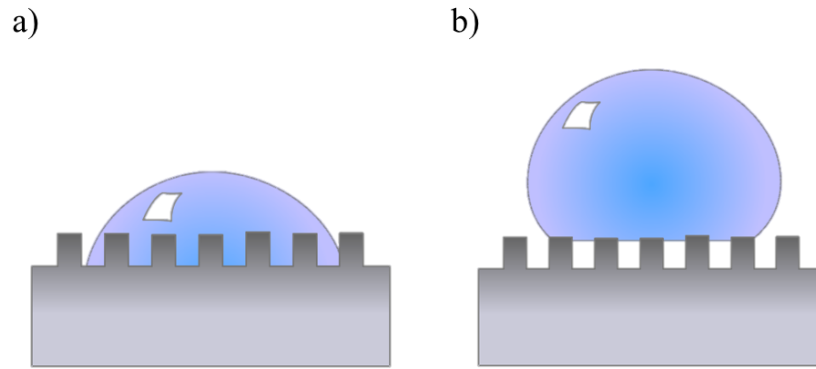


**Fig 2.9.** Sketch of rough surfaces in Wenzel wetting state (a) and Cassie-Baxter wetting state (b).

### 2.3.2 Measurement techniques

The most common ways to quantify the wettability of a surface are the static contact angle, previously mentioned; the sliding angle, which gives information of how drops are sliding or staying pinned in a surface when it is tilted; and the advancing/receding angle, whose difference is the hysteresis [33]. The most popular way is the static contact angle, due to its simplicity, accuracy and reproducibility.

The most extended technique to measure static contact angles is the sessile drop method. An optical goniometer consists in a mechanical stage where the measured surface is placed between a light source and a camera (Fig. 2.10a). A liquid dispenser deposits a drop with a specific volume on the surface, and then the camera captures the shape of the drop, which is analysed with a software, and finally the contact angle is given (Fig.2.10b).

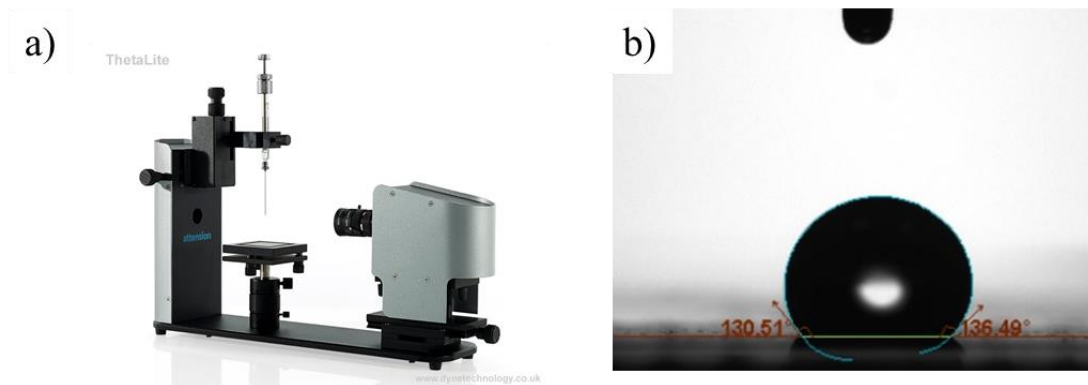


**Fig 2.10.** *Theta Lite optical goniometer from Biolin Scientific (a) and example of a contact angle measurement (b).*

There are some factors to take in account when measuring static contact angles in order to avoid errors. For example, the dispensing procedure, the correct positioning of the baseline, the flatness of the measured surface or the resolution of the camera and software used to analyse the shape of the drop. Furthermore, the measurements must be taken when the drop is stabilized and not spreading. Just after the contact between the drop and the surface takes place, the drop spreads dissipating energy and increasing the contact line (i.e. the contact angle is being reduced while the drop spreads), until the equilibrium is obtained and the spreading stops [34].

The size of the droplets has an effect on the contact angle measurements as well, if the drop size is too large, the influence of the gravity will affect the droplet and make it spread on the surface or induce a distortion, giving a wrong contact angle measurement [35]. Moreover, the drop volume must be large enough to avoid a significant distortion produced in the contact line due to the surface roughness [36].

The sliding angle gives information about whether a drop sticks or moves on a tilted surface. Usually surfaces with low sliding angles are related to super hydrophobic

surfaces with self-cleaning properties, as in the case of the lotus leaf. The sliding angle can be easily measured with an optical goniometer with a mobile stage (Fig. 2.11a). As the sample is being tilted, the gravity starts acting against the friction between the drop and the surface, when the gravitational forces are bigger than the friction, the drop slides and the inclination angle of the surface is recorded [37].

The advancing/receding angle measurement gives the information of the maximum and minimum contact angles a liquid can have in contact with a specific surface when a drop is placed and withdrawn, respectively, and if it is measured dynamically it can be plotted as a hysteresis loop. It can be measured when obtaining the sliding angle of a surface, as the maximum and minimum angles in the drop just before it starts sliding. The advancing/receding measurement with a tilted surface is only an approximation, and is more accurate to use the needle-embedded sessile drop method [38], where a drop is dispensed on top of the surface with a very slow flow rate, and then, after stabilization it is absorbed at the same flow rate, as shown in Fig. 2.11b.

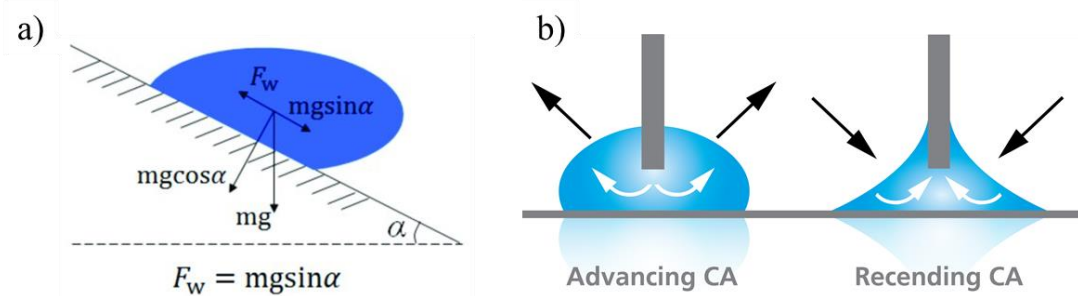


**Fig 2.11.** Sketches of (a) sliding angle measurement [39] and (b) advancing/receding angle measurement (Biolin Scientific Website).

## 2.4 Introduction to LASER technology

In 1916, Albert Einstein predicted the stimulated emission phenomenon [40], and described the mathematical model behind it, settling the basics of the LASER (Light Amplification by Stimulated Emission of Radiation). However, it was not until 1960 when Theodore H. Maiman [41] created the first working ruby laser. Since then, lasers have been in constant development and nowadays, laser technology is widely used in industry and research for many applications, as welding, cutting, surface treatment or laser cleaning [42].

### 2.4.1 Basic principles

An atom has certain energy levels where electrons can orbit around the nucleus, in such a way that orbitals closer to the atomic centre represent the lower energy levels and are more thermodynamically stable. Thus, as the energy required to be in the low energy levels is smaller, electrons will be more likely to occupy the closer orbitals. However, if an external source adds enough amount of energy to the system, an electron can jump to a higher orbital, where it would never be in a steady state. For example, given an atom with an electron in a low energy state ( $E_1$ ) (Fig. 2.12a), it can absorb energy from a photon ( $P_0$ ), and then jump to a high energy state ( $E_2$ ) (Fig. 2.12b), in a process called absorption. However, this is not a thermodynamically stable state, and at some point, the electron will decay to the original orbital, in an event called spontaneous emission, releasing the excess of energy in the form of a new photon ( $P_1$ ), with a random direction (Fig. 2.12c). Nevertheless, if during the time lapsed between the adsorption and the spontaneous emission, another photon hits the excited system, a different event occurs,

called stimulated emission, consisting in the decay of the electron to the lower energy state, together with the emission of a new photon identical to the incident one in terms of phase, direction, wavelength, and polarization (Fig. 2.12d).

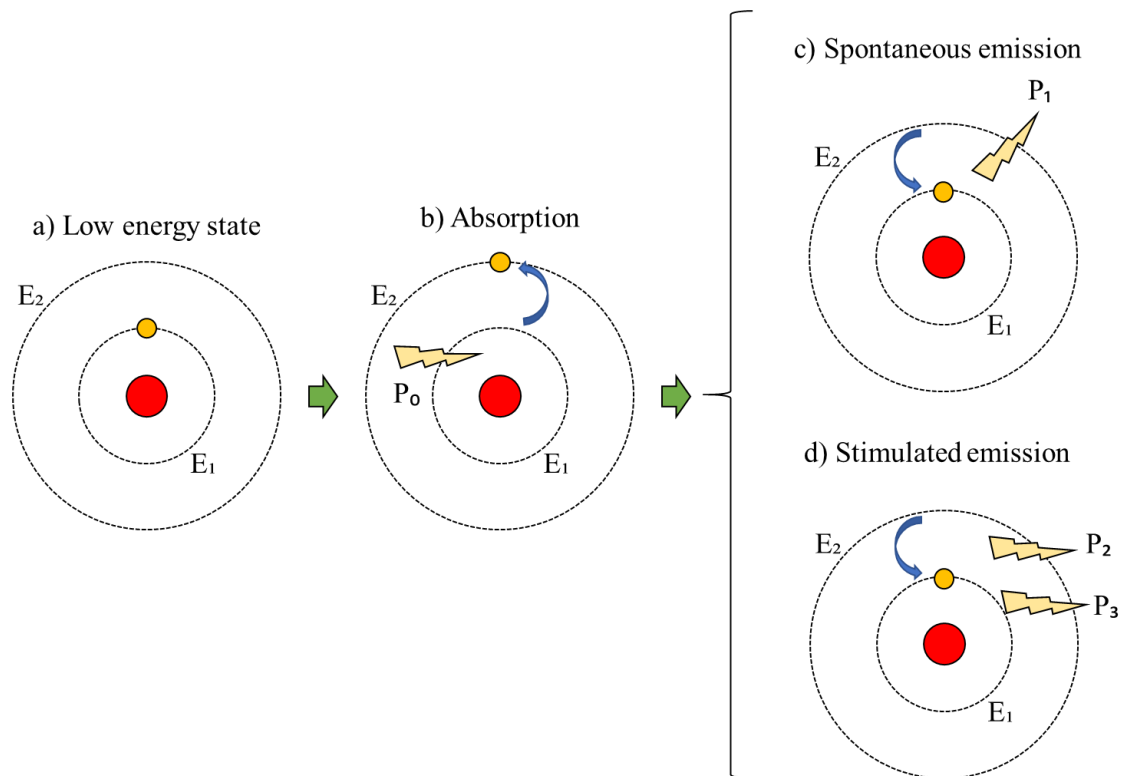


**Fig 2.12.** Sketch an atom in a low energy state (a) and the possible radiative processes: absorption (b), spontaneous emission (c) and stimulated emission (d).

Is this stimulated emission phenomenon what is behind the performance of lasers. Considering a large atomic population  $N$ , with  $N_1$  species with electrons in a low energy state and  $N_2$  excited species, in nature  $N_1$  is higher than  $N_2$ , as the opposite situation would be unstable. However, if enough energy is added to the system, the number of excited species raises until  $N_2 > N_1$ , achieving the so called population inversion, which makes the amplification of light possible [43].

A basic laser source is composed by an active medium, two opposing mirrors forming an optical oscillator and a pumping system [44], as can be observed in Fig. 2.13:

- Active medium: is the material containing the atoms, ions or molecules that are excited, and where the population inversion is produced. Almost everything can be used as active medium, but the most commonly used materials are gases (He-Ne, CO<sub>2</sub>...), alcohols with organic dyes solved, or rare-earth elements in a glass matrix (as Nd:YAG lasers). The composition of the active medium determines the wavelength of the produced laser beam.
- Pump: depending on the active medium, it can be an electric source or an optic device, as LEDs or lamps. The pump is where the process starts, giving energy to the active medium to drive the atoms to higher energy states and achieve the population inversion. The output power of the laser can be controlled with the energy supplied with the pump.
- Optical resonator: composed by two parallel mirrors, one of them semi-transparent, with the active medium located between them. When the active medium starts to be excited by the pump, the produced photons are reflected in the mirrors, going back and forth through the active medium, amplifying the light.

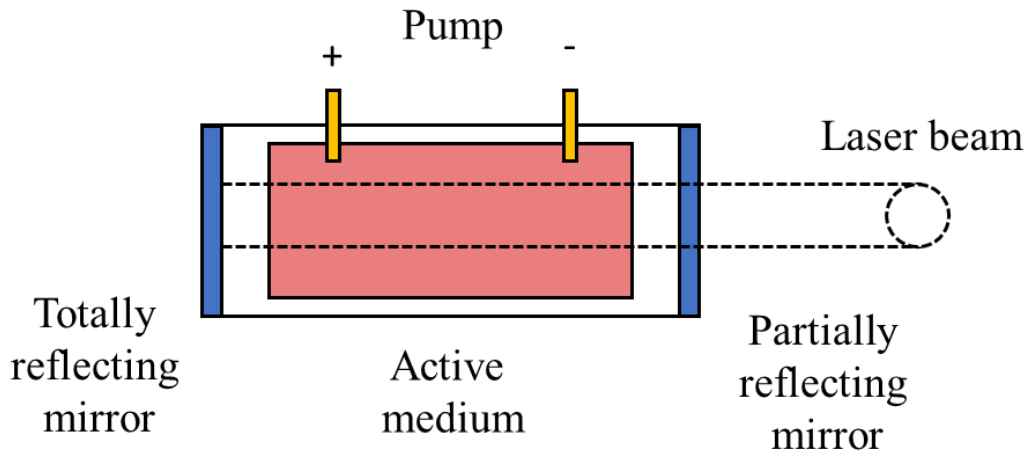


**Fig 2.13.** Sketch of a basic laser source.

## 2.4.2 Beam delivery

Lasers can be classified, regarding the temporal distribution of the power, in continuous or pulsed lasers. Continuous lasers have, as the name already announces, a continuous distribution of the power, and are commonly used for welding, cutting or surface marking in industrial applications. In the case of pulsed lasers, the output power is released in a train of consecutive pulses, reaching a higher peak energy per pulse ( $E_p$ ):

$$E_p = \frac{P}{f} \quad (2.4)$$

Where  $P$  is the average power of the laser source and  $f$  is the pulse repetition rate (frequency). Pulsed lasers are used in applications where high peak power is necessary, as machining or surface patterning.

Pulse duration ( $\tau$ ) is an important parameter to consider when processing with lasers, especially in the case of short (nanosecond range) and ultrashort (pico- and femtosecond range) laser pulses. Considering the distribution of the pulse power in time, the pulse duration is measured as the time lapse within which the output power

is half of the peak power [45]. If the pulse duration is in the nanosecond range (Fig. 2.14a), the material is melted and evaporated from the surface, and the heat diffusion can form a heat affected zone around the laser path. Furthermore, the molten material can solidify in the surroundings of the laser path. However, when the pulses are short enough (in the picosecond and femtosecond scales, as in Fig. 2.14b), the interaction between laser and material is so short that heat diffusion can be neglected [46]. The peak power ( $P_p$ ) depends on the pulse duration ( $\tau$ ) and can be calculated with the following equation:

$$P_p = \frac{0.94E_p}{\tau} \quad (2.5)$$

Being  $E_p$  the pulse energy.

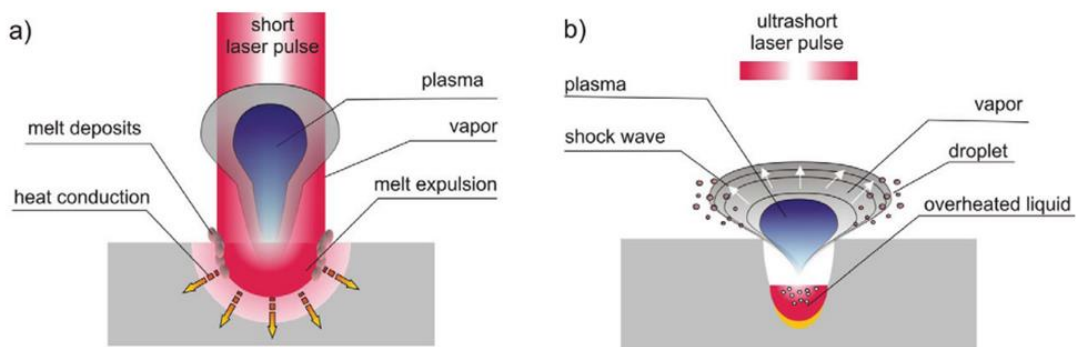


**Fig 2.14.** Differences between short (a) and ultrashort (b) pulses [46].

The laser beam can be delivered from the source towards the processed material by reflecting it with the appropriate set of mirrors, and focused with a stack of lenses, in order to obtain a smaller beam diameter and thus increase the energy density supplied on the targeted surface. Thus, considering a gaussian laser beam focused with a lens with focal distance  $F$ , the beam radius at focus ( $\omega_0$ ) will be:

$$\omega_0 = \frac{2(M^2)F\lambda}{\pi D_L} \quad (2.6)$$

Where  $M^2$  is the beam quality factor of the laser,  $\lambda$  is the wavelength of the laser beam and  $D_L$  is the diameter of the beam before the lens [47]. The pulse fluence ( $\varphi_0$ ) at focus can be calculated as follows:

$$\varphi_0 = \frac{E_P}{\pi\omega_0} \quad (2.7)$$

The Rayleigh length is the distance in the propagation direction of the beam where the beam radius is  $\sqrt{2}\omega_0$ , as depicted in the Fig. 2.15. The depth of focus (DOF) can be calculated as two times the Rayleigh length, and can be considered as the distance from the focal position where the defocusing can be neglected:

$$DOF = 2Z_R = \frac{2\pi(\omega_0)^2}{(M^2)\lambda} \quad (2.8)$$

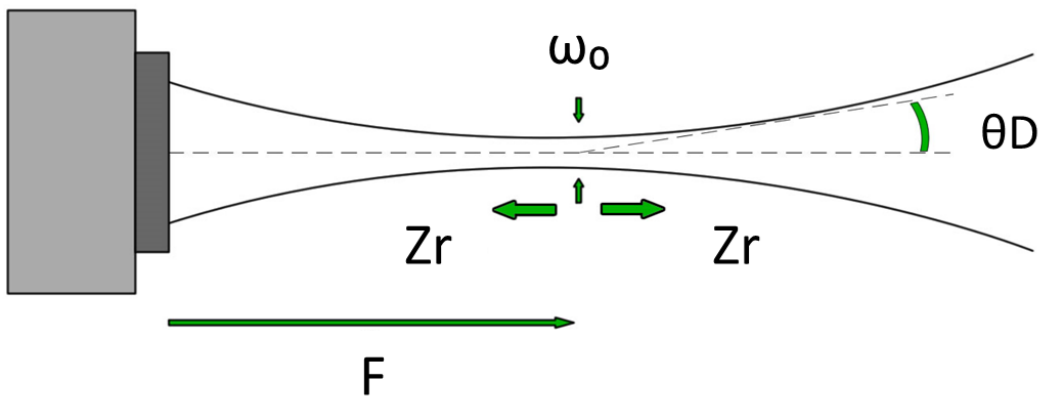


**Fig 2.15.** Sketch of the laser beam propagation through a focusing lens, with a focal distance  $f$ .  $\omega_0$  is the minimum spot diameter at focus.  $Z_r$  is the Rayleigh length and  $\vartheta_D$  is the divergence of the beam.

The relative movements between laser beam and workpiece can be performed either with a mechanical stage or with a galvanometric scanner. For the first one, the laser beam is fixed, and the workpiece is mounted in a mechanical stage, which realises the movements. In the second method, a pair of galvanometric mirrors controlled by a CAD software are deflecting the laser beam and scanning the working surface in x- and y-axes. The use of dynamic focusing modules, or Z-modules, enable the adjustment of the focal plane in a small range, usually a few millimetres, adding the possibility of movements in the z-axis as well [48].

## **2.5 Laser surface functionalization**

### **2.5.1 Patterning strategies**

One of the fields where lasers offer more interesting possibilities is surface functionalization. As introduced in the section 2.1, adding new functionalities to existing products or surfaces, inspired in nature, is a hot topic. In the case of laser functionalization, several strategies can be adopted to directly perform patterns on the surfaces, as direct laser writing (DLW), direct laser interference patterning (DLIP) or laser induced periodic surface structures (LIPSS), among others.

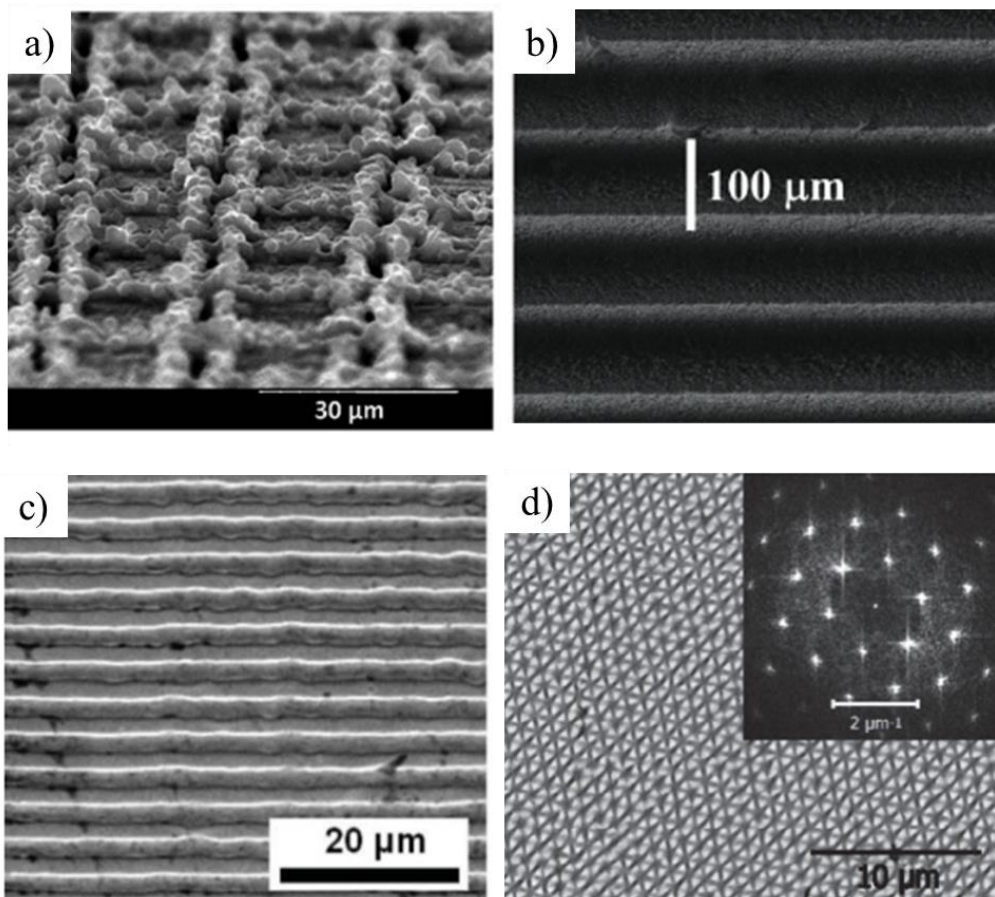


**Fig 2.16.** SEM images of patterns performed with (a) nanosecond DLW [49], (b) femtosecond DLW [50], (c) DLIP [51] and (d) triangular LIPSS [52].

As DLW is performed by the movements of the laser beam across the surface, it is a fast and versatile technique that allows the fabrication of many kinds surface topographies. Some of the most widely used ones are shark like structures [53], channels [54], pillars [17], lotus-leaf structures [55], single spot overlapping patterns [56], homogeneous polishing [57], dimples [58], and so on. When using ultra short pulses, patterns tend to be smoother [59,60], as in the case of Fig. 2.16b, whereas nanosecond and longer pulses tend to melt and solidify material on the edges of the laser path, forming bulges and rough structures [61,62], for example in Fig. 2.16a.

The causes of LIPSS formation are still under discussion, there are several theories to explain their appearance, as interferences between incident and scattered waves [63], inhomogeneous absorption [64], surface plasma polaritons [65] or convection flows due to thermal gradients [66]. The periodicity of LIPSS is usually closer to the wavelength of the laser used [67,68], and can be used in applications where smaller patterns are required, as antibacterial or optical devices (Fig. 2.16d).

DLIP is a very versatile technique, as the periodicity and shape of the patterns can be tailored varying the angles of incidence and the number of incident beams [69,70]. Spot sizes used in DLIP configurations are larger compared to DLW and their overlap enable the homogeneous patterning of large surfaces with complex patterns and dual scale topographies [71,72]. An example of DLIP channel like pattern is shown in Fig. 2.16c.

There are also some indirect techniques where lasers are used to produce a pattern in a master and after the topographies are replicated, usually in plastic parts, using roll to roll or injection moulding techniques [24,73].

One of the biggest challenges for laser patterning is the processing of 3-D surfaces. Most of the publications are focused in planar surfaces, however, industry requires the application of the patterns in real parts with 3-D shapes, requiring a combination of complex beam delivery systems and multi-axis mechanical stages. It is worth noting that, as lasers marking fields are usually a focal plane, when processing free form surfaces, the patterns will be deformed. Furthermore, the reflectance and fluence depend on the angle of incidence [74], deviations from the focal plane will result in differences in the pattern [75]. Moreover, surface curvatures change the beam spot shape, leading to alterations in the energy distribution [76].

Recent publications have been focused in the manufacturing of 3-D surfaces with lasers. Diaci. Et al. developed a method to pattern tilted and curved surfaces, where a CW laser scans the surface before the pulsed laser engraves it [77]. Cuccolini et. al. developed a method combining a 5 axis CAM with a software which, first, divides the CAD image in triangles, and then, controls the movements of the axes, synchronising it with the laser [78]. Jiang et al. proposed a method of layering considering the marking field of the laser, and dividing the IGES model file into partitions prior to the laser patterning [79].

## **2.5.2 Applications for laser patterned surfaces**

As it was already mentioned in section 2.2, there are many properties a surface can acquire by means of topographical or chemical modification. In particular, laser patterning targets the modification of the surface topography at micron or submicron scales, in order to induce changes in the final properties. Some of the targeted functionalities achieved with laser surface modification are discussed below.

Ice formation and growing can block air inlets in aeroplanes and helicopters, as well as increase the weight supported by the aircraft, leading to a higher fuel consumption. Thus, anti-icing surfaces are of great interest for aeronautics. Hydrophobicity and ice-repellence are sometimes related. Super cooled surfaces with micro-nano structural topographies can repel impacting water droplets, inhibiting ice formation [80]. Laser patterned micro-nano topographies with hydrophobic properties can slow down the formation of rime, improving static anti-icing properties of surfaces, as in the dark area observed in Fig. 2.17 [81]. However, as there are many icing scenarios and ice growing stages (i.e. drops impacting and condensing, ice nucleation, ice adhesion...), there is not

a master pattern with the properties to prevent ice formation and repel ice in all the cases. Thus, micro-nano roughness with hydrophobic properties can help, but is not enough to have anti-icing properties [82]. Furthermore, sometimes water repellent surfaces can worsen anti-ice properties during inflight conditions, as ice interlocking can happen with the roughness [83].

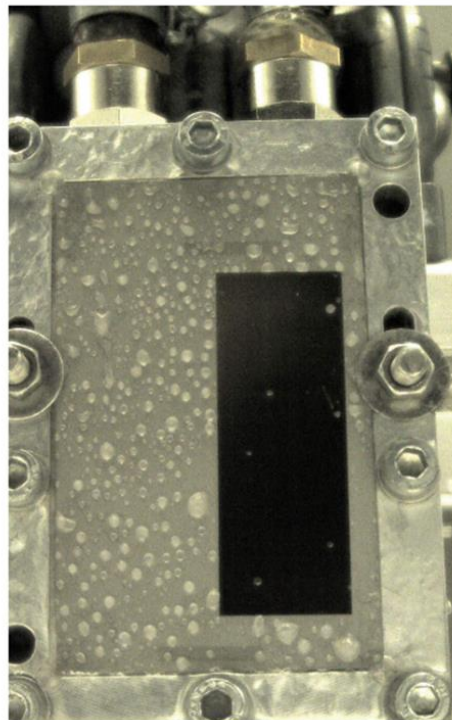


**Fig 2.17.** Example of a steel surface after an ice rain test, where the dark area was laser patterned [81].

Bacteria-repellence can be very beneficial in medical applications, as surgical material. Bacteria tend to attach in the surfaces where is energetically favourable to stay and where they are protected. The presence of surface roughness or topographies can lead to the bacteria repellence if the size of the patterns is slightly smaller than the size of bacteria [84–86], as for example in Fig. 2.18, it can be observed that the bacteria

population is reduced in smaller patterns. In the micro scale, Laha et. al. produced patterns by means of DLW with low bacteria adhesion and studied the relation between water repellence and bacteria growing [87]. Different topographies produced by DLW showed a reduction in bacteria colonization compared with the smooth surfaces [53]. Bacteria adhesion can be also reduced by smaller patterns, with sizes similar to the bacteria size, produced by DLIP [69,70] or LIPSS [88]. Other techniques involve the fabrication of masters and posterior replication in polymers [89] or the presence of microparticle arrays prior to the laser patterning [90].

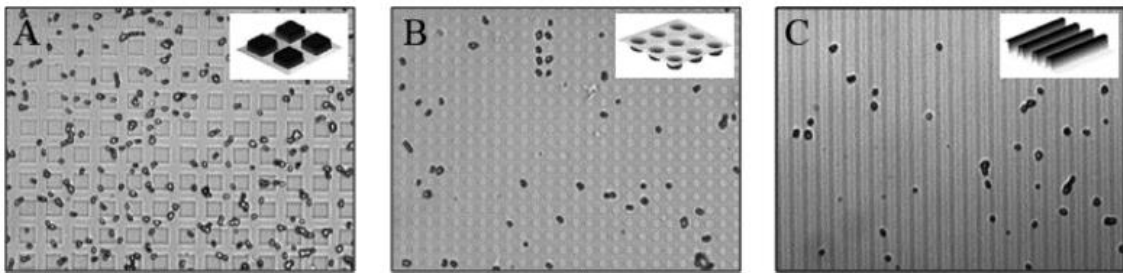


**Fig 2.18.** Examples of anti-bacterial patterns: (a) pillars, (b) circular holes and (c) channels [84].

Cell attachment and growing is of great interest in the field of medicine, in particular in scaffolds and implants, they must be biocompatible and allow cells to grow and remain strongly attached to form tissues around, as in the case of Fig. 2.19, where can be observed an increase on the cell attachment in patterned surfaces. The presence of hierarchical structures enhances the adhesion of cells [91], and surface laser patterning can be used to perform that kind of textures [17,88,92,93]. Depending on the cell type, some patterns can be beneficial or inhibit the adhesion, allowing the selective growing of cells in scaffolds [94].

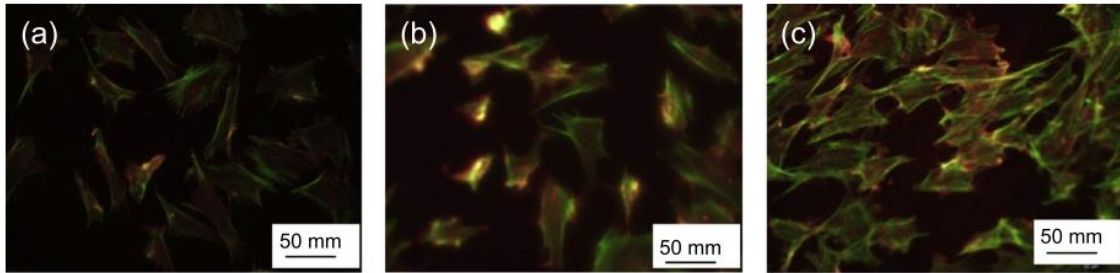


**Fig 2.19.** Examples of cell cultures: (a) non-irradiated surface and (b-c) irradiated surfaces [93].

Modification of the optical properties of the surface can be useful for aesthetical purposes or sensing applications. Colorization can be achieved by oxidation of the substrate with laser pulses [95], for example, titanium surfaces can be selectively oxidised by laser pulses achieving single spots which are composed by different oxides with various colours, allowing the imprinting of logos [56], as the Gioconda shown in Fig. 2.20c. Surfaces covered with LIPSS have a high potential for aesthetical purposes, for example, some kind of LIPSS offer light scattering properties and they show different colours depending on the observation angle [66,96], as in Fig. 2.20a, enabling the possibility to create aesthetical logos, as in Fig. 2.20b. In other cases, the presence of LIPSS have blackening properties, being useful for laser marking [97]. Following the same principle, DLIP can be successfully applied to obtain colours due to the light diffraction in PET surfaces for decorative purposes or light deflectors [98]. Apart from the aesthetic purposes, this kind of gratings can be patterned to fabricate holograms [99], sensors [100] or lenses [101], as shown in Fig. 2.20d.

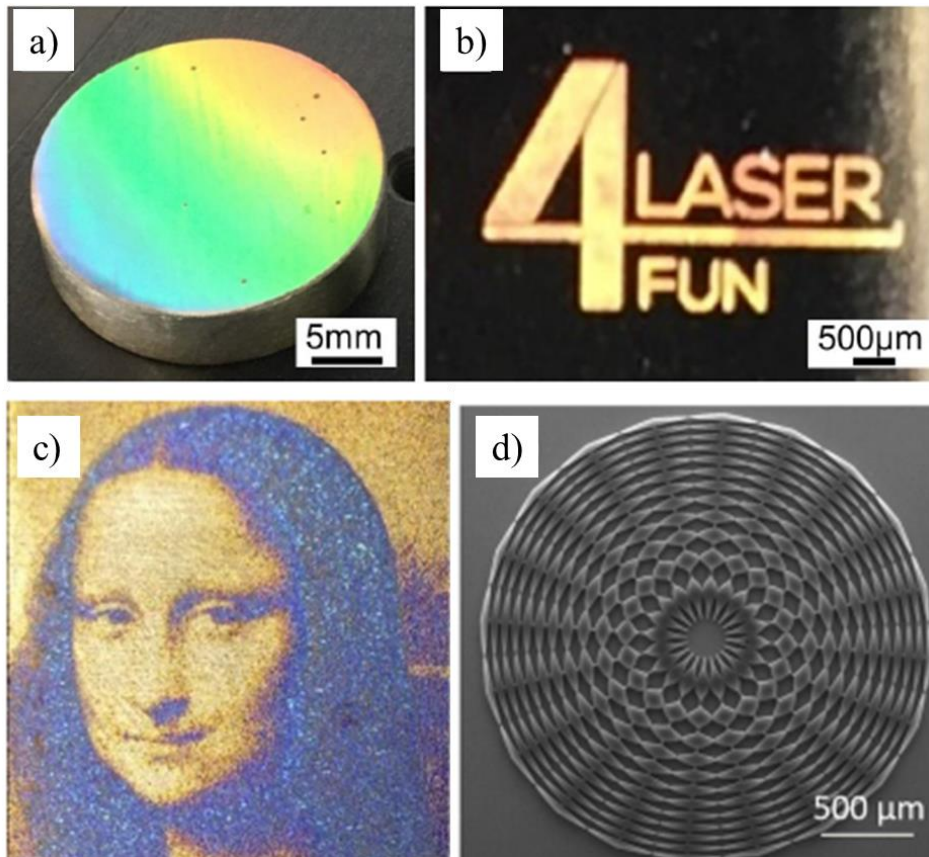


**Fig 2.20.** Examples of aesthetical patterns: (a-b) Surfaces covered with LIPSS showing light scattering effect [96]. (c) Image formed by combination of multiple oxidised single spot [56]. (d) Example of a Gabor zone plate lens for sensing applications [101].

Surface textures have been proven as an effective technique to reduce friction in mechanical parts working under lubrication regimes, and they can be used in real applications, as mechanical seals [102,103] or pistons, cylinders [104] and rings [112], as observed in Fig. 2.21. The presence of conformal contacts with surface textures, as holes, in moving parts working under loads with lubricants can change the hydrodynamic pressure in the contact area, reducing the friction and wear [105,106]. Furthermore, surface patterns can act as lubricant reservoirs and traps for debris produced by the wear, reducing the friction [107]. The density and size of the textures

was also proven as an important factor, and when the distribution is not adequate, the friction reduction can be negligible [13,108]. Tribological properties were successfully enhanced by laser surface texturing using different techniques, as DLW [109], DLIP [110] and LIPSS [111].

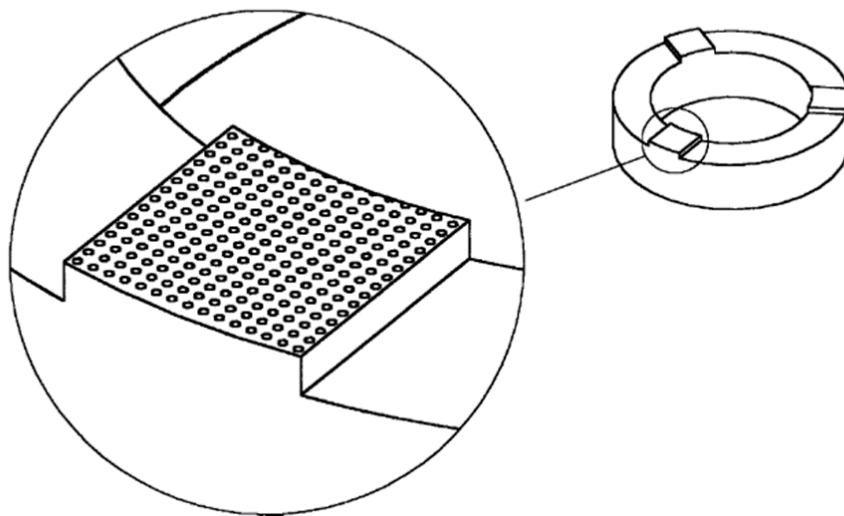


**Fig 2.21.** Sketch of a moving specimen ring patterned with dimples to reduce friction

[112].

As introduced in previous chapters, materials with special wetting properties, as hydrophobic surfaces, are of great interest, as they can be used for antifouling, self-cleaning, liquid transportation, drag reduction or corrosion resistance applications, among others [33]. Furthermore, hydrophobic surfaces are often related with other functionalities, as anti-icing [81] or bacteria adhesion [87]. Lasers are widely used to modify wetting properties; the main approach is to change the surface topography, which leads to an increase in the overall roughness of the surface, and thus, to an

increase in the contact angle, whether if the surface is in Wenzel or Cassie-Baxter wetting state.

Hybrid processes involving laser patterning and surface coatings have been reported. Channels [15,113,114], lotus-like [55] or rose-like patterns [115] processed with laser are combined with non-polar organic coatings, and the combination of both reduces the surface tension and leads to super hydrophobicity.

One-step processes, where the only surface modification technique used is laser patterning, are also successfully applied without a posterior chemical coating. In the range of submicron scales, LIPSS with different distributions were successfully applied, as triangular [52] or linear [116]. In the microscale range, DLIP has been proven to be an effective technique [117]. However, the most widely used way to fabricate one-step super hydrophobic surfaces is DLW, as it is the most cost effective, fast and easily up scalable technique, that can be used in a broad range of materials. Super hydrophobic surfaces were obtained by DLW in a wide range of metallic surfaces and patterns (i.e. channels or pillars, as shown in Fig. 2.22), with ultra-short lasers [28,116,118–120], and also with nanosecond lasers [54,121–125].

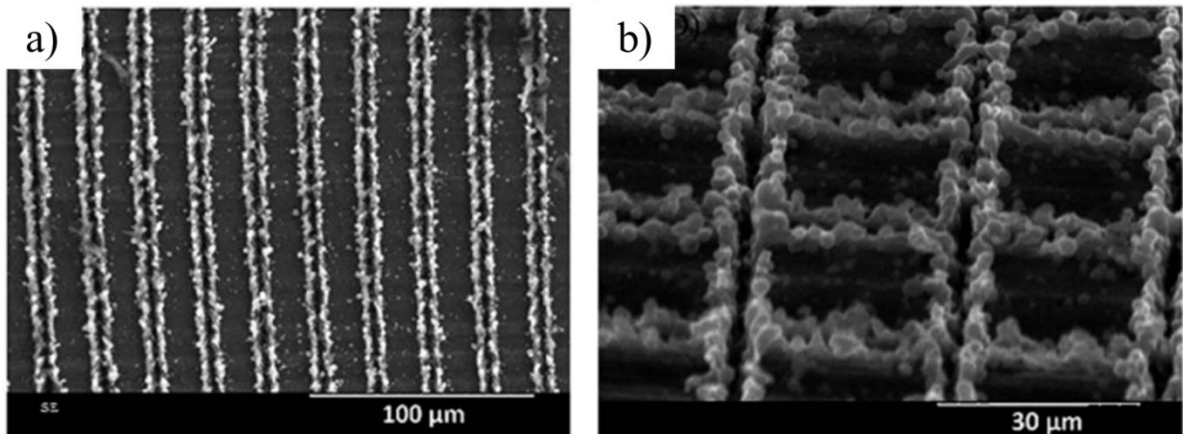


**Fig 2.22.** Hydrophobic channel-like (a) and cell-like (b) patterns [49].

It is worth noting that laser patterned surfaces manufactured by a one-step process, without adding a posterior coating, are highly hydrophilic just after the laser processing, and it is after time when that surfaces start changing and becoming hydrophobic. The mechanism involved in this change of wettability in time (i.e. aging process) is still not fully understood, however there are some hypotheses. The first one suggest that the evolution in wettability is due to partial deoxidation of the patterns [125], while other studies suggest that the change in contact angle is produced by airborne non-polar organic molecules absorbed by laser patterned surface [119,126], or the inhibition of water molecules deposition in the surface [127]. Furthermore, the storage conditions and the different atmospheres where the samples are kept after the laser patterning, can influence and accelerate the aging process [123] or inhibit it, resulting in long lasting hydrophilic surfaces [128].

### 2.5.3 Durability of laser patterned surfaces

Durability is one of the biggest concerns with functionalised surfaces. Coatings or surface patterns can disappear as wear and scratches are deteriorating them with the usage [106,129,130]. Thus, the functionality can be progressively lost, requiring the re-application of the coating or topography, or even the substitution of the product for a new one. In particular, wear, scratches and other factors can affect the performance of super hydrophobic surfaces, where the stability of the Cassie-Baxter state is crucial, and thus, standardized testing methods are required in order to bring out realistic applications for industry [131].

Recently, some publications studied the durability of hydrophobic surfaces manufactured by combining patterning with femtosecond lasers and surface coatings, where different kind of patterns, as cone-like structures [132] or surfaces with high roughness [133], behave as a protection for the chemical coating [19,134]. Nanosecond lasers were also employed to create protective structures and increase the surface roughness at the same time, in order to enhance air trapping and hydrophobicity of the manufactured surfaces [61,135]. Nevertheless, even if DLW has been successfully applied in many research groups to perform one-step processes to achieve hydrophobic surfaces, their durability remains unstudied.

It is well known that contact angles decrease drastically with wear, scratches and even after touching or wetting the surfaces, as grease or water particles can remain trapped on the surface, and they have an impact in the surface topography and chemistry. Performance of the produced functional surfaces after abrasion or surface contamination is reduced or even removed, and that is the main reason why almost all

the published papers only study the functional response in terms of contact angles and sliding angles only in the as-manufactured surfaces. Most of the published papers on laser patterned hydrophobic surfaces lack on durability tests due to the bad results obtained when those tests are performed. Furthermore, in the few papers that analyse the wear response of functional surfaces patterned with laser, the abrasion tests done are very basic. Usually the tests are carried out in a rudimentary way, by moving the samples over a rough surface, as can be a polishing sandpaper, measuring the distance with a rule while applying a load on the sample. However, that kind of tests are barely reproducible, and the results depend on the skills of the operator performing the experiment. Automatization of the abrasion tests is required in order to have a reproducible way to measure and quantify the behaviour of functional surfaces under real working conditions, in order to develop a standardised method to measure the impact of wear in functional patterns.

Wear resistance of the substrates is an important factor regarding the durability of patterned surfaces. A substrate with higher hardness will be more difficult to scratch and more resistant to wear, regardless the process applied (i.e. only DLW or DLW combined with a coating), thus, enhancing the characteristics of the substrate is a promising technique to increase wear resistance of a functionalized surface [136].

One of the techniques used to increase surface hardness in metals is the low temperature plasma surface alloying. This method consist in the diffusion of atoms into the surfaces, in order to create a thin layer of saturated solid solution [137]. The hardened layer can reach around 30  $\mu\text{m}$  thickness, and it tends to expand due to the high number of diffused atoms on it. As the bulk material remains unaltered, the expansion of the thin hardened layer is blocked by the rest of the material, resulting in

a compression in the surface, and the consequent increase in the surface hardness. Different gas mixtures can be used during the process, depending on the desired interstitial diffused element, being the most commonly used C and N. Fig. 2.23 shows a plasma furnace (DC KlöcknerLonon 40 kVA) located in the School of Metallurgy and Materials, in the University of Birmingham, used to perform plasma surface alloying with C or N based gases. The figure shows the white chamber where the samples are placed and the surface alloying takes place, the control panel to select the processing parameters (i.e. pressure, temperature, gas composition or processing time) and a photography taken during the process, when a set of stainless steel plates were carburised.

The method has been successfully applied in different metallic alloys, as Fe-Cr and Co-Cr [138], Ni-Cr [139], austenitic stainless steel [140], ferritic stainless steel [141] and iron aluminide [142].

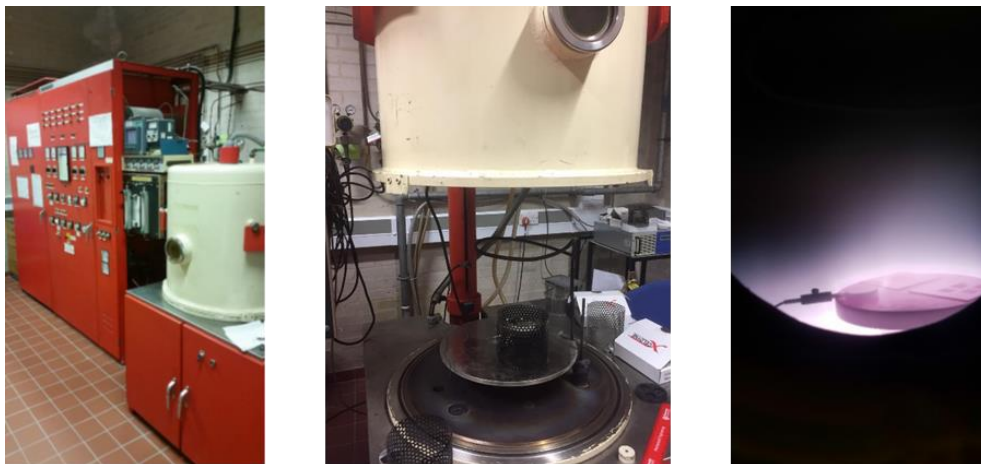


**Fig 2.23.** Images of a DC KlöcknerLonon40 kVA plasma furnace used for low temperature plasma surface alloying (University of Birmingham).

## Chapter 3

---

# Combined surface hardening and laser patterning approach for functionalising stainless steel surfaces

---

*A. Garcia-Giron<sup>1,\*</sup>, J. M. Romano<sup>1</sup>, Y. Liang<sup>2</sup>, B. Dashtbozorg<sup>2</sup>, H. Dong<sup>2</sup>, P. Penchev<sup>1</sup> and S.S. Dimov<sup>1</sup>*

*<sup>1</sup>Department of Mechanical Engineering, School of Engineering, University of Birmingham, Edgbaston, Birmingham, B15 2TT, UK*

*<sup>2</sup>School of Metallurgy and Materials, University of Birmingham, Edgbaston, Birmingham, B15 2SF, UK*

The objective of the first paper, corresponding to the Chapter 3, was to combine two processes in order to, first, increase the hardness of a material, and second, perform a surface patterning to modify the functional response, in this case the wettability. Surface functionalization is quite interesting for industry because by modifying the surface properties of a product it can be much more efficient, for example, if home appliances or kitchen goods are water repellent, they can have self-cleaning properties. As explained in the introduction, one way to perform that functionalization is by creating a surface pattern that modifies the topography and the roughness, like for example using a laser source. However, such patterns can only be applied in the surface, and when wear or scratches occur, they can be eroded and sometimes even totally removed, and once the pattern is lost, the functional response is also lost.

The target of the surface hardening was to enhance the material resistance to wear and scratches. By increasing the hardness of the substrate, the capability of other materials to penetrate the surface and scratch it is reduced, and hence, the durability of the patterns can be greatly increased, and thus the lifespan of the final product. The hardening method chosen was a low temperature plasma surface alloying. The material is introduced in a furnace with a gas, which is the alloying element, and during the process, atoms are being diffused through the surface, resulting in an increase of this element concentration just in the surface, which leads to a raise in the surface tensions. That surface tensions are responsible of the increase in the hardness. As the patterns are only present on the surface, a superficial alloying is enough to increase the pattern lifespan, and thus is not necessary to alloy the bulk material, reducing the final process cost.

Department of Mechanical Engineering and Metallurgy and Materials School, from the University of Birmingham, work together in several projects and collaborations. Professor H. Dong and his group are experts in low temperature plasma alloying and their labs are equipped with the required facilities to perform the surface alloying. Usually the process is carried out in

austenitic stainless steel grades, and the most common alloying elements are N and C, which are introduced from 25%N<sub>2</sub>:75%H<sub>2</sub> or 1.5%CH<sub>4</sub>:98.5%H<sub>2</sub> gas mixtures, respectively. Other alloying elements are used in the literature, but N and C were easier and faster to obtain, and their experience was higher with those gas mixtures.

The chosen substrate material was a ferritic grade stainless steel, imposed by the Laser4Fun project. Ferritic stainless steels are cheaper than austenitic ones, and are commonly used in industry, for example, the ones we used were the ones used to manufacture frontal panels in Bosch ovens.

Nanosecond laser writing was chosen to manufacture the surface functionalization due to the expertise of Professor S. Dimov' group in laser manufacturing. The group facilities include femtosecond and nanosecond laser sources, with ranges from 15 to 220 ns. Although femtosecond laser material interaction gives cleaner patterns and do not show thermal interaction, nanosecond lasers are 10 times cheaper than femtosecond sources, and commonly used in industry, and for this reasons nanosecond laser was the chosen one to carry out this work.

The main challenge on this research was that low temperature surface alloying results in metastable surfaces, stables up to 400°C, and as nanosecond laser is a thermal process, it was necessary to study if the combination of both methods was possible. For this end, low temperature surface was performed on ferritic steel plates, then nanosecond laser patterns were created, and finally, the resulting surfaces were analysed.

This research was published as a full length article in Applied Surface Science (2018) [143].

**Authors' contributions:** A. Garcia-Giron is the main author of this publication. He performed the laser processing and most of the characterization of the samples. Y. Liang and B. Dashtbozorg manufactured the plasma carburised and nitrided plates and contributed with the nano hardness tests. J. M. Romano assisted during the manufacturing of the samples and characterization. A. Garcia-Giron wrote the manuscript that was posteriorly revised by H. Dong, P. Penchev and S.S. Dimov.

**Keywords:** Laser patterning; nanosecond laser; hydrophobicity; plasma surface alloying; hardening; surface engineering.

## **Abstract**

The paper reports a laser patterning method for producing surfaces with dual scale topographies on ferritic stainless steel plates that are hardened by low temperature plasma surface alloying. Nitrogen and carbon based gasses were used in the alloying process to obtain surface layers with an increased hardness from 172 HV to 1001 HV and 305 HV, respectively. Then, a nanosecond infrared laser was used to pattern the plasma treated surfaces and thus to obtain super-hydrophobicity, by creating cell- or channel-like surface structures. The combined surface hardening and laser patterning approach allowed super-hydrophobic surfaces to be produced on both nitrided and carburised stainless steel plates with effective contact angles higher than  $150^{\circ}$ . The hardened layers on nitrided samples had cracks and was delaminated after the laser patterning while on plasma carburised samples remained intact. The results showed that by applying the proposed combined approach it is possible to retain the higher

hardness of the nitrided stainless steel plates and at the same time to functionalise them to obtain super-hydrophobic properties.

### **3.1 Introduction**

Surface functionalisation technologies have many industrial applications due to the added value that they offer to existing and new emerging products. Especially, these technologies allow the surface properties of products to be modified, i.e. to enhance or incorporate new properties such as hydrophobicity [144], bacteria repellence [87], self-cleaning [49], heat transfer improvements [145], wear resistance [146] and/or anti-icing [147]. In markets with many competing products, customers are more likely to choose those that offer a better performance and integrate more functions while are still produced cost-effectively and hence are competitively priced. Therefore, the technologies for surface functionalisation are of great importance in many industrial sectors, e.g. in life sciences, transport, energy and other application areas. The two main approaches to obtain such functionalities involve the use of either chemical treatments or require the surface compositions and topographies to be modified.

The surfaces can be classified depending on their wetting behaviour, in particular water droplets can be used to judge whether a given surface is hydrophilic (the drops spread) or hydrophobic (the drop stay rounded) [27]. To measure the surfaces' wetting properties, different techniques can be used, i.e. rolling angle, drop bouncing and static contact angle (CA). The latter is the easiest and quickest way to assess the wetting behaviour. When the static contact angle is lower than  $90^{\circ}$ , the surface is considered hydrophilic while if it is higher - hydrophobic. Furthermore, when CA is higher than  $150^{\circ}$

the surface is considered super-hydrophobic[148,149]. Hydrophobic properties are often related to other phenomena, like self-cleaning [4] or anti-icing [150], that are of significant industrial interest. CA depends on the chemical compositions of liquids and surfaces that are in contact and also on surface topography/roughness [11,16,151]. The chemical compositions affect directly the surface energy of the three phases in contact, i.e. liquid, solid and air, and water droplets always take a shape that minimise it. At the same time, the contact angle between liquids and solids is affected by the surface roughness. If the roughness is sufficiently high air trapping between the liquid and the solid can occur that results in super-hydrophobic properties [152]. This is known as Cassie-Baxter state where topographies act as small air pockets to decrease the contact area between solids and liquids and thus lead to super-hydrophobicity. The effective CA when air is trapped between the drop and the solid can be calculated using Cassie-Baxter equation:

$$\cos \theta_{Cassie-Baxter} = \varphi \frac{\sigma_{SV} - \sigma_{SL}}{\sigma_{LV}} - (1 - \varphi) \quad (3.1)$$

where:  $\varphi$  is the area fraction of the water-solid area to the projected area between a drop and a surface; and  $\sigma_{ij}$  - the surface tensions between the three interfaces, where ij are liquid-vapour (LV), solid-liquid (SL) or solid-vapour (SV) interfaces.

Processes employing chemical interactions with the substrate, such as chemical etching [153] or surface coatings [154], are widely applied by industry to obtain the desired surface properties. However, the use of chemical compounds results in wastes that are not environmentally friendly and require post processing to eliminate or manage them. Additionally, the chemicals can be applied only in special working areas as they can be hazardous to the workers.

While coatings are essentially applied to modify the surface tension, the wetting properties can be also changed by increasing the effective surface roughness, as shown in Eq. 3.1. To engineer such micro topographies on surfaces and thus to improve their wetting behaviour, several technologies have been used successfully, e.g. photolithography [20], vertically aligned carbon nanotubes [155], electron-beam lithography [22], etc. However, these are multi-step complex processes that are usually difficult to scale up cost effectively to meet the requirements of many applications. Therefore, laser processing of surfaces has attracted a significant industrial interest as it offers a cost effective alternative in terms of efficiency and flexibility.

Also, hybrid processes were developed where both laser patterning and chemical etching were utilised. First, lasers were used to modify the roughness and then organic compounds were applied to change the surface energy and thus to produce surfaces with hydrophobic properties [15,55,113,115].

Ultra-short pulsed lasers were utilised to create patterns on various metallic surfaces and thus to change their wetting behaviours without the use of any chemical processes or coatings. Hydrophobicity was successfully obtained on different metals, such as stainless steel [118], titanium alloys [156], aluminium [119], copper [120] or nickel [116] through direct laser patterning with pico- and femto-second lasers.

The long processing times and high investment associated with the use of ultra-short lasers are a major limiting factor for the take up of this technology by industry. Therefore, near infrared (NIR) nanosecond lasers have attracted a significant interest as a cost-effective texturing route, especially to achieve relatively low processing time while the investment required is also low. The use of nano-second lasers to obtain

hydrophobic surfaces on different metallic substrates has been reported, e.g. on aluminium alloys [121,122,157], stainless steel [158], copper and brass [159].

One of the major concerns when functionalising surfaces is their durability. If coatings are used due to wear or chemical interactions with surrounding environments the surface properties degrade and ultimately disappear over time. Consequently, the products' lifespans are reduced and also it may be necessary the coatings to be re-applied to recover the desired properties. The effect is similar on surfaces with functional topographies, where wear and scratches modify them [106,130,160] and ultimately again the properties are lost over time. Thus, the use of hard, wear resistant materials is becoming an important prerequisite to increase the lifespan of functionalised surfaces.

Low temperature plasma surface alloying is a process used to increase surface hardness of metals [137]. Materials are hardened by diffusing atoms into surfaces to create interstitial supersaturated solid solutions that form thin layers of hardened material with up to 30  $\mu\text{m}$  thickness. As the surfaces tend to expand while part's bulks are not affected, the hardened layers are stressed, in particular the surfaces are compressed and their hardness increases to up to 1500 HV. Low temperature plasma surface alloying has been successfully reported on several materials, e.g. Fe-Cr, Co-Cr [138] or Ni-Cr alloys [137], austenitic stainless steel [140], FeAl<sub>40</sub> iron aluminide [142] or ferritic stainless steel [141]. Different gas mixtures are widely used during the treatment, and depending on their composition the interstitials on surfaces are C or N.

The research reported in this paper presents a laser patterning method for producing surfaces with dual scale topographies on ferritic stainless steel plates hardened by low temperature plasma surface alloying. In particular, a nanosecond laser is used to

produce channels and cell-like surface structures on plasma treated surfaces and thus to obtain super-hydrophobic properties. The next section describes the experimental setup used in this research. Then, the results are presented and discussed and conclusions are made about the proposed approach that combines surface engineering with laser patterning to functionalise stainless steel surfaces.

## **3.2 Materials and Methods**

### **3.2.1 Sample preparation**

Ferritic stainless steel X6Cr17 plates with size of 50x50 mm and thickness of 0.7 mm were used in the experiments. The plates were grinded before the plasma treatments (1200 grit size) to remove surface contaminants and oxide layers. DC plasma carburising and nitriding processes were carried out in an adapted DC Klöckner Lonon 40 kVA plasma furnace. Any residual thin surface oxide films were removed by plasma sputtering to enable atomic diffusion into the surface. Samples were treated for 20 hours at 400°C in a gas pressure of 3 mbars and gas mixtures of 1.5% CH<sub>4</sub>: 98.5% H<sub>2</sub> and 25% N<sub>2</sub>: 75% H<sub>2</sub> for carburised and nitrided samples, respectively. Afterwards, all plates were cleaned in an ultrasonic bath with ethanol.

The depth of the treatment was determined using glow-discharge optical emission spectroscopy (GDOES) in Spectruma GDA 650HR analyser. Fig. 3.1 shows the chemical composition of the samples vs the depth after the plasma treatments. The depth of the hardened layer for the nitrided samples (25 µm) is higher than that obtained on the

carburised ones (1  $\mu\text{m}$ ). Also, the mass concentration of alloying elements on surfaces is 12.9% of C and 39.8% of N on carburised and nitrided samples, respectively.

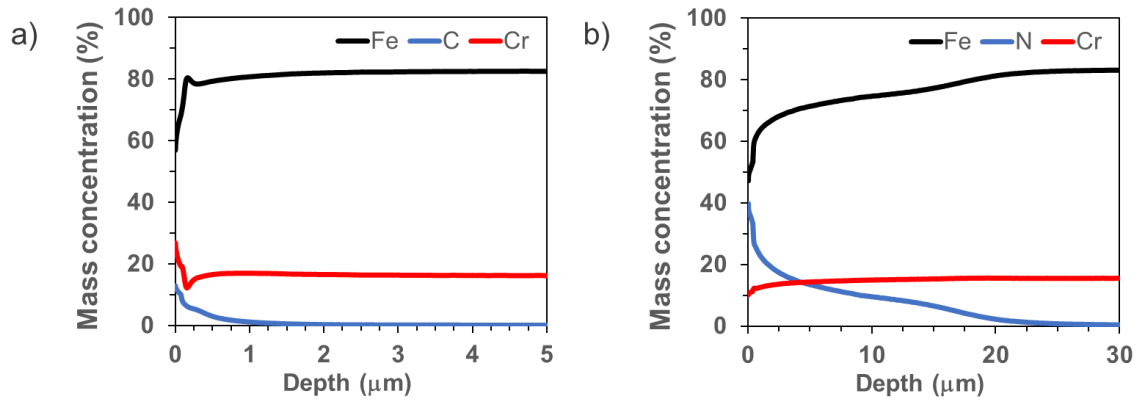


**Fig 3.1.** Mass concentration of the plasma carburised (a) and nitrided (b) samples vs the depth from the surface.

A Mitutoyo MVK-H1 micro-hardness tester fitted with a diamond Vicker's indenter and a load of 500 g was employed to measure the hardness of the surfaces before and after the plasma alloying process. The hardness of as-received ferritic stainless steel plates was 172 HV and 305 and 1001 HV for the carburised and nitrided samples, respectively. The roughness was measured using an Alicona G5 focus variation microscope (x100 lens). The roughness of as-received stainless steel plates was Ra 49.4 nm and respectively 39.3 nm and 149.5 nm for the grinded carburised and nitrided plates.

### 3.2.2 Laser processing

The samples were patterned using a laser micromachining system. The system integrates a MOPA-based Yb-doped fibre nanosecond (ns) laser source (SPI G4 50W HS-

S) with a maximum average power (P) of 50 W and wavelength of 1064 nm ( $\lambda$ ), and 100 mm telecentric lens to achieve a beam spot diameter of 35  $\mu\text{m}$ . The movements of the laser beam are CNC controlled and they are performed with a 3D scan head (RhoThor RTA) with maximum scanning speed of 2.5 m/s.

Two different pulse durations were used in the experiments, 15 and 220 ns, and laser parameters were adjusted to irradiate the processed surfaces with the same energy per line. The process setting for all samples produced with the two pulse lengths were as follows:

- 220 ns: a scanning speed of 150 mm/s, pulse frequency of 70 kHz and pulse energy of 50.14  $\mu\text{J}$ ;
- 15 ns: a scanning speed of 132 mm/s, pulse frequency of 100 kHz and pulse energy of 30.89  $\mu\text{J}$ .

The energy per line, E, was calculated as follows:

$$E = \frac{E_p f}{S} = \frac{E_p}{PD} \quad (3.2)$$

where:  $E_p$  is the pulse energy [ $\mu\text{J}$ ]; f - the pulse frequency; PD - the pulse distance [ $\mu\text{m}$ ]; S - the scanning speed [mm/s]. By using Eq. 3.2 E was maintained the same for both pulse durations, in particular 24.4  $\mu\text{J}/\mu\text{m}$ .

Two patterns were produced by changing the scanning strategies, in particular one with parallel lines/channels along the surface and the other with two intersecting lines at 90° to produce cell-like structures. The step over distance between two consecutive lines (hatch) was 100  $\mu\text{m}$  for all samples.

All plates were cleaned with compressed air after the laser patterning to remove any debris. No chemicals or alcohols were used to avoid the contamination of the patterned areas with organics that can affect the surface energy and thus the wetting properties.

### **3.2.3 Characterization techniques**

An Alicona G5 focus variation (FV) microscope was used to capture the 3D topographies of the produced patterns and thus to analyse the achieved ablation depths and also the volumes of redeposited material. Three samples were manufactured for each set of laser parameters and 9 measurements per sample were taken in order to have enough data to calculate the ablation depths and widths of the channels.

Micrographs of the patterned surfaces together with their chemical compositions were obtained using a Hitachi TM 3030 Plus Scanning Electron microscope with an integrated Energy Dispersive X-Ray (EDX) spectrometer Quantax70. The wetting properties were analysed using a sessile drop technique employing an optical CA measurement system (Attension Biolin Scientific Theta T2000-Basic+) based in a liquid dispenser with an integrated camera. 6  $\mu$ l drops of Milli-Q water were used in all measurements under ambient conditions. Static contact angles and rolling angles were measured.

Samples were cut and polished to mirror finish to perform hardness measurements at different depths from the processed surface. The measurements were performed on a NanoTest Vantage nano indenter (Micro Materials Ltd).

To test the abrasion resistance of the produced samples, a polisher device that integrates a Buehler Vector Power Head and a Buehler Phoenix Alpha grinder-polisher have been employed. Silicon carbide sandpapers, Buehler CarbiMet 600 (P1200), were

used as an abrasive with an average grain diameter bigger than the patterns, in particular 15.3  $\mu\text{m}$ , to study the samples' wear resistance. The rotation speeds of the grinder and the head were set at 150 rev/sec and 60 rev/sec respectively, while the load applied was 1.36 kg for 20 seconds and water was used to assist the process and remove the generated debris in the test. The samples were cut prior to the abrasion test in order to have the same surface area of 325  $\text{mm}^2$  and thus to apply the same pressure on all of them. The topographies of the patterns were captured before and after the tests by using an Alicona G5 Focus Variation Microscope, and the depth of the patterns was measured and the volume of the removed material was assessed, too.

### **3.3 Results and discussion**

#### **3.3.1 Ablation threshold**

Prior to the laser patterning, ablation thresholds of as-received and the plasma treated plates were calculated using Liu's method [161]. The ablation thresholds were higher when the pulse duration of 220 ns was used in comparison with those obtained with 15 ns pulses as shown in Table 3.1. In addition, the ablation thresholds were higher after the plasma alloying both on carburised and nitrided plates.

Ablation thresholds (J/cm<sup>2</sup>)

	220 ns	15 ns
<i>Stainless steel</i>	3.98	2.23
<i>Nitrided</i>	5.25	2.38
<i>Carburised</i>	4.95	2.67

**Table 3.1.** Ablation thresholds of as-received, carburised and nitrided samples obtained with pulse durations of 220 ns and 15 ns.

### 3.3.2 Microstructure analysis

Channels and cell-like structures were produced on as-received and plasma treated stainless steel plates by laser patterning, and their topographies were analysed employing a FV microscope. As the laser processing was carried out with pulses in the nano-second range, the ablation was followed by plasma expansion, ejection and re-deposition of molten material along the laser beam path. This led to the formation of dual scale patterns on surfaces, i.e. channels/cells produced by ablation and bulges around them resulting from the re-deposited molten material as shown in Fig. 3.2a-b. Fig. 3.2c shows a cross section of the produced structures. As the step-over distance between the lines was the same during the laser patterning both with channels and cells, only two geometrical parameters were studied, the ablation depth (D) and the height of the solidified material (H). Multiple measurements on surfaces were taken to calculate the average values of H and D.

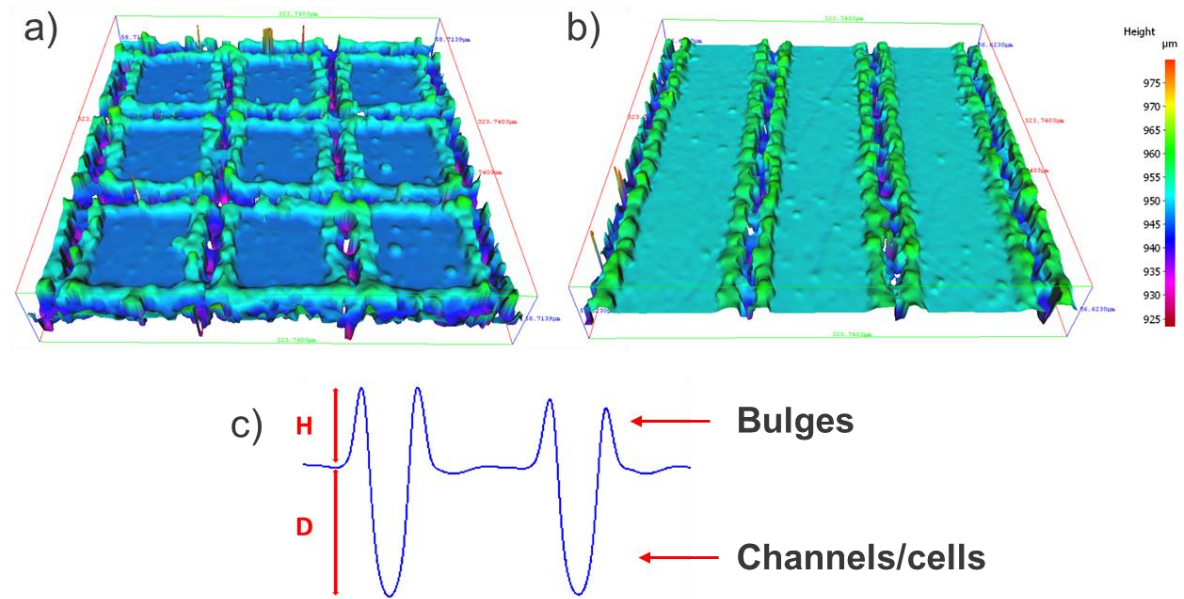


**Fig 3.2.** 3D topography of a cell-like pattern (a) and 3D topography of a channel like pattern (b), on an area of 323x323  $\mu\text{m}$ ; (c) cross-section of the 3D patterns, showing the height of redeposited material (H) and depth of ablation (D).

The D and H values obtained after laser patterning are given in Fig. 3.3. As can be seen the results obtained on as-received and plasma carburised samples are very similar, while those on the nitrided ones are different. The similarities between as-received and carburised samples can be attributed to the very small thickness of the hardened layer obtained with C, only 1  $\mu\text{m}$ . As D of channels and cells are in the range from 4.07 to 8.83  $\mu\text{m}$ , the hardened layer was removed with the first pulses and then the following pulses ablated the bulk of the stainless steel plates. In the case of the plasma nitrided samples, the thickness of the hardened layer is much higher, 25  $\mu\text{m}$ , and therefore the bulk of the plates was not reached as D achieved with both pulse lengths were from 4.46 to 6.05  $\mu\text{m}$ .

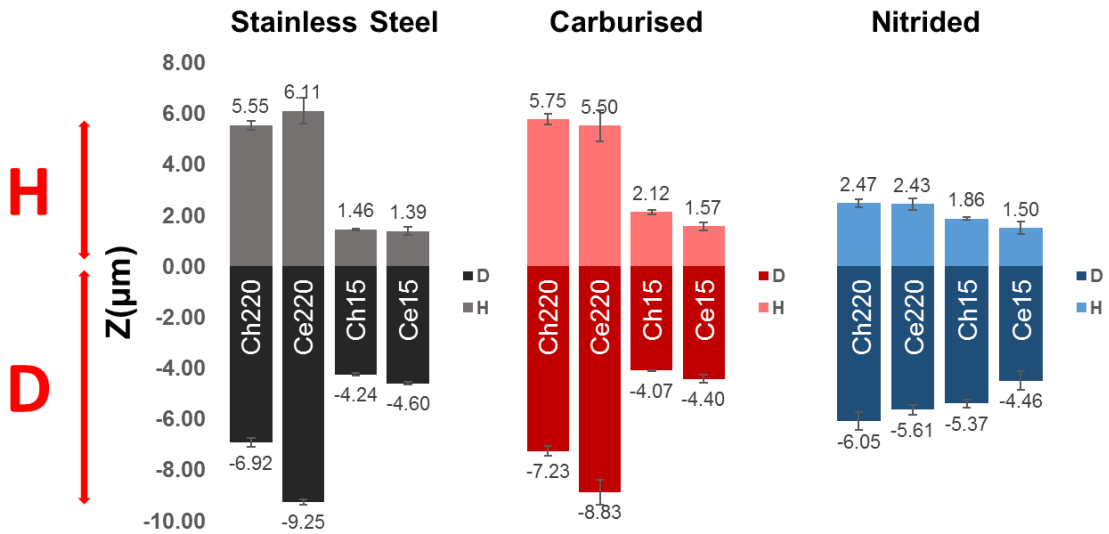


**Fig 3.3.** Ablation depths (*D*) and heights of bulges (*H*) for as-received and plasma treated samples.

**Note:** *Ch* or *Ce* denote samples with channels or cells, respectively, while *15* or *220* - the pulse length used for their patterning. For instance, the sample denoted as Ce220-Carburised would mean a cell-like pattern produced with a pulse length of 220 ns on a plasma carburised plate.

As can be expected the patterns produced with 220 ns pulses are deeper than those produced with 15 ns, due to the higher heat diffusion and subsequently the ejection and re-deposition of a bigger volume of molten material. Thus, the bulges resulting from the longer pulses are bigger and also the channels are deeper but the defences are less pronounced on nitride samples. On all samples the ablated volumes are in line with the ablation thresholds of as received and plasma treated stainless steel plates. In particular, the deeper patterns were produced with the longer pulses on the as-received and

carburised plates as their ablation threshold were lower. Regarding the patterns produced with 15 ns pulses they had a similar depth as this is in line with the similar ablation thresholds of the three different types of plates investigated in this research.

The cell-like patterns are deeper than the channel-like ones on as-received and plasma carburised samples. In Fig. 3.3, the plotted depths for the cell-like patterns were measured along the lines only in order to compare the results with those obtained for the channel-like patterns. The depth at the intersections was measured, too and as expected it was almost twice higher, in particular the depths obtained with 220 and 15 ns pulses were 18.63  $\mu\text{m}$  and 8.51  $\mu\text{m}$  and 22.73  $\mu\text{m}$  and 10.42  $\mu\text{m}$  for as-received and plasma carburised samples, respectively. This can be explained with the twice high number of scans in the intersections and associated with the heat accumulation in producing the cell-like patterns. However, this response was not observed on plasma nitrided samples, especially the depths obtained were 11.65  $\mu\text{m}$  and 12.01  $\mu\text{m}$ , respectively, and this could be explained with the recast formations that led to shallower and narrower channels and cells.

The SEM micrographs of the patterns produced on the three different types of plates investigated in this research are given in Fig. 3.4. In particular, one channel is shown or in the case of cell-like patterns the intersection between two lines is depicted where the effect of the heat accumulation is more pronounced. It can be observed that for all surfaces patterned with 220 ns pulses there is a higher volume of re-deposited material along the laser paths (see Fig. 3.3). In addition to the ejected material as a result of the plasma expansion, the dynamic effects of consecutive pulses reaching the surface contributed to the higher volume of re-deposited material. Especially, the trains of 220 ns pulses led to a higher agglomeration of solidified metal and also to the formation of

thick and non-homogeneous structures with solidified drops on top. At the same time, when the patterning was performed with 15 ns pulses, the dynamic effects were much less pronounced and the resulting patterns were more homogeneous and uniform. Contrary to longer pulses, the effect of each 15 ns pulse can be seen and also the result of the overlap of consecutive pulses.

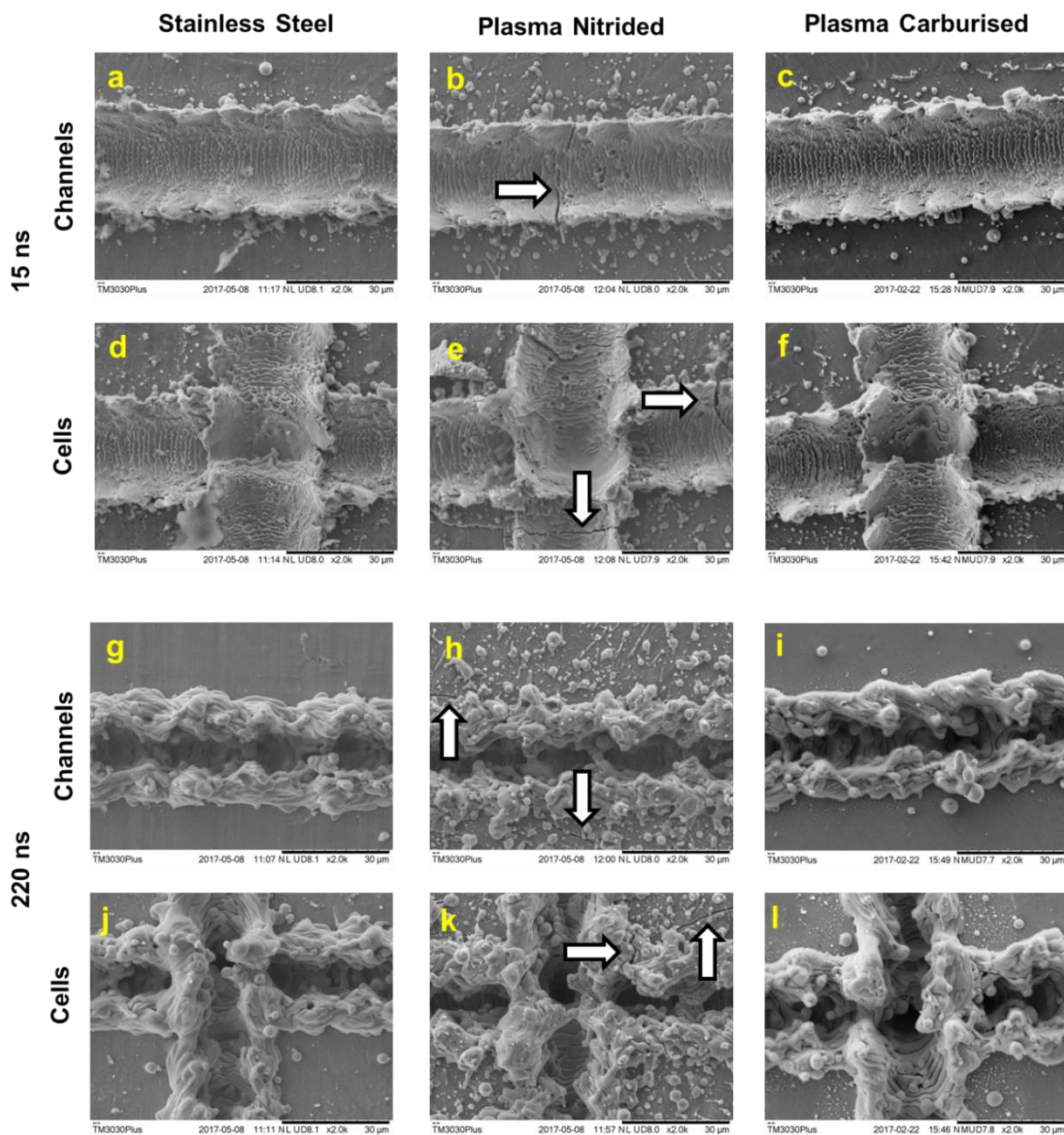


**Fig 3.4.** SEM micrographs of stainless steel and plasma treated samples patterned with 15 and 220 ns pulses. Cracks produced on the nitrided surfaces are pointed out with white arrows.

Surface quality obtained on plasma nitrided samples is slightly different, especially the splashes along the beam path are bigger and this is more pronounced when longer pulses were used. Also, cracks can be seen along the beam path and they are pointed out with arrows in Fig. 3.4. The presence of cracks can be explained with the plasma hardening and laser patterning mechanisms. As discussed above, during the plasma nitriding process a high concentration of the alloying element, N, is diffused in the material and leads to a hardness increase due to solid solution hardening mechanism. Then, when the surface is laser patterned, the highly nitrogen containing surface was abraded and the re-deposition material was radically solidified and/or self-quenched. As a consequence the re-deposited material becomes cracked in the surroundings of the processed area under the combined effects of the tensile stress caused by the rapid solidification and the brittle nature of quenched high-nitrogen steel. This is supported by the observation that the appearance of cracks was observed only on plasma nitrided samples mainly due to the mass concentration of the alloying element, N.

### **3.3.3 Chemical analysis**

Chemical compositions of the processed samples were analysed employing EDX spectrometry. The normalised elementary composition of the surfaces, calculated in weight, is shown in Table 3.2. The measurements were carried out on as-received and plasma treated samples after the laser patterning while the compositions of non-patterned surfaces were used as references.

	Stainless steel			Plasma carburised			Plasma nitrided		
	220 ns	15 ns	Ref	220 ns	15 ns	Ref	220 ns	15 ns	Ref
Fe	71.8	69.9	79.2	69.4	66.9	72.7	71.3	64.1	72.6
C	6.7	5.9	4.0	9.1	9.3	11.4	4.6	7.5	2.9
O	6.2	8.8	0.2	6.6	9.2	1.0	4.4	10.8	0.2
Cr	13.5	13.2	14.7	13.2	12.7	13.4	13.2	11.9	13.0
N	1.4	1.8	1.7	1.4	1.7	1.3	6.2	5.3	11.1
Mn	0.6	0.4	0.2	0.5	0.4	0.2	0.5	0.5	0.3

**Table 3.2.** Normalised chemical composition in weight (%) of stainless steel and plasma treated samples without (the reference one) and after laser patterning with 220 ns and 15 ns pulse durations.

As expected, an increase of the alloying element was found after the plasma treatments, in particular the amount of carbon and nitrogen increased from 4.0% to 11.4% and from 1.7% to 11.1% on plasma carburised and nitrided samples, respectively. At the same time the amount of other elements remained the same and there were no traces of oxidation after the plasma treatment.

However, the oxygen content increased after laser patterning on all samples. This can be easily explained with the steel melting and solidification during the laser patterning that result in iron reacting with the oxygen present in air to form oxides along the beam path. The oxygen content was higher on the plates patterned with 15 ns pulses, most likely due to the higher patterns' depth achieved with 220 ns pulses that impeded the oxygen measurement at the bottom of the channels.

The amount of nitrogen detected on plasma nitrided samples was lower after the laser patterning and this can be attributed to the release of nitrogen in the processed area

and/or some diffusion in the bulk due to the thermal load. On the contrary, the content of carbon on plasma carburised samples remained the same. This suggests a higher stability to thermal loads present in nanosecond laser patterning.

### **3.3.4 Wettability**

Static CA measurements were performed to assess the wettability of the patterned surfaces with a droplet size of 6  $\mu\text{l}$ . The wetting behaviour of the surfaces prior to laser patterning were measured, too and the results were used as a reference. The measurement showed that they did not have super-hydrophobic properties, in particular CA of as-received, carburised and nitride surfaces were  $78.9 \pm 1^\circ$ ,  $84.3 \pm 6^\circ$  and  $101.4 \pm 1^\circ$ , respectively.

It is widely reported that laser patterned metallic surfaces show hydrophilicity just after the processing and with time CA increases until the surface is stabilized. The topographies remain the same and therefore any CA changes are attributed to surface chemistry, especially to the oxidation states of the processed surfaces [159] and the absorption of organic compounds from the air, due to the high porosity of the oxidised surfaces [25].

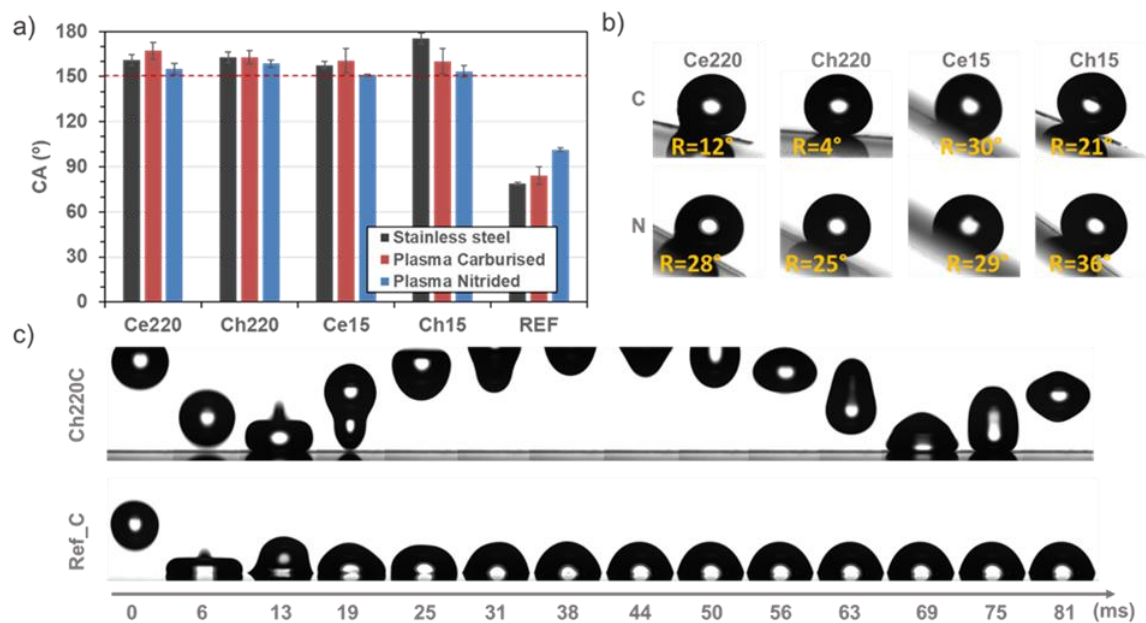


**Fig 3.5.** (a) Stabilized CA of laser patterned and reference surfaces. The dashed red line indicates the transition from hydrophobic to super-hydrophobic (CA higher than 150°). (b) Sliding angles for the plasma carburised and nitrided samples after laser patterning. (c) Examples of water drops bouncing on plasma carburised stainless steel before (Ref\_C) and after laser patterning.

All samples were highly hydrophilic just after the laser patterning. The water spread over the surface and therefore it was not possible to measure CA. Samples were analysed again after 10 days and then all of them were super-hydrophobic with CA higher than 150°, as shown in Fig. 3.5a. As can be judged from the figure there was no significant difference in wetting behaviours of laser patterned as-received and plasma treated plates.

Drops on patterned areas did roll out when the samples were tilted, both on plasma nitrided and plasma carburised surfaces, as shown in Fig. 3.5b. Rolling angles were

smaller for the samples patterned with 220 ns pulses, especially on the plasma carburised samples due to the patterns' higher aspect ratio. The impact of water drops was analysed, too, by employing a high speed camera at 160 frames per second. An example of a drop bouncing on a plasma carburised sample is provided in Fig. 3.5c. It can be clearly seen in the figure that drops bounced several times only on the sample with the channel-like pattern.

Thus, it could be assumed that the Cassie Baxter state was achieved and water drops did not spread into the channels/cells. This phenomenon can be attributed to the hydrophilic iron oxides formed after the patterning that are porous and absorb organics from the air. Then, as a result, the patterned surfaces become non-polar [157] and in combination with the air pockets in the channels/cells they repel the water.

### **3.3.5 Hardness**

The effects of heat dissipation on stability of the hardened layer were investigated. In particular, hardness measurements at different depths were performed with a nano-indenter on plasma treated surfaces after the laser patterning. After cutting the samples and polishing their cross section, the surface integrity was analysed with an optical microscope.

As it was already noted in Fig. 3.4, all nitrided surfaces were covered with cracks after the laser patterning, due to the high concentration of stresses on treated surfaces. This led to delamination of the nitrided layer and hence the loss of the surface properties. In the case of laser processing with shorter pulses (15 ns), the nitrided layer was

significantly damaged after cutting the sample (see Fig. 3.6b), while the layer was fully removed in the case of 220 ns pulses (see Fig. 3.6a).

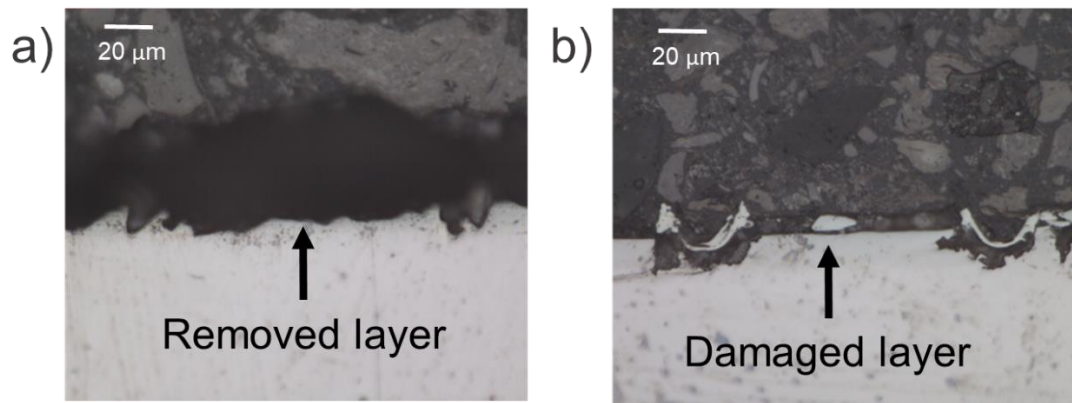


**Fig 3.6.** Cross-sections of the plasma nitrided samples after laser patterning with 220 ns (a) and 15 ns (b) pulses.

On the contrary, hardened layers on plasma carburised samples remained after laser patterning and there were no signs of any damage. Three different samples for each of the two considered pulse durations were analysed and typical micrographs of studied cross sections are given in Fig. 3.7. Channels produced with 220 ns and 15 ns pulse durations are shown in Fig. 3.7a and Fig. 3.7b, respectively. The volume of redeposited material and the height of the bulges produced with the longer pulses were bigger. However, at the same time the hardness was similar and there were no other noticeable differences on the patterns produced with the two pulse durations considered in this research.

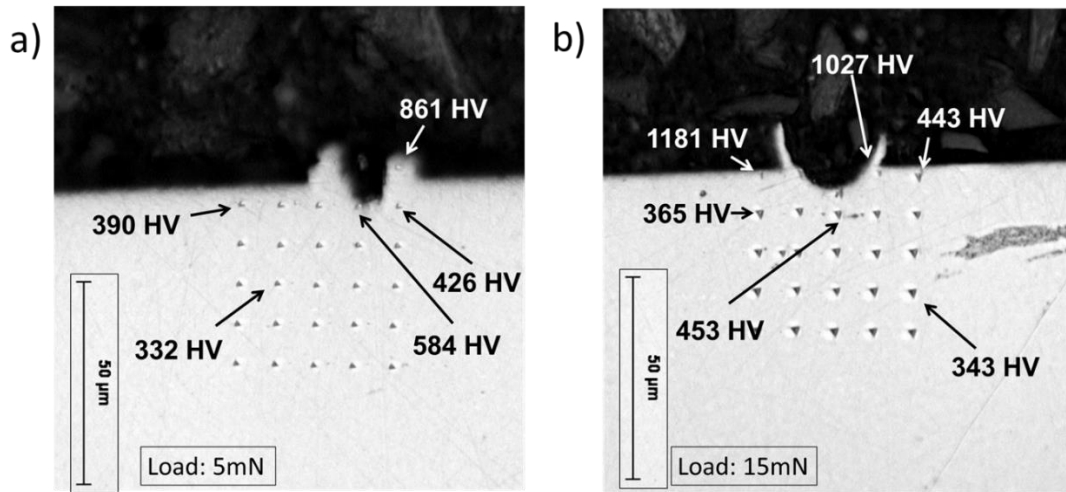


**Fig 3.7.** Cross sections of the channels produced with 220 ns (a) and 15 ns (b) pulse durations on plasma carburised samples with nano indentations at different depth from the processed surface.

The examination of both cross sections shows that the hardness close to the bottom of the channels is higher, approximately 600 HV, and it is gradually reduced to reach 300 HV away from the patterns that are the hardness values achieved after the plasma treatment.

The hardness of the bulges and their surroundings were also measured and the obtained values were higher than 800 HV as shown in Fig. 3.7a. This higher hardness can be explained by the thin carburised layer formed during the plasma treatment. It was also possible to measure the thin hardened layer on the patterns produced with the shorter pulses and values higher than 1100 HV was obtained, see Fig. 3.7b. This very high hardness value can be attributed to the thin carburised layer and the formation of martensite due to rapid self-cooling or quenching. The increased hardness of laser patterned areas can be explained with the heat dissipation into the bulk and the follow up self-cooling and quenching during the nanosecond laser-material interactions. At the

same time should be stated that the heat affected zone is small and the thermal load does not modify the properties of the hardened layer.

### **3.3.6 Abrasion test**

As discussed, the plasma nitrided surfaces had cracks after the laser patterning, and also the hardened layer delaminated. Therefore, the wear resistance of only as-received and plasma carburised samples were analysed and compared after channel-like patterning with the same pulse duration of 15 ns. In particular, both samples underwent the same abrasion tests, especially the same time and conditions were used, and also the topographies were analysed before and after the tests as shown in Fig. 3.8. It can be seen in the figure that in both cases the recasts were removed after the abrasion tests as they were mainly formed of brittle oxides. However, there was a significant difference in the depth of the channels, especially 41% and 18% reductions on as-received and plasma carburised samples, respectively, and hence there was a much higher loss of the patterns' depth on the as-received sample.

The static CA was measured after the abrasion tests, too, and they were  $121.7 \pm 1^\circ$  and  $138.5 \pm 1^\circ$  for the as-received and plasma carburised samples, respectively. This difference can be attributed to the smaller loss of channels' depth and also the remaining presence of carbon into the surface as the depth reduction after the abrasion test was smaller than the depth of the carbon diffusion shown in Fig. 3.1.

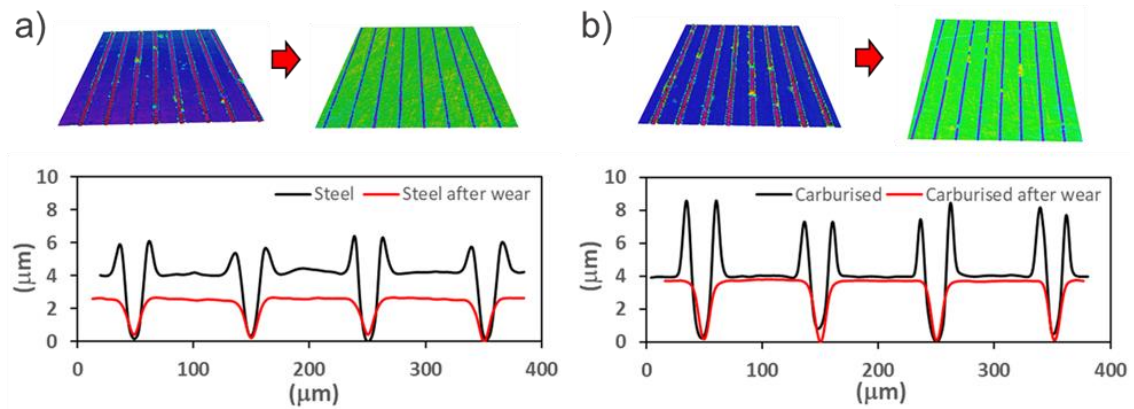


**Fig 3.8.** The topography and cross-sections of stainless steel (a) and plasma carburised (b) samples with channel-like patterns produced with 15 ns laser, before and after the abrasion test.

### 3.4 Conclusions

The combined effects of plasma surface alloying and nanosecond laser patterning on surface properties of stainless steel plates were studied in this paper. A laser patterning method was investigated for producing surfaces with dual scale topographies on ferritic stainless steel plates hardened by low temperature plasma surface alloying. The combined surface engineering and laser patterning approach allowed super-hydrophobic surfaces to be produced on both nitrided and carburised stainless steel plates with effective contact angles higher than  $150^{\circ}$ . However, the nitrided samples exhibited cracks on the surfaces that led to delamination of the harden layer after the laser patterning. On the contrary, hardened layers on plasma carburised samples remained intact after the laser patterning. The results showed that by applying the proposed combined surface engineering - laser patterning approach it is possible to retain the higher hardness of the carburised stainless steel plates and at the same time

to functionalise them and obtain super-hydrophobic properties. It was shown that the plasma carburised samples experienced much less wear compared with the as-received stainless steel substrates. Potentially, these combined effects can address one of the major concerns in functionalising stainless steel surfaces, in particular their resistance to wear and scratching. The future research will be focused on investigations of tribological properties such functionalised surfaces in the context of specific application in consumer products, automotive and tool making industries.

## **Acknowledgements**

The research reported in this paper was carried out within the framework of European Commission H2020 ITN programme “European ESRs Network on Short Pulsed Laser Micro/Nanostructuring of Surfaces for Improved Functional Applications” ([www.laser4fun.eu](http://www.laser4fun.eu)) under the Marie Skłodowska-Curie grant agreement No. 675063. In addition, the work was supported by two other H2020 FoF programmes, i.e. the projects on “Modular laser based additive manufacturing platform for large scale industrial applications” (MAESTRO) and “High-Impact Injection Moulding Platform for mass-production of 3D and/or large micro-structured surfaces with Antimicrobial, Self-cleaning, Anti-scratch, Anti-squeak and Aesthetic functionalities” (HIMALAIA).

# Chapter 4

---

## **Durability and wear resistance of laser-textured hardened stainless steel surfaces with hydrophobic properties**

---

*A. Garcia-Giron<sup>1,\*</sup>, J. M. Romano<sup>1</sup>, A. Batal<sup>1</sup>, B. Dashtbozorg<sup>2</sup>, H. Dong<sup>2</sup>, E. Martinez Solanas<sup>3,4</sup>, D. Urrutia Angos<sup>3,4</sup>, M. Walker<sup>5</sup>, P. Penchev<sup>1</sup> and S.S. Dimov<sup>1</sup>*

*<sup>1</sup>Department of Mechanical Engineering, School of Engineering, University of Birmingham, Edgbaston, Birmingham, B15 2TT, UK*

*<sup>2</sup>School of Metallurgy and Materials, University of Birmingham, Edgbaston, Birmingham, B15 2SF, UK*

*<sup>3</sup>ATRIA Innovation, C/Alaún 14, nave 5, 50197, Zaragoza, Spain*

*<sup>4</sup>Center for Corporate Technology and Innovation Spain, BSH Electrodomésticos España, S.A, Av. de la Industria 49, 50016 Zaragoza, Spain*

*<sup>5</sup>Department of Physics, University of Warwick, Coventry CV4 7AL, UK*

A preliminary study about the durability of the hardened and laser patterned stainless steel plates was performed on the first paper, however, a more detailed test was required in order to determine whether the dual process increased the lifespan of the functional surfaces.

It is worth noting that there is not a standard method to measure and quantify the wear resistance of functional patterns and, as mentioned in Chapter 2, each research group uses their home made setup to perform durability tests. Automatization is very important in order to avoid uncertainties due to human errors during the measurements, such as pressure variations applied on the tested samples, or moving speed, if the tests are done by moving the samples manually. For this reason, an abrasion and washability tester was used to perform all the experiments. This device is designed following the standards given by the ISO 11998:2006 – “Paints and varnishes – Determination of wet-scrub resistance and cleanability of samples”, and the one used for this experiments is placed in the B/S/H/ Home Appliances Group facilities. They use this setup to study the durability of functional coatings and mimic the cleaning process on kitchen surfaces and home appliances. A soft cleaning cloth is used to perform the aforementioned tests, however, it was observed that the affect on the laser patterned surfaces with conventional soft cloths was negligible, and after 3000 reciprocating cycles the erosion in the patterns was minimal. Furthermore, the time consumed to perform 3000 cycles was 81 minutes, and due to the large number of samples needed to erode.

Thus, a more abrasive counterpart was selected, in this case a heavy duty scouring pad (Scotch-Brite™) in order to reduce the time consumed to perform the abrasion tests. Nevertheless, the abrasion yield was increased, and the patterns were fully removed after 400 cycles. Due to this, a maximum of 300 cycles was chosen for the experiments, and measurements were taken each 100 cycles in order to be able to observe the behaviour of the patterned surfaces during the abrasion.

Once the abrasion was carried out in the samples, topographies of the patterns were taken and static contact angle measurements were done, in order to study the links between functional response and remaining topography.

Furthermore, chemical analysis were performed in some samples, to analyse the potential contamination of the surfaces from the counterparts and observe the influence of surface contaminants on the functional response. It was not possible to study all the samples, as the XPS analysis is very expensive and the data post processing and study is very time consuming, however, measurements were performed in the most representative surfaces, to observe differences between carburised and as received stainless steel, before the laser patterning, just after the laser processing (When surfaces are hydrophilic), some weeks after the laser patterning (When surfaces are hydrophobic) and after 300 wear cycles.

This research was published as a full length article in Langmuir (2019) [163].

**Authors' contributions:** A. Garcia-Giron is the main author of this publication. He performed the laser processing, wear tests and characterization of the samples. B. Dashtbozorg manufactured the plasma carburised plates. J. M. Romano and A. Batal assisted during the manufacturing of the samples and characterization. E. Martinez Solanas and D. Urrutia Angos helped with the wear tests. M. Walker performed the XPS chemical analysis and helped with the analysis of the obtained data. A. Garcia-Giron wrote the manuscript that was posteriorly revised by H. Dong, P. Penchev and S.S. Dimov.

**Keywords:** Laser patterning; nanosecond laser; hydrophobicity; plasma surface alloying; wear resistance; surface engineering.

## **Abstract**

Hydrophobic surfaces are of high interest to industry. While surface functionalization has attracted a significant interest, both from industry and research, the durability of engineered surfaces remains a challenge, as wear and scratches deteriorate their functional response. In this work, a cost-effective combination of surface engineering processes on stainless steel was investigated. Low temperature plasma surface alloying was applied to increase surface hardness from 172 to 305 HV. Then, near-infrared nanosecond laser patterning was deployed to fabricate channel-like patterns that enabled superhydrophobicity. Abrasion tests were carried out to examine the durability of such engineered surfaces during daily use. In particular, the evolution of surface topographies, chemical composition and water contact angle with increasing abrasion cycles were studied. Hydrophobicity deteriorated progressively on both hardened and

raw stainless steel samples, suggesting that the major contributing factor to hydrophobicity was the surface chemical composition. At the same time, the samples with increased surface hardness exhibited a slower deterioration of their topographies when compared with non-treated surfaces. A conclusion is made about the durability of laser-textured hardened stainless steel surfaces produced by applying the proposed combined surface engineering approach.

## **4.1 Introduction**

Surface functionalization technologies have attracted a significant industrial interest due to the wide range of properties that can be created on the surface. By applying chemical coatings or by modifying surface topographies at micron or sub-micron scales, surface properties can be enhanced, modified or even new ones introduced to products. For example, anti-bacterial [164], hydrophobicity [149], tribological [130] or anti-icing [14] are some of the properties that can be achieved when using such techniques.

The term wettability refers to the way a surface responds to the interaction with a liquid. In particular, when water is the liquid, the surface can be classified as hydrophilic when droplets spreads, or hydrophobic if the droplets stays rounded or are repelled. Depending on the surface response to water droplets, different wetting states can be identified, i.e. (i) the hemi-wicking state is present when the droplets spread over the surface; (ii) the Wenzel state or the homogeneous wetting regime is present when the droplets can wet the “valleys” within the surface topographies but does not spread; and (iii) the Cassie-Baxter state or heterogeneous wetting regime, when there is air trapped between the droplets and the surface, and thus, the droplets do not wet the “valleys”

within the topographies [165]. Cassie-Baxter state often leads to high hydrophobicity. Water repellence is an important characteristic of hydrophobic surfaces that is closely related to corrosion resistance improvements, anti-icing, anti-fouling, liquid transportation or self-cleaning [4,33,49,150,166] properties. Thus, hydrophobicity is of great interest to a wide range of engineering applications, e.g. in aerospace, naval or home appliances industrial sectors, and also to many product development projects. Different metrics can be used to quantify wettability, i.e. rolling angle, drop bouncing, hysteresis measured with the advancing and receding contact angle, or static contact angle (SCA) measurements [167]. However, SCA is the metric that is the most commonly used due its simplicity. When SCA is smaller than 90° the surface is classified as hydrophilic, while when it is higher the surface is considered to be hydrophobic. SCA values equal or exceeding 150° are one of the main conditions for a give surface to be considered superhydrophobic [27,149], together with low roll-off angles[28]. SCA is the angle at which the liquid–vapor and solid-liquid interfaces meet.

In the case of a homogeneous wetting regime, i.e. the Wenzel state, the contact angle is calculated by using the following equation:

$$\cos \theta = r \frac{\sigma_{SV} - \sigma_{SL}}{\sigma_{LV}} \quad (4.1)$$

where:  $r$  is the ratio of true area of the solid surface to the apparent area; and  $\sigma_{SV}$ ,  $\sigma_{SL}$  and  $\sigma_{LV}$  are the surface tensions between solid-vapour, solid-liquid, and liquid-vapour interfaces, respectively, that are determined by the respective liquid, surface and air compositions.

When the surface is heterogeneous and the Wenzel model is not sufficient, the contact angle can be calculated using the Cassie-Baxter equation:

$$\cos \theta = f_1 \frac{\sigma_{SV} - \sigma_{SL}}{\sigma_{LV}} - f_2 \quad (4.2)$$

where:  $f_1$  and  $f_2$  are the area fractions of solid and air in contact with the liquid, respectively.

Based on Eq. 4.1 and Eq. 4.2, it could be inferred that the contact angle depends on two main factors, i.e. surface chemistry and topography. Thus, if the surface energy is assumed constant, a change in topography will always lead to a change of wetting properties.

Different methods have been employed to create hydrophobic surfaces, e.g. photolithography [20], electron-beam lithography [22] or chemical coatings [11,168,169]. Recently, laser processing has emerged as a viable alternative for producing hydrophobic surfaces with a potential for upscaling that is a very important factor for its broader use by industry. There are two main approaches for producing superhydrophobic surfaces through laser processing. First is a two stage process that involves laser patterning/texturing to change the surface topography, i.e. for creating channels [15,113,114], lotus-like patterns [55] or rose petal shapes [115], followed by a chemical non-polar coating to change the surface energy. The second approach employs only laser patterning and there are different alternatives for producing superhydrophobic surfaces depending on the scales of the generated topographies. Submicron patterns with different periodicities and distributions, like honeycomb [52] or linear [116], can be obtained by generating laser induced periodic surface structures (LIPSS). Whereas at the micro scale, direct laser interferences [117] or direct laser writing (DLW) can be deployed, with the latter being the most widely used method due to its simplicity, faster processing times and cost effectiveness; which comes as a result of the relatively low cost of nanosecond laser sources. DLW has been applied

successfully to produce superhydrophobic surfaces on a wide range of metals, e.g. aluminium [54,122], stainless steel [124] and brass or copper alloys [159].

It has been widely reported that metallic surfaces are hydrophilic initially, just after laser patterning, and then they become hydrophobic with time [28,118]. However, the mechanism of this wettability evolution in time (so called aging process) is not fully understood. Some studies suggest that the contact angle changes are the result of some partial deoxidation of the laser patterned surfaces [159], while others attribute this to the presence of induced non-polar molecules on surfaces, especially due to the adsorption of organic elements from air [126,162] and inhibition of water molecules deposition [127]. Nevertheless, surface topographies produced by laser patterning remain unaltered while the wettability evolves and thus the changes in contact angle must be influenced by surface chemistry, which can be also inferred from Eq. 4.1 and Eq. 4.2.

Irrespective of the processing method employed, a major concern is durability of the obtained surface functionality as a result of wear and scratches that could have a progressive detrimental effect on their properties [131]. Recently, several researchers have reported investigations into the mechanical durability of hydrophobic surfaces. In most of them the surface functional response was achieved by combining surface texturing with some chemical modifications [170–173]. Wang et al. developed a method to produce hierarchical micro-nanostructures on steel surfaces, where the microstructures behaved as a protection for the nanoscale roughness, and then a chemical etching with ultrasonic treatment was applied to modify them chemically [170,171]. Su et al. combined electrodeposition with heat-treatment in a chemical solution to fabricate cone-like microstructures on copper substrates [172].

Another approach was reported by She et al. [173], where electrodeposition followed by a chemical modification was used on magnesium alloys. Other researchers investigated laser microstructuring, especially femtosecond laser processing to create cone-like dual scale patterns on pristine metal plates [132] or surfaces with high roughness on aluminum alloys [133]. Moreover, nanosecond lasers were also employed to create hydrophobic surfaces with enhanced wear resistance by applying hydrophobic coating over channel-like patterns on stainless steel [61] or by inducing roughness on aluminum-magnesium alloyed surfaces [135]. A common aspect of all research referred to so far was that the surface topography was first modified and only then a chemical coating was applied to modify the surface energy. Particularly, patterning or other approaches were employed to create a topography or just to increase the surface roughness and thus to protect [134] and potentially to enable air trapping in the resulting topography.

However, despite the fact that hydrophobic surfaces can be produced by one-step DLW, their durability remains unstudied, especially with regards to the evolution of their topographies and respective properties due to wear and scratches. Specifically, water contact angles decrease drastically after scratching, touching or even after wetting the surfaces, due to topography changes and chemical contaminations that lead to surface tension modifications. The wear resistance of the substrate material is an important factor affecting the durability of any functionalized surface irrespective of its treatment by one-step DLW or just patterning as protection for a hydrophobic coating. Enhancing substrates physicochemical characteristics, e.g. hardness [136], before any surface functionalization step, seems a promising approach to increase their wear resistance.

In this research, the durability and wear resistance of hydrophobic patterns on untreated and plasma treated stainless steel [143] plates produced using an infrared nanosecond laser source is investigated. The impact of substrate hardness on wear resistance and durability of hydrophobic surfaces produced by one-step DLW is analysed. Specifically, rubbing tests were conducted and the topographical evolution and accompanying chemical composition changes were studied together with their effects on surface functionality. The results from wettability and chemical analyses are reported and discussed and conclusions are made.

## **4.2 Materials and methods**

### **4.2.1 Sample preparation**

Circular ferritic stainless steel X6Cr17 samples were cut with a diameter and thickness of 36 and 0.7 mm, respectively. After the cutting, all plates were ground and polished to remove any oxides and contaminants. Half of the plates were hardened by DC plasma carburising, i.e. by using an adapted DC Klöckner Ionon 40 kVA plasma furnace. Samples were freshly polished to remove any residual oxides on the surfaces and also to allow atomic diffusion during the hardening process. The carburising process was performed for 20 hours at 400°C, using a mixture of 1.5% CH<sub>4</sub>: 98.5% H<sub>2</sub> at 3 mbars of gas pressure. The stainless steel and plasma carburised plates were cleaned using an ultrasonic bath with ethanol.

Glow-discharge optical emission spectroscopy (GDOES) was carried out on the alloyed samples to measure depth and mass concentration of the treatment, using a Spectruma

GDA 650HR analyser. Hardened layers of 1  $\mu\text{m}$  thickness were obtained, with a C mass concentration of 12.9% at the surface.

Hardness was measured using a Mitutoyo MVK-H1 micro-hardness tester with a diamond Vicker's indenter; the load was set at 500 gf for the analysis. Measured hardness of as-received and plasma carburised stainless steel samples were 172 HV and 305 HV, respectively.

## **4.2.2 Laser processing**

A laser micromachining system was used to produce the surface patterns that integrates a MOPA-based Yb-doped fibre nanosecond (ns) laser source (SPI G4 50W HS-S) with a near infrared wavelength (1064 nm) and a maximum average power of 50 W and a 100 mm telecentric focusing lens for achieving a beam spot size of 35  $\mu\text{m}$ . The laser beam movements were controlled employing a 3D scan head (RhoThor RTA) and thus to be able to produce predefined patterns. A maximum scanning speed of 2.5 m/s can be achieved with the used laser processing setup.

Channel-like patterns were created on the sample surfaces. The distance between scan lines was set at 100  $\mu\text{m}$ . This laser processing strategy was chosen over other possible patterns, e.g. cell-like or dimples' patterns, due to the higher anisotropy of the resulting topographies. This is important in order to be able to study how the wear directionality in respect to the pattern orientation can affect the functionality in the laser processed surfaces.

The pulse durations used to produce the patterns were 15 and 220 ns, the lowest and the highest achievable with this particular laser source and thus to judge about the

trade-offs between speed and quality in producing the patterns and their impact on wear resistance. The other processing parameters were chosen in order to maintain the same accumulated energy per line based on previous experimental results [143] as follows:

- 220 ns: scanning speed of 150 mm/s, pulse frequency of 70 kHz and pulse energy of 50.1  $\mu\text{J}$ .
- 15 ns: scanning speed of 132 mm/s, pulse frequency of 100 kHz and pulse energy of 30.9  $\mu\text{J}$ .

### **4.2.3 Hydrophobic coating**

Two of the plasma carburised samples patterned with the 220 ns laser pulses were coated by immersion in Mecasurf<sup>®</sup> (Surfactis, Angers, France), a hydrophobic monolayer coating commercially used in aeronautics to reduce surface tension. This was done in order to compare the durability of naturally aged samples against the coated ones.

### **4.2.4 Abrasion test**

Abrasion tests were performed on the samples to study the behaviour of the patterns under heavy wear conditions and thus to analyse any changes in functionality, chemistry and surface topography. The test was specially designed to be able to study the mechanical durability of the engineered surfaces in conditions as close as possible to those they could be exposed to in a real working environment. As there is not a standardised method to measure the durability of patterned/textured surfaces, all tests

were performed by adapting the ISO 11998:2006 “Paints and varnishes – Determination of wet-scrub resistance and cleanability of samples” [174], used to test the resistance of coated surfaces. An Elcometer 1720 Abrasion and Washability Tester was used for this purpose. The test setup includes a moving mechanical arm with a counterpart holder and a load as shown in Fig. 4.1a to perform reciprocating movements on a surface and thus to induce a tangential abrasion. Dimensions of the counterpart holder used were 90 x 39 mm, and a cadence of 37 cycles per minute was kept constant during the tests. A total stroke length of 180 mm with a load of 0.05 kgf/cm<sup>2</sup> was used, and the number of cycles performed were 100, 200 and 300.

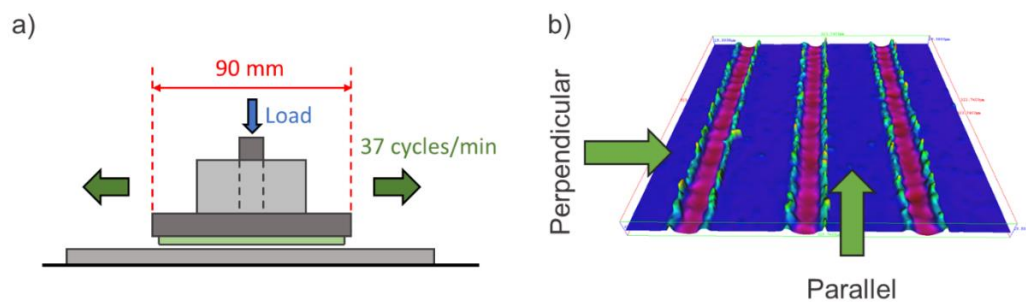


**Fig 4.1.** (a) a sketch of the Elcometer 1720 Abrasion and Washability Tester. (b) the relative orientation between the two abrasion directions and channel-like patterns.

Commercially available heavy-duty scouring pads (Scotch-Brite™) were used as counterparts during the tests. The composition of the pad in percentage weight was given by the manufacturer: aluminium oxide (45-67%), cured resin (15-40%), nylon fiber (5-15%) and titanium oxide (0.5-2.75%). The scouring pads are chemically stable and therefore it was considered that no chemical interactions between the pads and engineered surfaces took place in the tests. Counterparts were replaced after each 100

cycles to avoid the build-up of stainless steel particles during the cycles and thus to minimise their potential contribution to wear in subsequent cycles.

As is shown in Fig. 4.1b, the relative orientations between the channel-like patterns and reciprocating movements were varied, i.e. they were parallel and perpendicular to the channels. After the tests, the samples were rinsed with water and dried with compressed air to remove all debris on their engineered surfaces and fibers from the scouring pads.

## **4.2.5 Characterization methods**

A focus variation microscope, Alicona G5, with a 20x magnification lens was used to analyse the topographies of the engineered surfaces, before and after the wear cycles. The vertical resolution of the system is 50 nm. In particular, the initial depth of the channel, the height of the bulges resulting from the redeposited material after the laser patterning and then their changes after the abrasion tests were measured to quantify the wear. Uncertainty of the measurements was calculated based on the standard deviation of 10 consecutive measurements in different areas of the patterned surfaces and it was less than 0.6  $\mu\text{m}$  in all cases.

A JEOL JCM-6000 Benchtop Scanning Electron Microscope (SEM) was used to obtain the micrographs of the produced patterns before and after the abrasion tests.

Wettability of the surfaces was studied using a sessile drop technique and thus to obtain their respective SCAs, with an Attension Biolin Scientific Theta T2000-Basic+ contact angle measurement system employed for these measurements. Milli-Q water droplets of 6  $\mu\text{l}$  were used for all SCA measurements.

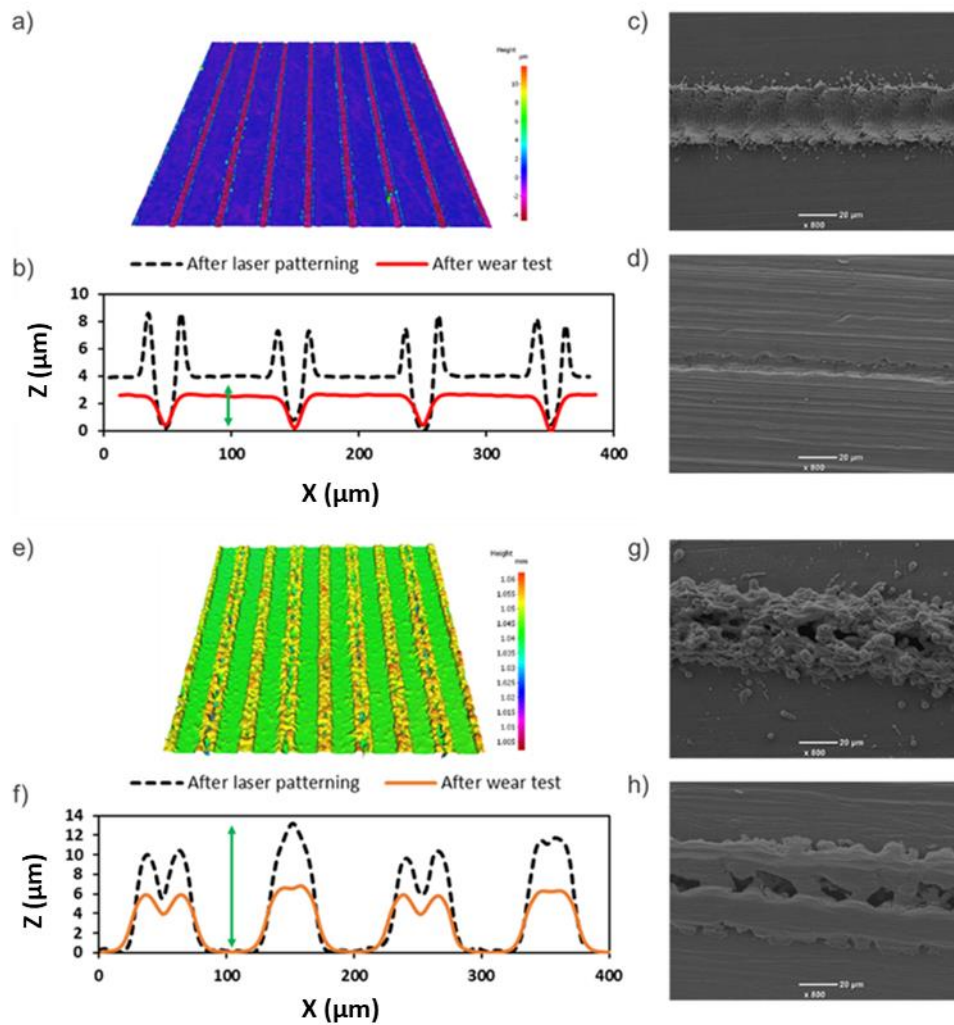
X-Ray photoelectron spectroscopy (XPS) measurements were performed on both, stainless steel and plasma carburised surfaces. The reference surfaces were analysed prior to patterning them and also on a “freshly” laser processed samples (within the 24 hour time period before the surfaces become hydrophobic), “aged” laser patterned surfaces (i.e. when the surface is hydrophobic) and “aged” surfaces after undergoing 300 wear cycles. A Kratos Axis Ultra DLD spectrometer (Kratos Analytical, UK) with a monochromated Al K $\alpha$  X-ray irradiation source was used for the XPS analysis. Analysis areas of 300 x 700  $\mu\text{m}$  were scanned at room temperature under a base pressure of  $2 \times 10^{-10}$  mbar and the estimated depth of the XPS analysis was 5-10 nm. The measurements were calibrated by using the Fermi edge and 3d $_{5/2}$  peak recorded from a polycrystalline Ag sample. Data analysis was carried out with the CasaXPS package.

## **4.3 Results and discussion**

### **4.3.1 Surface analysis**

Laser patterning in the nanosecond regime is a thermal process. In particular, the substrate material is molten as a result of the irradiation with nanosecond laser pulses and pulse trains lead to splashes of molten material that then solidify to create bulges on the surface. The increase of pulse duration leads to bigger volumes of molten material and thus to bigger bulges along the laser path. Therefore, two different pulse durations, i.e. 15 ns and 220 ns, were used to investigate how they could affect the wear resistance of laser functionalised surfaces. As shown in Fig. 4.2a, the obtained topographies with 15 ns pulses were well defined patterns with small volumes of solidified material along the trenches; whereas when the patterning was performed

with 220 ns pulses, relatively big bulges were formed along the trenches and therefore they were less well defined (see Fig. 4.2e). Therefore, the tribological contacts between the counterpart and the patterned areas were different when the abrasion tests were performed.



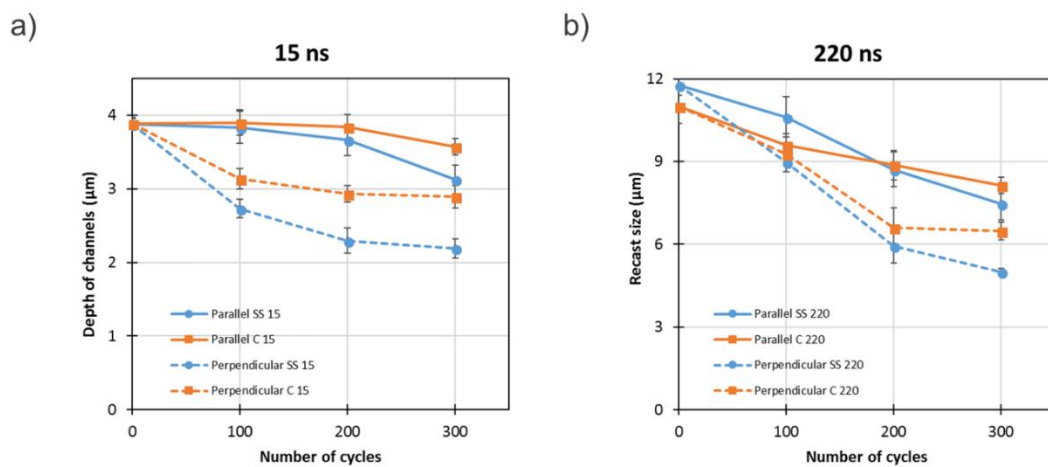
**Fig 4.2.** 3D images of patterns produced with pulse durations of 15 ns (a) and 220 ns (e); topographical profiles resulting after irradiation with 15 ns (b) and 220 ns (f) pulses before and after the wear tests (300 abrasion cycles); SEM images of the topographies produced with 15 ns and 220 ns before (c & g) and after (d & h) the wear tests, respectively.

Fig. 4.2b shows representative profiles of the patterns produced with 15 ns pulses, the black dashed line before and the red line after the abrasion tests. The size of the resulting bulges could be considered negligible, i.e. only 1.1 and 1.8  $\mu\text{m}$  on as-received and carburised stainless steel sample, respectively, in comparison with the channels' width of 100  $\mu\text{m}$ . Furthermore, these bulges were thin and brittle, were removed quickly at the start of the abrasion tests and thus the non-processed surface was in a tribological contact with the counterpart. Then, due to the wear during the abrasion cycles the depth of the channels was reduced, as depicted in Fig. 4.2b and Fig. 4.S1. Fig. 4. 2c-d show the SEM images of the 15 ns topographies before and after the wear tests, respectively, clearly demonstrating the removal of the bulges and the reduction in the depth of the channels.

Fig. 4.2f shows representative profiles of the patterns produced with 220 ns pulses where the black dashed and orange lines represent the profiles before and after the abrasion tests, respectively. In this case, the bulges are in a tribological contact with the counterpart and thus the resulting abrasion had reduced their size. The height reduction of these bulges as a result of the wear can be clearly seen in Fig. 4.2f and Fig 4.S2. Fig. 4. 2g-h show the SEM images of the 220 ns patterns before and after the abrasion tests. It can be clearly seen that first, the channels are almost buried under the bulges and there is a high amount of splashes and a relatively high roughness on the patterned surfaces. After the abrasion tests, the pattern is still visible on the surface, however, the bulges are smoother and as a result the surface roughness is reduced.

Fig. 4.3 depicts the impact of wear on the dimensions of the pattern with the increase of abrasion cycles. In particular, the depth changes of the channels produced with the 15 ns pulses are plotted in Fig. 4.3a while in Fig. 4.3b the height evolution of the bulges

generated with the 220 ns pulses is shown. In both graphs, the profile of the pattern changes on the plasma carburised and as-received stainless steel samples are represented. Furthermore, the continuous and dashed lines depict the results obtained by performing the wear tests with abrasion directions parallel and perpendicular to the patterns, respectively.



**Fig 4.3.** Topography and bulges' evolutions after abrasion cycles: (a) the depth changes of the channels produced with 15 ns pulses after 100, 200 and 300 cycles; (b) the height changes of the bulges generated with 220 ns pulses after 100, 200 and 300 cycles.

As can be seen in Fig. 4.3a, the depth of 15 ns channels is the same both on as-received and plasma carburised stainless steel samples, i.e. 3.9 µm deep, before the abrasion tests. Whereas in case of 220 ns patterns (see Fig. 4.3b), the height of the bulges is slightly higher on the as-received sample, i.e. 11.8 µm, compared to that on the carburised steel one, i.e. 11.0 µm. This height difference could be explained with the lower ablation threshold of as-received stainless steel at this pulse duration [143] and thus a bigger volume of material is melted and splashed on the surface.

The total reduction,  $R$ , represents the decrement in the size of the patterns after the abrasion tests in percentages and was calculated with the following equation:

$$R (\%) = \frac{X_i - X_f}{X_i} * 100 \quad (4.3)$$

where:  $X_i$  is the initial value of channel depth or bulge height obtained for the 15 ns or 220 ns patterns, and  $X_f$  - their final values after 300 abrasion cycles. Table 4.1 includes the values of  $R$  calculated for the patterned samples after the wear tests.

	R after 300 cycles	
	Parallel	Perpendicular
SS 220 ns	36.4	57.4
C 220 ns	26.1	41.1
SS 15 ns	19.4	43.4
C 15 ns	8.0	25.5

**Table 4.1.** The total reductions ( $R$ ) after 300 parallel and perpendicular abrasion cycles.

*Note: SS and C denote as-received (Stainless steel) and carburised stainless steel samples respectively, while 220 and 15 ns the pulse durations used to produce them.*

Similar trends can be observed for both graphs in Fig. 4.3. Especially, the wear rates, i.e.  $R$  in Table 4.1, are consistently higher on the as-received stainless steel samples in comparison to the plasma carburised ones and quantify the effects of the abrasion cycles on surface topography.

The effects of the orientation of the patterns with regards to the abrasion direction are also depicted in Fig. 4.3. The wear rates were constantly higher for all tests when the abrasion direction was perpendicular to the patterns compared to when the abrasion

direction was parallel to them (dashed and continuous lines in Fig. 4.3, respectively). In particular, the applied forces are along the channels in the case of the parallel abrasion and thus the surface works under compression. At the same time, when a perpendicular abrasion is performed, the forces induce a tangential/tensile stress on the bulges generated with the 220 ns pulses that lead to flexion and a higher wear.

In the case of the 15 ns patterns on plasma carburised surfaces, the depth reduction of the channels after the abrasion cycles is less than 1  $\mu\text{m}$  for both the parallel and the perpendicular abrasion. As the thickness of the carbon layer after the plasma treatment is approximately 1  $\mu\text{m}$ , this means that during all abrasion cycles this harder layer and not the as-received stainless steel is in a tribological contact with the counterpart. The effect of this carbon layer is quantified in Table 4.1, in particular R is reduced from 19.4 % to 8.0 % and from 43.4 % to 25.5 % when the abrasion was parallel and perpendicular to the patterns, representing corresponding improvements of 59 % and 41 %.

For the 220 ns patterns, the pattern wear was assessed again using R. In particular, R was reduced from 36.4 % to 26.1 % and from 57.4 % to 41.1 % when parallel and perpendicular abrasion cycles were performed, respectively, representing an improvement of 28 % in both cases.

The higher improvement in wear resistance of 15 ns patterns in comparison with the 220 ns ones can be attributed to the specific tribological conditions between counterpart and functionalised surfaces. First, the contact area on the 15 ns surfaces is significantly bigger as can be clearly judged in Fig. 4.2, and thus the applied force is better distributed and hence the exerted pressure is lower. Secondly, the contact occurs predominantly on the bulges in the case of 220 ns patterns, both on as-received and plasma carburised stainless steel samples. The bulges are recasts mainly formed of iron

oxides (see the results in Section 3.3) and therefore, the tribological contact with the hardened non-patterned carburised surface is reduced substantially and hence the wear is higher when compared with the 15 ns samples.

### **4.3.2 Wettability**

SCA measurements were carried out to quantify the wettability of the patterned surfaces and also to analyse their evolution as a result of the abrasion cycles. SCAs measured on as-received and plasma carburised stainless steel samples were 92° and 98°, respectively, before the laser patterning.

It is well known that laser patterned metallic surfaces are hydrophilic just after the processing and with time they become hydrophobic due to an aging process that leads to changes in surface chemistry while their topography remains unaltered. All samples were analysed after the laser patterning and all of them exhibited high hydrophilicity. After 10 days, the samples were analysed again and then SCAs were closer to 170° while the rolling angles were low [143], indicating a transition to Cassie-Baxter state. SCAs for all samples before the laser patterning (used as references) and after 10 days following their processing are shown in Fig. 4.4.

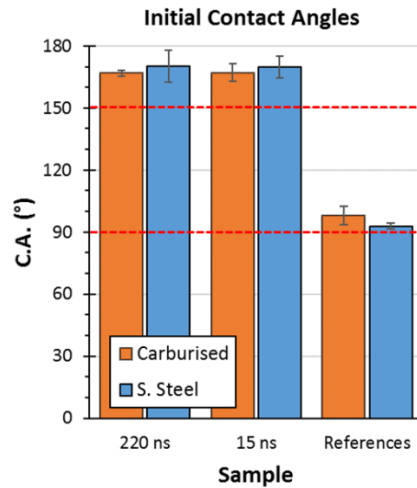


**Fig 4.4.** SCAs of the reference and patterned samples after 10 days stabilization.

Following the 10 day stabilization, patterned samples were used to analyse their wear resistance, with SCAs measured on the samples after undergoing 300 abrasion cycles and then cleaning them to remove any debris. Fig. 4.5 shows the SCA evolution with the increase of abrasion cycles. SCAs dropped from 170° to values in the range from 100° to 110° after the first 100 parallel abrasion cycles as shown in Fig. 4.5a and were between 95° and 105° at the end of the tests, similar to the values obtained with the reference samples. This demonstrates a quick loss of hydrophobicity, regardless of the laser and plasma treatments of the four analysed samples that underwent parallel abrasions cycles. In addition, it is worth noting that on all four samples the droplets spread along the channels and became elongated following the parallel abrasion cycles (See Fig. 4.S3). In the case of the abrasion cycles that were performed perpendicular to the channels, the SCA decrease was not so sharp and the change of the wetting properties was progressive as can be seen in Fig. 4.5b. The patterns were continuously eroded and SCAs decreased following the Wenzel model. SCAs remained higher during the first 200 cycles on the 220 ns samples, due to the relatively higher aspect ratio of the patterns compared

to those produced with 15 ns pulses. After 300 cycles, SCA values were in the range from 100° to 110°, slightly higher than the references.

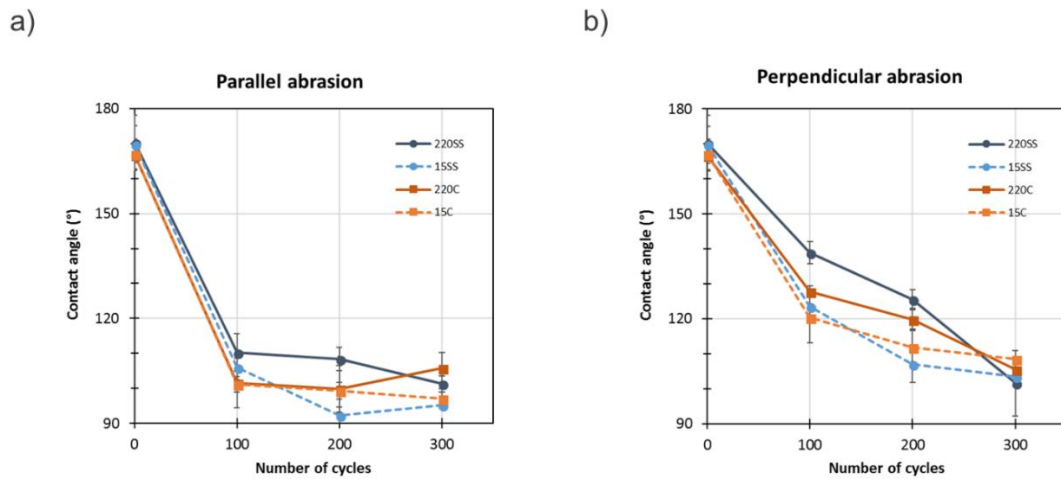


**Fig 4.5.** SCA evolution after 100, 200 and 300 parallel (a) and perpendicular (b) abrasion cycles.

As discussed in Section 3.1, and considering the evolution of surface topographies, the impact of wear is higher when the abrasion cycles were performed perpendicular to the channels. However, when the functional response of the surfaces was analysed, the patterns that underwent abrasion cycles perpendicular to the channels have shown a slow deterioration of their hydrophobicity. Fibers from the scouring pads used for the abrasion cycles were retained inside the channels during the tests when the reciprocating movement of the counterpart was parallel to the channels. Therefore, the fibers eroded the channels from inside and thus their surface chemistry was modified. In the case of the perpendicular abrasion, the bulges prevented the pad fibers from being deposited inside the channels, inhibiting them from wearing the channels from inside, and thus their surface chemistry was altered at much slower rate.

### 4.3.3 Chemical analysis

X-Ray photoelectron spectroscopy (XPS) analysis was performed on the samples to analyse the surface chemical compositions at different stages of the aging process and after the abrasion cycles. Similar trends in composition changes were obtained for the samples patterned with both pulse durations as shown in Fig. 4.S4. However, differences in chemical compositions were bigger for the 220 ns samples due to the larger patterns (the increased surface damage due to the longer pulse duration) and therefore only the results for 220 ns samples are presented below. As-received and plasma carburised stainless steel samples were compared. Measurements were taken on all samples before any laser processing in order to use them as references. Then, measurements were taken on freshly patterned samples while they were still hydrophilic and also on aged samples, when they were super hydrophobic. Finally, the last set of measurements were taken after the wear tests, when the samples lost their hydrophobicity.

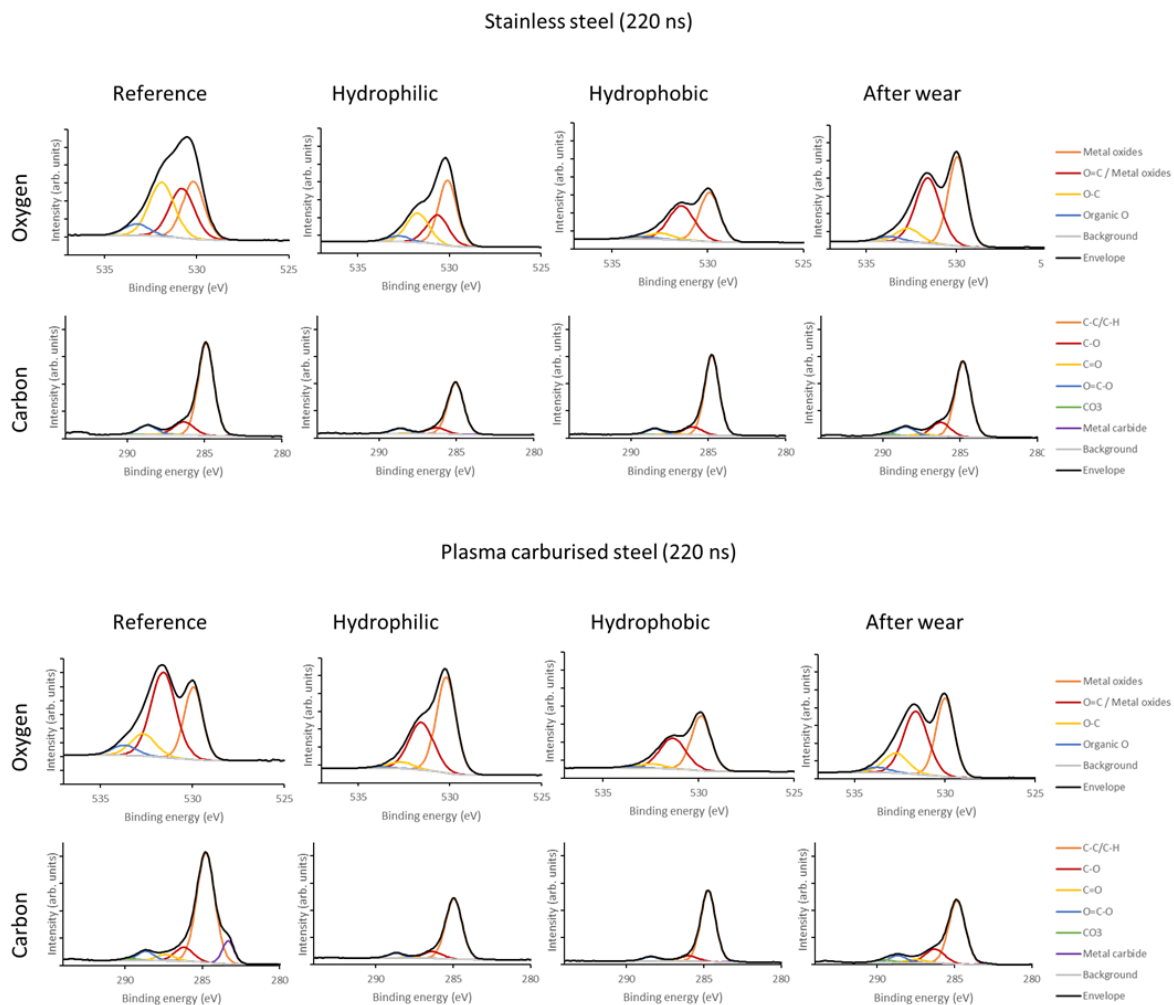


**Fig 4.6.** Deconvolution of the carbon (C 1s) and oxygen (O 1s) regions of as-received and plasma carburised samples patterned with 220 ns laser pulses.

Note: reference – the measurements on the samples before patterning, hydrophilic – the set of measurement taken on the “freshly” patterned samples, hydrophobic – the measurements after stabilization and wear tests – the set of measurements after 300 abrasion cycles.

After comparing the XPS survey spectra of the samples, differences were identified in the peaks corresponding to carbon and oxygen. Deconvolution of the C 1s and O 1s

regions are depicted in Fig. 4.6, including measurements taken on the sample before and after the laser patterning and also after the wear tests. The reference measurements on as-received and plasma carburised stainless steel showed differences in their oxygen peaks. While the component corresponding to metal oxides at 530 eV were the same, there was a shift in the O=C/Metal oxide peaks from 530.8 to 531.6 eV and also in the peaks corresponding to O-C, from 531.9 to 532.7 eV, respectively. These shifts are most likely due to a change in the surface potential due to the carburisation process, with two components arising from metal oxides due to the different metal oxides present on stainless steel. The intensity of the O-C peak was higher on as-received stainless steel, while the O=C/metal oxide peak was higher on plasma carburised surface. These differences in oxidation states can be attributed to the high amount of carbon present on the plasma carburised samples before the laser processing. A peak at 533.5 eV can be identified on both samples, corresponding to organic oxygen, possibly enhanced by water molecules on the surface. Considering the carbon peaks on as-received and plasma carburised reference samples, this could be explained with the high amounts of surface contaminants due to the C-O, O=C-O and C-C/C-H bonds. In the case of plasma carburised stainless steel, the C-C/C-H peak is higher due to the carbon alloying process. Additionally, a peak at 283.3 eV could also be observed on this sample, indicating the presence of metal carbides.

Deconvolution of the O 1s region after laser processing on hydrophilic as-received and carburised stainless steel samples also revealed some interesting changes as a result of the laser process. An increase in the metallic oxide component at 530 eV can be identified on both surfaces, to the detriment of the other peaks, explained by the solidification and subsequent oxidation of molten metal during the laser patterning and

the formation of bulges along the channels. For both surfaces, the C 1s profiles are similar but reduced in intensity compared with the references, suggesting a reduction in the concentration of surface contaminants. No carbides were observed in any of the hydrophilic samples, indicating that carbon present in the as-received and carburised stainless steel was vaporised or dissolved into the lattice.

Oxygen peaks are similar on hydrophobic as-received and carburised stainless steel samples after stabilization, indicating identical oxidation states with metallic oxide peaks at 529.9 and 531.4 eV on both samples. Comparing them with the hydrophilic samples, an overall reduction in the relative intensity of the O 1s region was observed due to the increase of the carbon content. In addition, there is a change in the relative ratio of the peaks at 529.9 and 531.4 eV. For the as-received sample, a shift in the peak to higher binding energy can be identified, too, i.e. from 530.6 to 531.4 eV. These differences in the oxygen peaks suggest a change in the surface potential that could be attributed to the surface activation after the laser processing, and a posterior surface contamination during the samples aging. Regarding the carbon peaks, an increase of the peak at 284.7 eV can be observed when comparing the hydrophobic with the hydrophilic sample, corresponding to the C-C/C-H bonds, while the other peaks remain constant.

After the wear tests, the relative intensity of the C 1s region was reduced, as the contaminants from the surface were partially removed, in particular the C-C/C-H peaks are smaller compared with those on the hydrophobic samples. Furthermore, an increase of C-O and O=C-O peaks can be observed on both as-received and plasma carburised samples. On both surfaces, the oxygen peaks are at the same positions and their relative sizes are similar compared to the hydrophobic samples, suggesting that there is no change in oxidation states or surface potential after the wear tests. However, the

intensity of all the peaks is higher, due to the total reduction in carbon-based contaminants.

Carbon-carbon (C-C) and hydrocarbon species (C-H) are known to be non-polar molecules, while carbonyl groups (C=O), carbon-oxygen (C-O) and carboxyl molecules (O=C-O) together with metal oxides, are polar. Water molecules are polar, and thus if a surface polar as well, bonds form between them, leading to hydrophilicity. Furthermore, non-polar surfaces are associated with hydrophobicity. The presence of such polar and non-polar molecules on the surfaces and the change in the oxidation states explain the SCA evolution during the stabilization.

Table 4.2 shows the contributions of non-polar organic molecules, metal oxides and polar organic molecules to the compositions detected on the surfaces, measured in atomic weight (%). In accordance with the results in Fig. 4.6, the reference surface compositions were different due to the high amount of carbon present on the alloyed material. After the laser patterning, a small reduction in organic based compounds was detected, especially on the carburised surfaces, due to the cleaning effect of the laser. Furthermore, an increase in metallic oxides was found on both as-received and carburised stainless steel samples that could explain the high hydrophilicity of the “freshly” patterned surfaces.

On both hydrophobic samples, the presence of non-polar molecules is higher in comparison with the “freshly” patterned ones, while the presence of polar molecules is smaller. In addition, as previously pointed out in Fig. 4.6, a difference in oxygen peaks was observed on hydrophilic and hydrophobic surfaces, indicating a change in surface potential, and as topographies remained unchanged, this clearly indicates chemically active/unstable surfaces after the laser patterning. Oxidation is followed by a

chemisorption of organic non-polar molecules from the atmosphere [123], and thus in combination with the resulting surface topography after the laser patterning leads to hydrophobicity.

After the wear tests, surfaces lost the hydrophobicity, and this can be explained with the reduction of non-polar molecules, due to material removal during the abrasion cycles. Furthermore, as the surfaces reached an equilibrium state after stabilization, no changes in chemical composition occurred, suggesting that the surfaces were not chemically active anymore, and thus this could explain why the surfaces did not recover the hydrophobicity again after some time.

	Sample	Non-polar organics	Metal oxides	Polar organics	Rest
As-received	Reference	29.0	20.3	20.0	30.8
	Fresh sample	29.5	29.1	17.3	24.1
	Aged sample	42.7	27.4	8.4	21.5
	After wear	28.2	33.4	10.6	27.9
Carburised	Reference	41.7	16.9	11.1	30.2
	Fresh sample	29.4	41.3	5.7	23.5
	Aged sample	42.2	31.5	6.2	20.2
	After wear	26.4	32.2	12.4	29.0

**Table 4.2.** Surface compositions at the four investigated states on as-received and carburised stainless steel samples.

#### 4.3.4 Durability of coated samples

As shown in Section 3.1, the wear rates (see Table 4.1) are consistently higher on the as-received stainless steel samples in comparison to the plasma carburised ones.

Furthermore, the progressive loss of hydrophobicity with the increase of abrasion cycles was discussed in Section 3.2. Therefore, a feasibility study was conducted to investigate the effect of a commercially available hydrophobic monolayer coating on top of topographies resulting after laser processing on two plasma carburised stainless steel samples. Especially, the surface response of uncoated and coated carburised samples patterned with 220 ns pulses was investigated under the same wear conditions, and for both parallel and perpendicular abrasion. The reference SCA on the coated surface without laser patterning was measured, too, and it was 114°, slightly higher than the reference for an unpattern carburised sample without the coating, and the response during the wear test was studied as well.

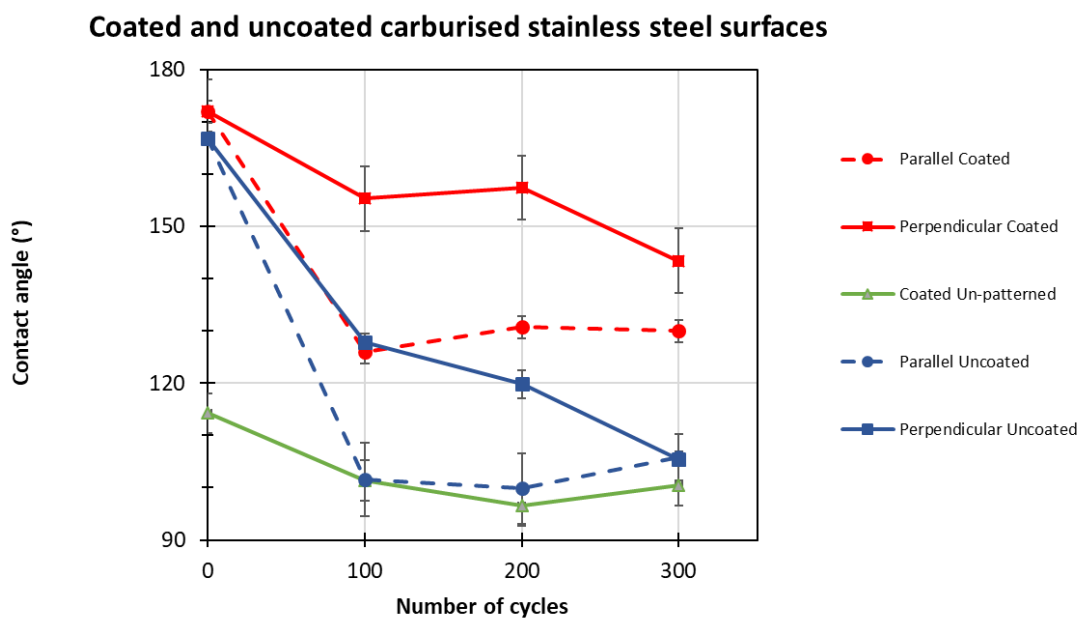


**Fig 4.7.** SCA evolution after 100, 200 and 300 wear cycles on uncoated and coated carburised samples patterned with 220 ns pulses, as well as the reference coated un-patterned surface.

The SCA evolution on uncoated and coated carburised 220 ns samples after perpendicular and parallel abrasion cycles is shown in Fig. 4.7. It can be clearly seen that the coated samples showed higher SCAs after the abrasion. This suggests that the applied coating was strongly attached to the surface not only on the bulges, as it was the case with the organic layer formed during the stabilization, but also inside the channels and on not laser processed areas. As discussed earlier, the bulges acted like a mechanical shield for the coating. Especially, as can be clearly seen in Fig. 4.7, the wear of the coating is higher as a result of the parallel abrasion cycles, as the pad fibers of the counterpart got inside the channels and were progressively wearing the coating. However, when the abrasion cycles were performed perpendicular to the channels, the bulges shielded the coating and therefore SCAs were higher than  $140^\circ$  even after 300 cycles. Furthermore, the combination of both surface topography and coating is the key in achieving high SCAs, as can be clearly seen in Fig. 4.7. The coating on un-patterned surfaces is not sufficient to achieve high SCA values and thus the presence of the bulges has a double effect, i.e. increasing hydrophobicity and at the same time shielding the coating.

## **4.4 Conclusions**

In this paper, durability, both mechanically and functionally of surface topographies produced by laser patterning was studied. Channel-like patterns were fabricated with an infrared nanosecond laser on as-received and plasma carburised stainless steel samples to investigate the evolution of their wear and wettability after abrasion cycles.

The patterns produced with longer pulse durations were more wear resistant, due to the larger volumes of melted and quenched material during the laser patterning process. Furthermore, the patterns produced on plasma treated harden surfaces showed consistently a higher wear resistance, especially a higher mechanical durability. The pattern mechanical durability improvements on plasma carburised surfaces were 28 % and 59 % after laser processing with 220 and 15 ns pulses, respectively, compared to the durability achieved on as-received stainless steel substrates.

Also, the results revealed that the abrasion cycles orientation relative to the channels was important factor affecting the surface durability. From a mechanical viewpoint, the wear resistance was higher to the parallel abrasion cycles because the patterns were exposed to compression forces compared to the tangential stress experienced during the perpendicular abrasion cycles. However, from the wettability viewpoint, surfaces were more resistant to the perpendicular abrasion cycles. The bulges formed along the channels during the laser processing behaved as a mechanical shield, absorbing most of the abrasion, and thus inhibiting the wear by pad fibers and thus the changes of surface chemistry inside the channels. In case of the parallel abrasion cycles, pad fibers were freely moving inside the channels and thus causing a homogeneous wear along the entire surface topography.

The reasons for the wettability evolution of laser patterned surfaces in time was also investigated. XPS analysis of laser patterned surfaces on as-received and carburised stainless steel samples revealed changes in their oxide peaks in time and also an increase of carbon based molecules. This suggests a surface activation after the laser processing that leads to changes in the surface potential and a chemisorption of non-polar molecules onto the surface. Furthermore, hydrophobicity attained in time could be

explained with the combined effects of absorbed non-polar molecules and the topography attained after laser patterning.

In addition, it was possible by combining surface hardening, laser patterning and surface coating to retain higher hydrophobicity after wear tests, especially contact angles higher than  $140^\circ$  were maintained after 300 abrasion cycles by using the bulges resulting after laser patterning as a shield for the coating. Particularly, the mechanical properties were enhanced by carburizing substrates and thus to increase the wear resistance of the patterns and hence to prolong their shielding effect and protect the hydrophobic coating. Thus, the proposed combined surface treatment by first carburizing the substrates and then laser patterning them could offer increased durability and wear resistance of functionalized surfaces that is one of the critical obstacles toward their broader use in many application areas. Further research is necessary regarding the effects of the abrasion orientation and thus propose laser patterns that could withstand heterogeneous wear cycles. Furthermore, other alloying elements should be investigated to increase even further the substrate hardness and thus the lifespan of laser-based functionalized surfaces.

## **Acknowledgements**

The research reported in this paper was carried out within the framework of European Commission H2020 ITN programme “European ESRs Network on Short Pulsed Laser Micro/Nanostructuring of Surfaces for Improved Functional Applications” ([www.laser4fun.eu](http://www.laser4fun.eu)) under the Marie Skłodowska-Curie grant agreement No. 675063 and the UKIERI DST programme “Surface functionalisation for food, packaging, and

healthcare applications”. In addition, the work was supported by two other H2020 FoF programmes, i.e. the projects on “Modular laser based additive manufacturing platform for large scale industrial applications” (MAESTRO) and “High-Impact Injection Moulding Platform for mass-production of 3D and/or large micro-structured surfaces with Antimicrobial, Self-cleaning, Anti-scratch, Anti-squeak and Aesthetic functionalities” (HIMALAIA). The authors would like also to acknowledge the support and assistance of Airbus Defence and Space GmbH and B/S/H/ Hausgeräte GmbH in conducting this research.

## 4.5 Supporting information

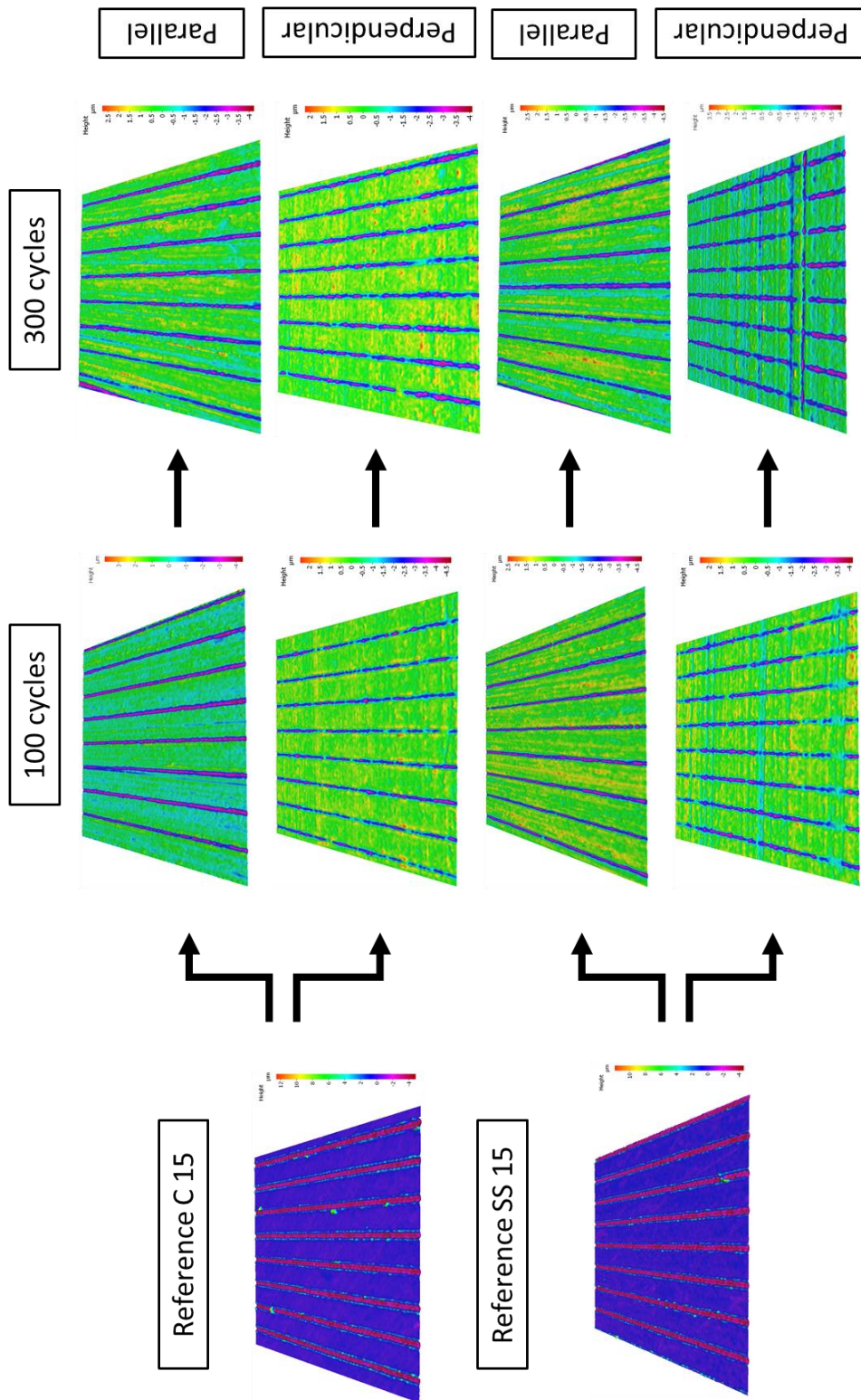
Captions:

Figure S4.1. 3D images of the samples produced with 15 ns pulses on both, as-received and carburised stainless steel, before, during and after the wear tests.

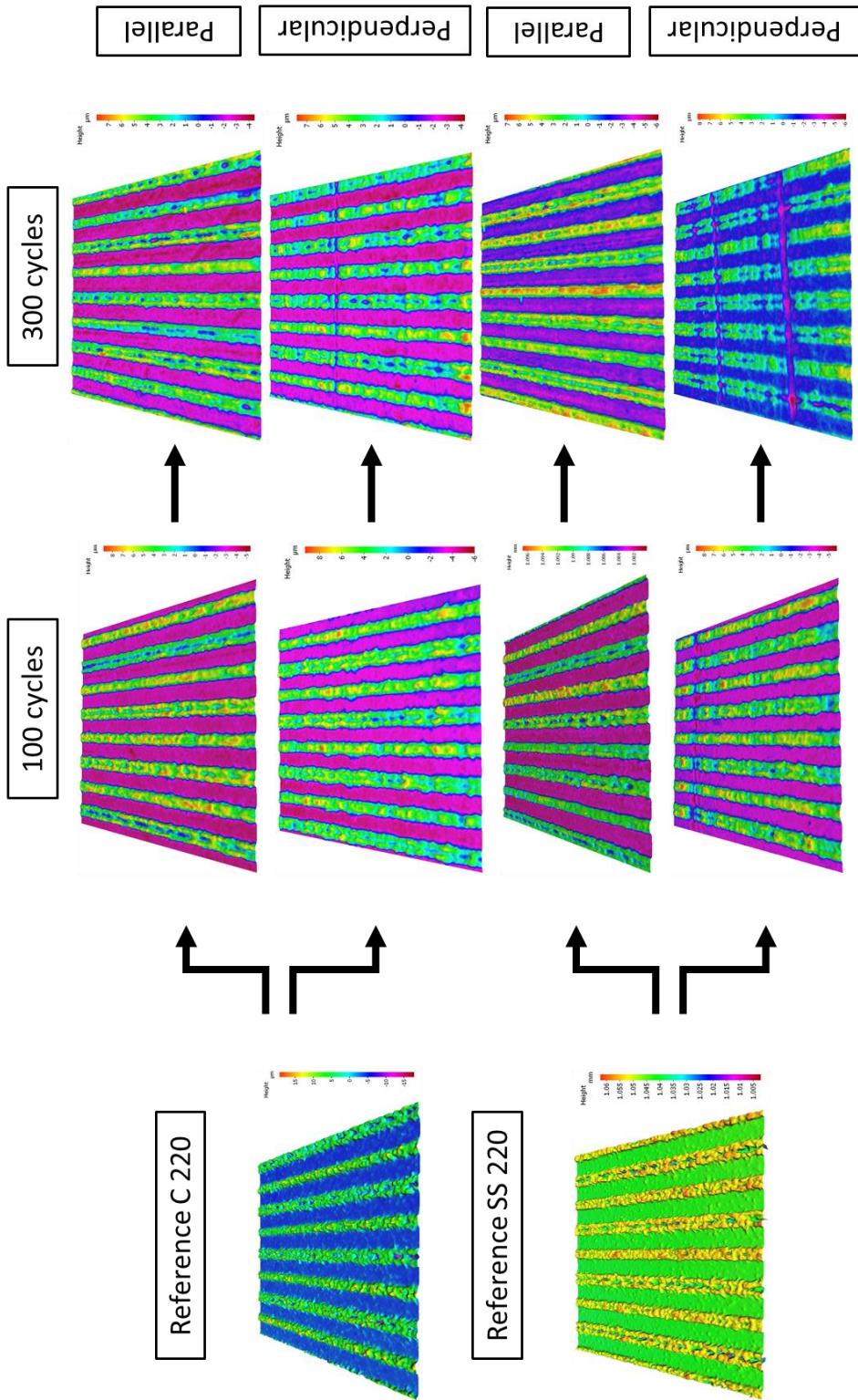
Figure S4.2. 3D images of the samples produced with 220 ns pulses on both, as-received and carburised stainless steel, before, during and after the wear tests.

Figure S4.3. Side and front views of the drop shape before and after parallel abrasion, showing the drop spreading along the channel direction, for sample 220C.

Figure S4.4. XPS surveys for both, as-received and carburised stainless steel, before and after laser patterning with 220 and 15 ns of pulse durations.



**Figure S4.1.** 3D images of the samples produced with 15 ns pulses on both, as-received and carburised stainless steel, before, during and after the wear tests.



**Figure S4.2.** 3D images of the samples produced with 220 ns pulses on both, as-received and carburised stainless steel, before, during and after the wear tests.

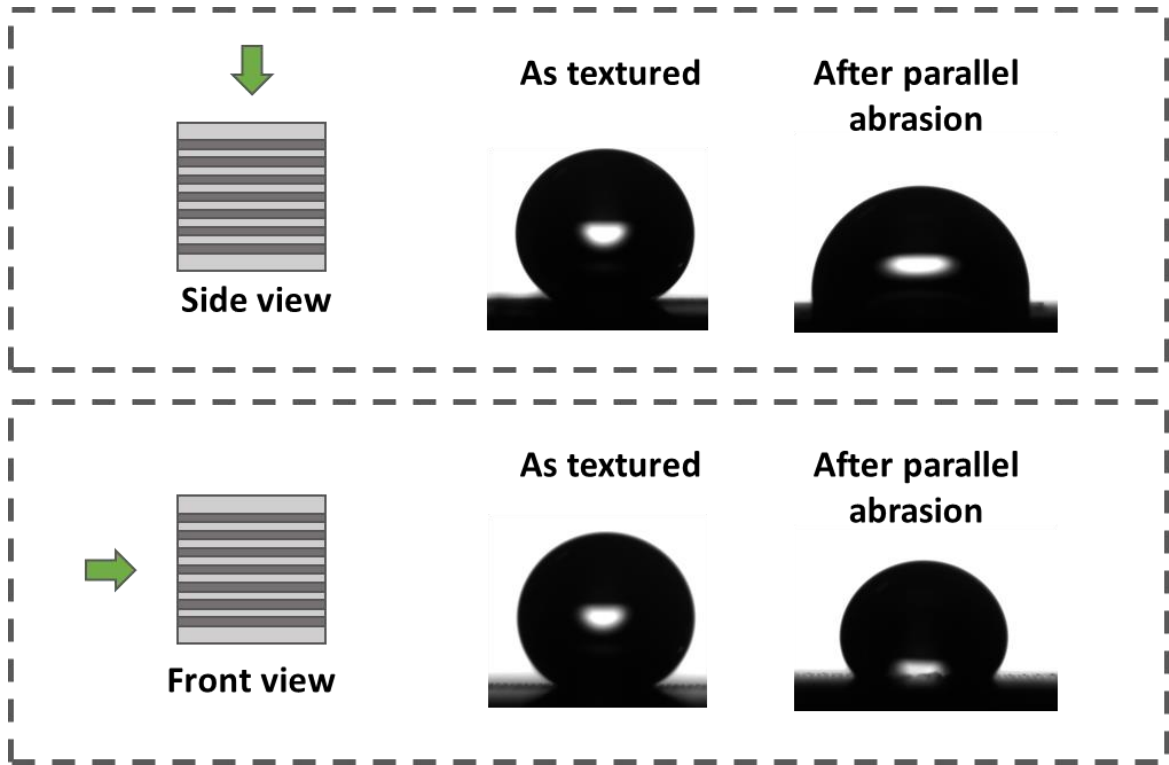


**Figure S4.3.** Side and front views of the drop shape before and after parallel abrasion, showing the drop spreading along the channel direction, for sample 220C.

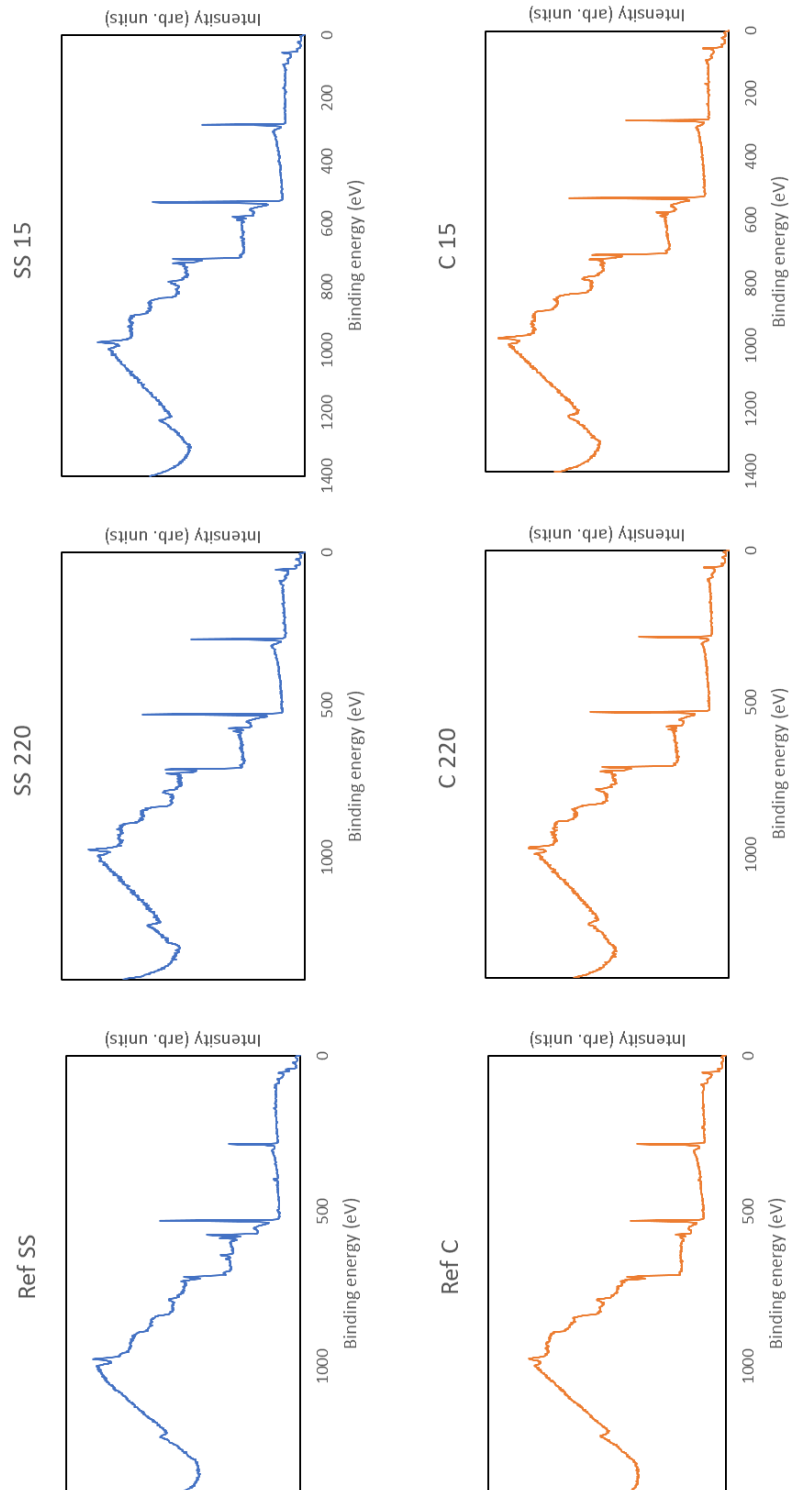


**Figure S4.4.** XPS surveys for both, as-received and carburised stainless steel, before and after laser patterning with 220 and 15 ns of pulse durations.

# Chapter 5

---

## Experimental investigation of processing disturbances in laser surface patterning

---

*A. Garcia-Giron<sup>1,\*</sup>, J. M. Romano<sup>1</sup>, A. Batal<sup>1</sup>, A. Michalek<sup>1</sup>, P. Penchev<sup>1</sup> and S.S. Dimov<sup>1</sup>*

*<sup>1</sup>Department of Mechanical Engineering, School of Engineering, University of Birmingham, Edgbaston, Birmingham, B15 2TT, UK*

Lasers have a reduced working volume, as every optical device where lenses are involved, they are limited by the depth of focus and the marking area of the setup. The depth of focus limits the processing freedom to a plane, and that is why lasers are most commonly used to process surfaces, like for example towards surface functionalization, laser writing or cutting. Processing free form or 3D surfaces with lasers is a challenge, and the most widely spread method to achieve this consist in dividing the surface into smaller discrete planar tesserae, in such a way that either the working piece or the laser source are moving after processing each discrete field, repositioning to the next marking field and so on.

There are some manufacturing solutions where the laser source is equipped with mechanical platforms to allow the movement of the laser beam around the workpiece, while the processed piece is static, as for example, the ones integrated by GF Machining Solutions. The other approach is to have the laser source in a static position and move the workpiece to the focal plane to be processed, using a mechanical platform for this purpose.

In both cases it is possible to have a continuous relative movement between the laser beam and the workpiece, in such a way that the surface does not need to be tessellated, so each processed point is at focus and the incidence of the laser beam is perpendicular to the surface, however, this is limited only to simple shapes, as for example curved or cylindrical surfaces, and it requires a specific setup. For example, in B/S/H/ Home Appliances Group, direct laser writing is used to mark some plastic curved panels for washing machines, and for this, the nanosecond IR laser source is fixed while a mechanical platform moves the panel, in such a way that the full piece is processed without dividing it into smaller working areas. This process requires a perfect coordination between the laser and the mechanical stage, to keep constant the focal distance, number of pulses per area, scanning speed, and so on. Nevertheless, the capacity to perform the laser marking without dividing it into smaller marking fields, as in the case of the aforementioned example, is limited by the available laser source, the mechanical stages and the necessary configuration between them, i.e. due to machine limitations.

The alternative is to divide the surface into smaller discrete fields and process them separately. However, this method has some drawbacks. Even if the discrete fields are small, some points will be at focus, and some will be out of focus, and in some points the laser beam incidence will be perpendicular to the surface, but in others it will not.

When performing a functional pattern into free form surfaces, these uncertainties will result into deviations from the designed pattern, that can affect the resulting topography and functional response.

This research was published as a full length article in Optics and Lasers in Engineering (2019) [1].

**Authors' contributions:** A. Garcia-Giron is the main author of this publication. He performed the laser processing, characterization of the samples and analysis of the data. J. M. Romano, A. Batal and A. Michałek assisted during the manufacturing of the samples and characterization. A. Garcia-Giron wrote the manuscript that was posteriorly revised by P. Penchev and S.S. Dimov.

**Keywords:** Processing disturbances; hydrophobic surfaces; 3D laser patterning; inline monitoring

## **Abstract**

Laser surface patterning has attracted a significant interest from industry and research due to its promising applications in surface functionalisation. However, there are specific issues and limitations associated with the beam delivery, especially when processing 3-D surfaces and/or setting up routines for executing complex multi-axis processing strategies. In particular, there are common processing disturbances that affect the resulting surface topographies and profiles and their respective functional responses, i.e. geometrical distortions of resulting surface patterns, focal offset distance (FOD) and variations of beam incident angle (BIA). A method to investigate the effects of these factors in laser patterning 3-D surfaces is presented in this research, especially how their effects can be analysed independently by conducting empirical studies on planar surfaces. A pilot implementation of the proposed methodology is reported for producing channel-like patterns on stainless steel plates with a super-hydrophobic functional response. The results are discussed in detail to show how the effects of

processing disturbances on topographies, profiles and areal parameters together with the respective functional responses of patterned planar surfaces can be analysed and then used to set constraints in pre-processing 3-D surfaces for follow up laser patterning.

## **5.1 Introduction**

There is constant drive for improving the performance of existing products and also for integration of more functions in new products due to competitive advantages that such advances offer to companies. Therefore, technologies that can be deployed for improving the performance of products have attracted a significant interest from industry and research. An important group of such technologies have been applied successfully to functionalise surfaces and thus to improve and/or integrate novel and attractive properties into existing and new products, e.g. to incorporate surfaces exhibiting anti-icing [14], anti-bacterial [12], cell growth enhancement [17], hydrophobic [157] and friction reduction [110] properties. One of the common objectives in such applications is to control the wetting response of functionalised surfaces [27] as it is often related to other properties [33,166], i.e. corrosion resistance [19], ice repellence [150] or self-cleaning [49].

One of the technologies that have attracted a significant industrial and research interest, recently, is the laser patterning process, especially as a tool for selective functionalisation of surfaces. And, this is not surprising taking into account its flexibility and capabilities to achieve high accuracy, repeatability, reproducibility and efficiency [175,176] in processing different materials. Furthermore, the laser processing does not

require the use of any chemical substances and also as a non-contact technology there is only a negligible material waste. Therefore, it is considered an environmentally friendly process [47]. Moreover, laser surface functionalization can be applied on a wide range of materials, from metals [114,127] to polymers [177], and thus can be deployed in different industrial sectors, e.g. in aeronautics, automotive or medical applications.

Laser-based surface functionalization has been widely studied by many research groups but most of them have been focused on processing planar surfaces. At the same time, it is recognised that laser patterning of 3-D surfaces is a challenging task that requires complex multi-axis beam delivery systems and therefore has been investigated by a number of researchers, recently. In particular, Diaci et. al. developed a method for engraving curved and tilted surfaces that employed a sensor for measuring the shape of workpieces before the laser processing [77]. Overmeyer et. al. reported the fabrication of sensors on tilted and freeform surfaces and showed interdependences between the beam incident angle (BIA) and respective fluence and reflectance variations that affected the laser-material interactions [74]. Cuccolini et. al. created a method employing a 5 axis CAM procedure for laser milling of 3-D surfaces, especially by partitioning surfaces into overlapping triangular areas to generate beam paths and control/synchronise the movements of the mechanical axes and beam deflectors [78]. Jiang et. al. proposed another method that again generated the scanning paths by partitioning free form surfaces and then the necessary programmes for positioning scan heads and for controlling a five axes gantry machine tool while processing each working area [79]. In another research, Wang et. al. investigated the effects of surface curvature on beam spot shape and energy distribution at the focal point and then used the results

to develop a method for partitioning surfaces and thus to laser process them with required accuracy and quality [76].

The focus of all these investigations was predominantly on developing methods for partitioning 3-D surfaces into fields and then generating the necessary scanning paths for processing each of them following a pre-determined sequence of scan head positions. In particular, these methods generate the necessary beam paths and strategies for laser processing 3-D surfaces but without investigating systematically the factors or processing disturbances that can affect the laser patterning process and ultimately the functional response of the resulting surface topographies. For example, Fig. 5.1a-b depicts a laser processing setup where a 3-D surface is approximated/tessellated into planar fields and each of them is laser processed sequentially. In particular, each field is approximated with a discrete planar field (the red line segments of the curved surface) with different relative angles between their normals and the laser beam ( $\alpha_0, \alpha_1, \alpha_2, \dots$ ). Thus, if this laser processing approach is adopted for patterning 3-D surfaces three factors can affect the resulting topographies and their respective functional response, i.e. focal offset distance (FOD), BIA and spatial differences between the nominal and produced patterns on 3-D surfaces, also referred as geometrical distortions in this research. These factors can be considered as processing disturbances, too, and their effects should be investigated independently, e.g. by patterning planar surfaces/fields that approximate 3-D surfaces as illustrated in Fig. 5.1c.

The processed area of any conventional beam deliver system that integrates a F-theta scan lens is determined in size by its field of view while the pattern quality is affected by its theoretical depth of focus (DOF), defined as two times the Rayleigh range [48]:

$$DOF = \frac{2\pi(\omega_0)^2}{(M^2)\lambda} \quad (5.1)$$

where:  $\omega_0$  is the radius of the beam spot at the focal plane,  $M^2$  - the beam quality factor and  $\lambda$  - the laser wavelength. Thus, as depicted in Fig. 5.1, when an area on a 3-D surface approximated as a tessellated field is processed some points on the workpiece will be in focus, e.g. Point A, while others will be outside of the respective lens's DOF, e.g. Point B (see Fig. 5.1). Sola et. al. demonstrated that laser ablation yields are very dependent on FOD [75,178]. Thus, when a beam delivery system that integrates a F-theta lens is used to process a 3-D surface, homogeneity of the resulting patterns is affected [159].

The other disturbance commonly present when processing 3-D surfaces are deviations of BIA ( $\alpha$ ) from normal. BIA affects the resulting surface patterns and thus the final topography and potentially its functional response due to three reasons mainly, i.e.: i) alterations in reflectance and fluence [74], ii) the fluid mechanics of the molten material when ns and ms laser sources are utilised, and iii) the evacuation of ablated material from the produced patterns [179].

Finally, the other factor that affects the resulting patterns on 3-D surfaces and potentially again their functional response are some geometrical distortions. Such distortions are caused again by deviations of BIA from normal due to the surface curvature, but it is worth investigating their effects separately. For example, as shown in Fig. 5.1c, the nominal design of a channel-like pattern requires the distances between the channels to be equal to  $\Delta l$  however due to the deviation of BIA,  $\alpha$ , from normal the distance will be  $\Delta l'$ , in particular:

$$\Delta l' = \frac{\Delta l}{\cos\alpha} \quad (5.2)$$

Thus, the patterns produced with BIA different from normal will be always distorted compared with their nominal design.

These three processing disturbances can affect not only the patterns created on 3-D surfaces, but also on any surface when it is not correctly positioned in respect to the focal plane (see Fig. 5.1c), or when the beam delivery system is not properly calibrated. In this research, a method to investigate the effects of these three factors in laser patterning 3-D surfaces is presented, especially how their effects can be analysed independently by conducting empirical studies on planar surfaces. A pilot implementation is reported, especially by applying the proposed methodology for producing channel-like patterns on stainless steel plates with a super-hydrophobic functional response. The results are discussed in detail to illustrate how the effects of processing disturbances on topographies, profiles and areal parameters together with the respective functional responses of patterned planar surfaces can be analysed and then used to set constraints in pre-processing 3-D surfaces for follow up laser patterning.

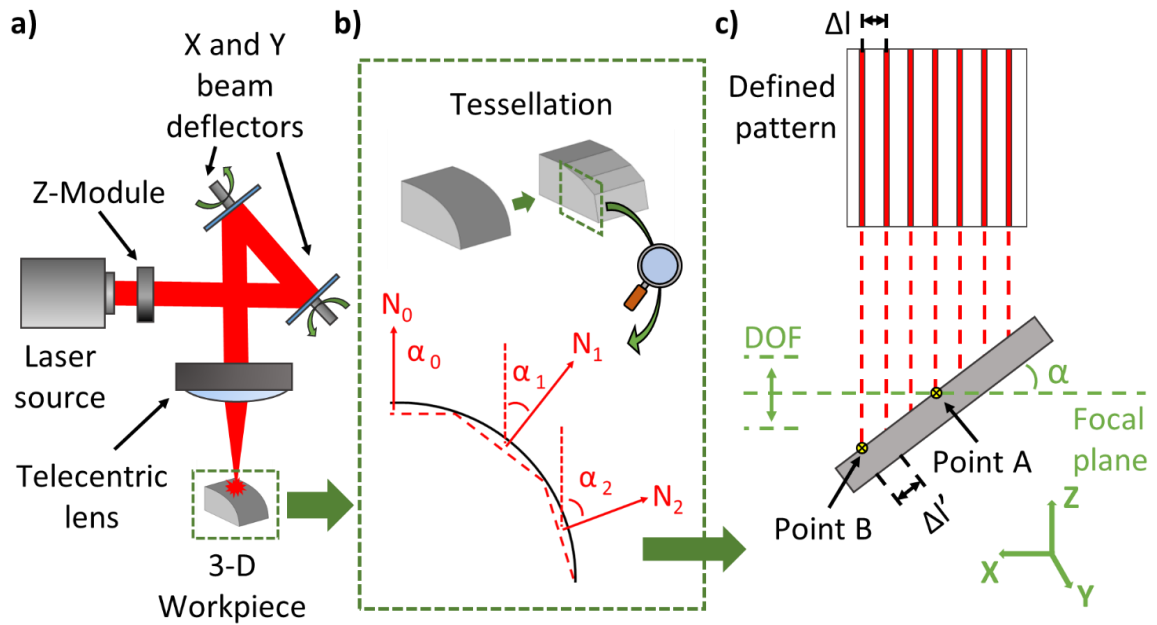


**Fig 5.1.** The laser processing setup (a) employed to produce channel-like patterns on: b) 3-D and c) planar surfaces.

## 5.2 Methods and Experiments

### 5.2.1 Methodology

A methodology is proposed to study the effects of processing disturbances in laser patterning 3-D surfaces. Fig. 5.1b shows a general case of a free-form surface (the black curve) which has to be laser patterned. All three factors affecting the laser patterning process are present in this case, i.e. pattern distortions and FOD and BIA variations. Therefore, a common solution to limit their effects on resulting topographies and hence on their respective functionalities, too, is to pre-process such 3-D surfaces by partitioning/tessellating them into planar fields. For example, the 3-D surfaces can be represented by triangular and square fields, for follow up laser patterning as depicted in Fig. 5.1b, i.e. where the planar fields are represented by line segments of the curve

[78,79]. However, the processing disturbances will be still present when patterning 3-D surfaces partitioned into planar fields (see Fig. 5.1c) together with their effects on topography and functionality. Therefore, the effects of each disturbance should be investigated independently while patterning planar surfaces and so to inform/guide partitioning/tessellation processes by setting constraints. In particular, three different sets of samples on planar surfaces can be produced to investigate their effects independently. Especially, the samples in each set can be patterned by varying the values of only one factor at a time as follows:

- *Pattern distortion*: For example, the distance between the channels will vary when patterning a 3-D surface as shown in Fig. 5.1c due to variations of BIA. To investigate this factor independently from the BIA variation a set of samples should be patterned in focus with a beam normal to the surface while the distance between channels should be varied gradually, e.g. as in the pilot implementation of the proposed methodology from 100 to 350  $\mu\text{m}$  with an increment of 50  $\mu\text{m}$ .
- *FOD*: When patterning a field on a 3-D surface, the FOD will depend on the set focal plane as shown with the green line in the general case depicted in Fig. 5.1c while the other two factors will be present, too. Therefore, a set of samples should be patterned with a beam normal to the surface without any pattern distortion. For example, in the pilot implementation the channel distance was maintained at 100  $\mu\text{m}$  while only FOD was varied along the Z axis from 0 (patterning in focus) with an increment of 250  $\mu\text{m}$ , both above and below the focal plane. The FOD convention sign in this research was positive when the focal plane was above the sample and negative when it was below.

- *BIA*: Again, to investigate independently the *BIA* effects in patterning 3-D surfaces from other two factors, a set of samples should be patterned in focus without any pattern distortion, e.g. constant channel distance, while varying only *BIA*.

Then, the resulting topographies on the samples in each of the three sets should be analysed to determine quantitatively if there are any deviations due to the considered three factors. For example, Fig. 5.2a-c depicts representative profiles on the three sets of samples produced in the pilot implementation of the proposed methodology. By analysing them it is possible to determine the deviations caused by each factor (the continuous coloured profiles in the figure) in comparison to the reference pattern (the black dashed profiles), i.e. the profiles of a sample produced at focus, with normal *BIA* and without pattern distortion, i.e. with the nominal channels' distance, respectively.

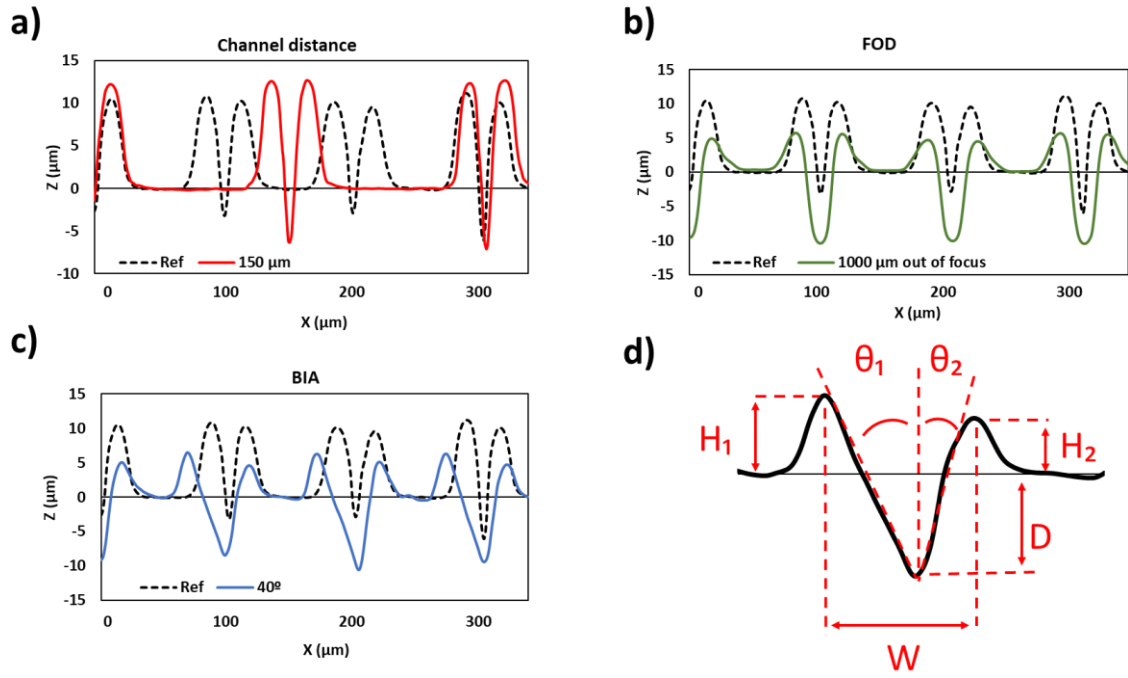


**Fig 5.2.** Representative examples of profiles for the three sets of samples produced with: a) varying channel distance, b) FOD, c) BIA and d) the different surface parameters measured on profiles of the samples produced with BIA deviations. The black dashed lines represent the reference sample produced at focus with 100  $\mu\text{m}$  distance between lines and BIAS of  $0^\circ$  while the coloured solid lines represent the patterns' profiles.

In particular, the surface profiles of the samples can be analysed quantitatively by calculating the deviations ( $Dev$  [%]) of surface profiles in respect to the reference one, using the following equation:

$$Dev (\%) = \frac{|Ref - Measured|}{Ref} 100 \quad (5.3)$$

where:  $Ref$  is the value of the considered surface profile parameters, e.g.  $D$ ,  $W$ ,  $H_1$ ,  $H_2$ ,  $\theta_1$  or  $\theta_2$  in Fig. 5.2d, obtained on the reference sample, and  $Measured$  are the

respective values obtained on profiles produced when the processing disturbances were present, i.e. the increasing FOD and the BIA deviation from normal.

Altogether, the effects of the considered three factors on surface functionality should be used to set limits on any considered profile variations in order to obtain acceptable results when processing 3-D surfaces. In particular, the results from the investigated dependences between the surface functional response, e.g. its wettability, and the considered three processing disturbances can be used to set limits on channel distortions, FOD and the BIA deviations when patterning 3-D surfaces (see Fig. 5.1). Then, indirectly through these limits, it will be possible to set constraints in pre-processing 3-D surfaces, i.e. to drive their partitioning/tessellation into planar fields, for follow up laser patterning. For example, the maximum offset of the fields representing the 3-D surface, i.e. the distance between the line segments and the surface in Fig. 5.1, can be set at a given value in order to retain the desired functional response. In addition, the results can be entered in proprietary software as Smartpatch [180] and CALM [181] to optimise the partitioning process, e.g. to minimise the laser patterning time.

## **5.2.2 Experiments**

A pilot implementation of the proposed methodology required three set of samples to be produced as described in Section 2.1. The patterns selected for this empirical study are channel-like structures that are commonly used and also investigated by many researchers for fabricating surfaces with a hydrophobic functional response [20,54,148,163].

The three set of samples were patterned using a SPI redEnergy G4 50W HS-S MOPA-based Yb-doped fibre nanosecond (ns) source with a wavelength of 1064 nm and random polarisation, integrated into a laser micro-machining (LMM) platform. The laser source had  $M^2$  better than 1.2 and a maximum repetition rate of 1MHz, while the pulse duration could be modulated from 15 to 220 ns. The beam delivery system of the LMM platform integrates a 3-D scan head, i.e. a Z-module and X and Y beam deflectors (RhoThor RTA), and a 100 mm telecentric focusing lens (See Fig. 5.1). A spot size of 35  $\mu\text{m}$  was obtained at focus on this system, while the maximum achievable scanning speed was 2.5 m/s. Furthermore, the 3D scan head through the use of the Z-module allowed high dynamics movements of the focal plane in a range up to 7.7 mm along the lens' axis and thus to enable laser processing within a 35 x 35 x 7.7 mm volume.

In addition, the LMM platform integrates a stack of mechanical stages that allows the sample positioning in X, Y and Z together with rotary movements around X and Z axis, with positioning resolutions of 0.25  $\mu\text{m}$  and 45  $\mu\text{rad}$ , respectively. In the pilot implementation of the proposed methodology the Z stage was used to investigate the FOD effects, i.e. to reposition the focal plane along the Z axis. At the same time, the X rotary stage was used to vary BIA with an increment of 5°. Especially, after setting up the samples at a given BIA, the Z-module of the 3-D scan head was used to reposition the focal plane when processing each channel [23]. At the same time, the nominal distance between channels ( $\Delta l$ ) was varied to keep the actual distance ( $\Delta l'$ ) on the produced samples the same, i.e. 100  $\mu\text{m}$  (see Fig. 5.1).

Also, the LMM platform was equipped with a confocal displacement sensor, i.e. a CCS Prima sensor, for positioning the processed surfaces, especially for setting up very accurately the origins of samples' coordinate systems in regard to the focal plane.

However, it was necessary to limit the maximum BIA investigated in this research to 40° due to limitations of the used setting up procedure, especially the reflectivity of the stainless steel plates impeded the correct performance of the confocal sensor when the tilting angle was bigger than 40°.

Processing parameters	
Scan strategy	Channels
Scan speed (mm/s)	150
Hatch distance (μm)	100
Pulse duration (ns)	220
Pulse frequency (kHz)	70
Pulse energy (μJ)	172.1

**Table 5.1.** Laser processing parameters

All samples in the three sets were produced on ferritic stainless steel X6Cr17 plates with 0.7 mm thickness and a diameter of 36 mm. The same laser processing parameters were used to pattern all samples and they were selected based on previous results [28]. Laser processing parameters are shown in Table 5.1, especially, channel-like patterns were produced by consecutive parallel scans of the laser beam with a speed of 150 mm/s while the distance between scanned lines was 100 μm. Pulse duration was set at 220 ns to produce deeper channels and higher bulges, i.e. the deposited molten material on the sides of the channels. Pulse repetition rate and energy were set at 70 kHz and 172.1 μJ, respectively. Each sample was produced 3 times, and 3 different measurements in different areas of the patterned surfaces were taken, and thus 9 measurements in total were obtained from each sample. Then, the average values with their standard deviations were calculated based on these 9 measurements.

The produced patterns were analysed with SEM micrographs created using a JEOL JCM-600 Benchtop Scanning Electron Microscope. An Alicona G5 focus variation microscope was utilized to inspect the patterned areas. In particular, the effects of investigated three factors on areal surface parameters and 3D topographies of the patterned surfaces were analysed using a x20 magnification lens, with a vertical resolution of 50 nm. Surface topographies of the samples were captured and the profiles of the patterns, cross-sections perpendicular to the channels, were measured using the Profile Form Measurement tool integrated in the Alicona software, which calculates the average values of considered profile parameters. Especially, the specific measurements taken on the samples produced in the pilot implementation of the methodology (see Fig. 5.2) were the depth (D) and width (W) of the channels, and the height of the bulges (H). Regarding the set of samples produced with different channel distances, only the areal surface parameters were studied, as the profile differences were marginal. For the set of samples produced with the BIA deviations, the channels' profiles were not symmetric, and therefore the height of the bulges on both sides was analysed separately, i.e. as  $H_1$  and  $H_2$  in Fig. 5.2d. Furthermore, the tapering angles of the channels' walls were different, in particular bigger on one side ( $\theta_1$ ) and smaller on the other ( $\theta_2$ ). It should be noted that the bigger  $H_1$  and  $\theta_1$  were for the wall side incident to the beam.

Furthermore, the areal surface parameters were obtained for each sample, in particular, the arithmetic mean height of the surface (Sa) and the true to projected area ratio (Ar) were found relevant, and were analysed further in this research. Ar was selected because this areal parameter represents the relation between the true area of a surface and its projected area and provides information about the aspect ratio of the patterns that affects the wettability of surfaces [6]. Pearson correlation analysis was conducted

to identify potential correlations between the three disturbances and areal parameters and functionality of patterned surfaces.

Areal surface parameters were obtained using the x20 magnification lens with a measured field of 811.645  $\mu\text{m}$  x 811.645  $\mu\text{m}$ , and vertical resolution of 50 nm. The integrated software applies a Gaussian filter for inclined planar surfaces, as specified in the ISO 11562 standard for areal surface roughness measurements. The cut-off value for roughness and waviness dataset used ( $\lambda_c$ ) was 162.329  $\mu\text{m}$  and was automatically selected by the Alicona MeasureSuite software in order to obtain the primary surface dataset.

All together, the impact of investigated processing disturbances on functional responses of patterned surfaces were studied by measuring the static contact angles (CA) with an optical tensiometer, i.e. Attension Biolin Scientific Theta T2000-Basic+, with 6  $\mu\text{l}$  Milli-Q water droplets. It is worth noting that samples were only cleaned with compressed air after the laser patterning to remove debris. No chemicals were used to clean the surfaces to avoid surface contamination and any other side effects. Samples were kept in plastic boxes in ambient conditions, and the contact angles were measured after one month.

### **5.3 Results and discussion**

The results from the pilot implementation of the proposed methodology obtained from the three set of samples produced as described in Section 2.2 are reported and discussed in this section. Especially, the effects of channel distance, FOD and BIA on

surface topography, profiles, surface parameters and functional response together with their potential use in partitioning 3-D surfaces are reported and discussed.

### **5.3.1 Effects on surface topography**

The effects of the investigated three factors, i.e. channel distance, FOD and BIA, on resulting surface topographies are depicted in Fig. 5.2. Especially, the resulting topographies on the samples produced by varying channel distance, FOD and BIA from 100  $\mu\text{m}$ , 0 mm and 0 degrees to 150  $\mu\text{m}$ , 1 mm and 40 degrees, respectively, are provided there. The SEM micrographs of the same samples shown in Fig. 5.2 are given for comparison in Fig. 5.3. Fig. 5.3a-b depict the reference pattern that corresponds to the black dashed profile in Fig. 5.2.

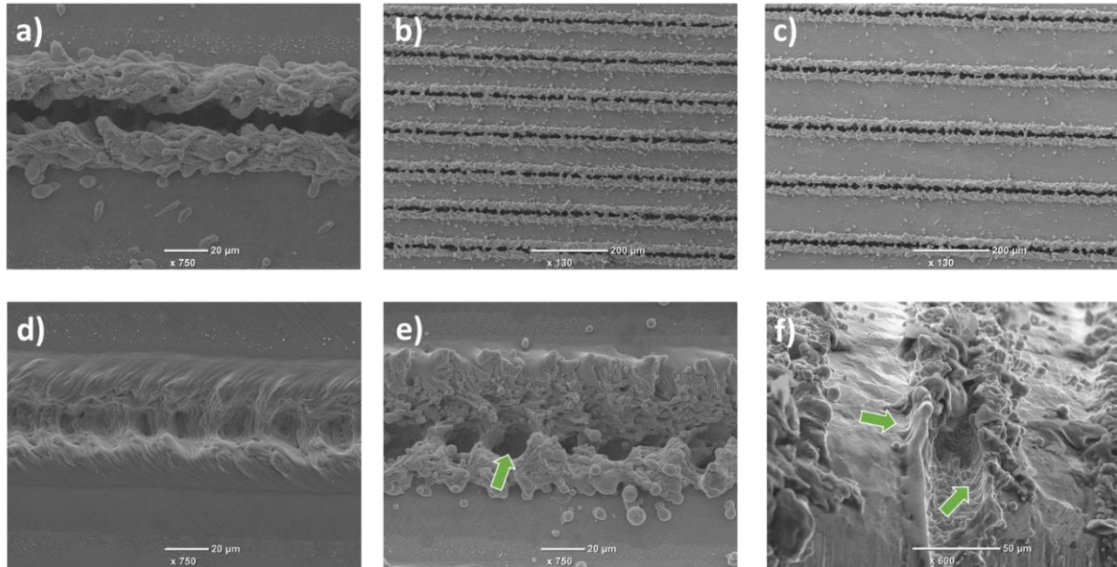


**Fig 5.3.** SEM micrographs of channels on a reference sample produced with 100  $\mu\text{m}$  distance between them and without FOD and BIA deviations in a) and b) with x750 and x130 magnifications, respectively. SEM micrographs of channels on samples produced with: c) an increased distance between them to 150  $\mu\text{m}$ , d) FOD of 1 mm, and e-f) BIA of 40°.

As expected, due to relatively high thermal load when a nanosecond laser is used, the channels are surrounded by bulges, i.e. depositions of molten material along the beam path. As a result of the quick solidification the bulges are relatively rough and porous and this can explain the changes of wetting properties, especially the transition to hydrophobicity of patterned surfaces [15, 28].

The analysis of micrographs in Fig. 5.3b-c suggest that the change of the channel distance from 100 to 150  $\mu\text{m}$  did not affect the resulting topography and therefore are not discussed further. At the same time, FOD of 1 mm led to a clear increase of channels' width and depth, while the resulting bulges were less pronounced compared to the reference pattern (see Fig. 5.2b and Fig. 5.3d) and also the porosity was greatly reduced.

As a result of the other processing disturbance, i.e. the BIA increase to 40° from normal, the channel profiles were not symmetrical anymore (see Fig. 5.2c and Fig. 5.3e-f). In particular, the deposition of ablated and melted material led to different bulges' height and tapering angles along the channels, especially a higher deposition and bigger tapering angles were observed on the beam incident wall side. This can be explained with the competing phenomena when laser processing is performed with a beam not normal to the surface, especially due to alterations in reflectance and fluence [19], the fluid mechanics of the molten material and also one sided evacuation of ablated material from the channels [27]. In addition, it is worth noting that there were some deep craters and even some small undercuts formed on the channels' side opposite to the beam incident one where the melted material was evacuated (see green arrows in Fig. 5.3e-f).

## **5.3.2 Effects on surface profiles**

The laser patterns produced in the presence of FOD and BIA deviations were compared with the reference one, i.e. processed at focus with a beam normal to the surface.

### **5.3.2.1 FOD effects**

The surface profiles on the samples produced with FOD were measured and the results are provided in Fig. 5.4. The height of the bulges (H) on the reference sample was the highest and then it decreased with the FOD increase as shown in Fig. 5.4a. At the same time, the depth of the channels (D) increased initially, as expected [75], and picked at

FOD of 1 mm (see Fig. 5.4b) with two maximums, both above and below the focal plane. The width of the channels increased when FOD was above the focal plane, while initially decreased when FOD had negative values up to 1 mm but only marginally before it started increasing again as depicted in Fig. 5.4c.

The standard deviations of D were higher, and this can be attributed to the bigger volume of molten material deposited along the channels' edges that even led to closures of the laser path (see Fig. 5.3a). The other reason for this big standard deviation are the limitations of the focus variation technology, in particular its capabilities to inspect high aspect ratio channels. At the same time, DOF of the laser used in this research was calculated with Eq. 5.1 and it was 1500  $\mu\text{m}$ . Thus, theoretically acceptable patterning results should be expected within a range of 750  $\mu\text{m}$  above and below the focal plane.

The deviations of the resulting profiles from the reference one were calculated using Eq. 5.3 and plotted in Fig. 5.4d. The maximum deviations of H, D and W values were 87%, 196% and 64%, respectively, D was the most affected profile parameter by the FOD increase and therefore it could be considered a critical constrain in producing surfaces with designed topographies. Especially, the maximum deviations of D resulted from FOD values of 1000  $\mu\text{m}$  and 750  $\mu\text{m}$ , below and above the focal position, respectively, that were only marginally outside the calculated DOF. In the case of H and W, the deviations obtained within the calculated DOF were smaller than the 30% and 15% respectively, as can be seen in Fig. 5.4e.

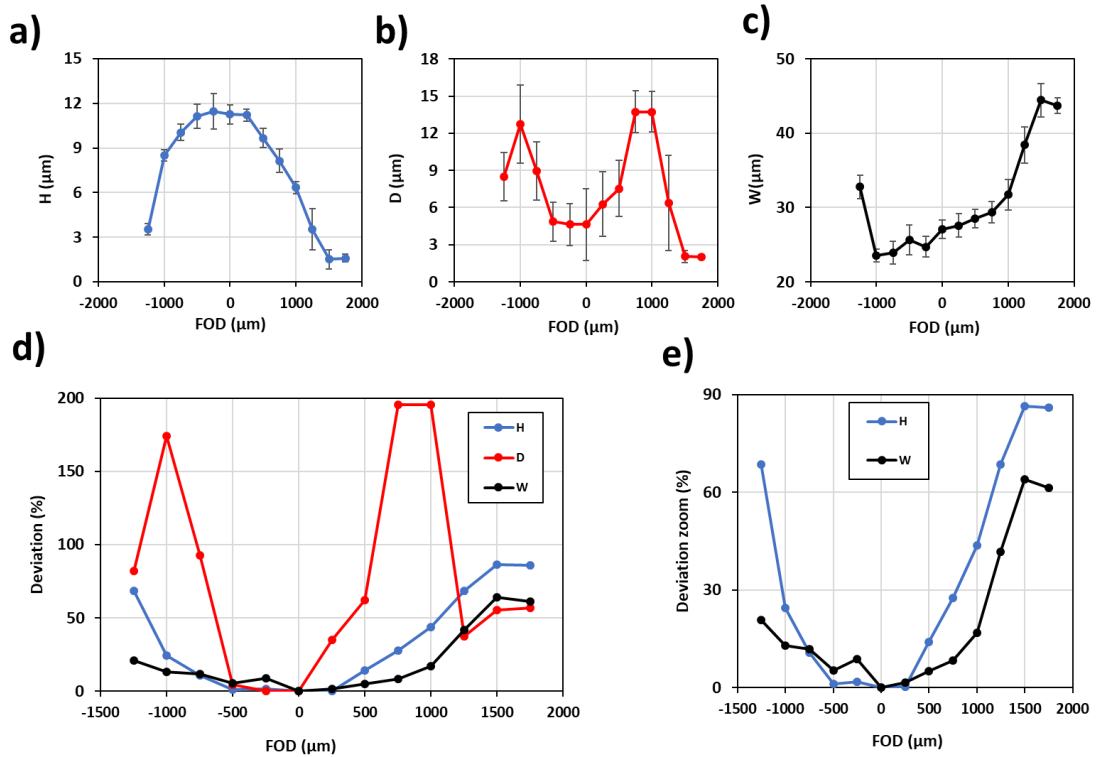


**Fig 5.4.** Surface profile parameters of samples produced with increasing FOD, i.e.: a) bulges' height,  $H$ ; b) channels depth,  $D$ ; c) channels width,  $W$ ; and d-e) their deviations from the reference profile.

### 5.3.2.2 BIA effects

The evolution of surface profiles on the samples produced with BIA deviations from normal is depicted in Fig. 5.5. As it can be clearly seen, the bulges' height on both sides of the channels was reduced almost equally, especially  $H_1$  on beam incident side was only slightly higher than  $H_2$  (see Fig. 5.5a). The channels depth,  $D$ , varied within a small range when BIA deviated from normal, however the standard deviation of the measurements was relatively high (see Fig. 5.5b) due to the same reasons as those in the case of FOD. The standard deviation of  $D$  was reduced with the BIA increase as the channels were getting wider ( $W$  increased as shown in Fig. 5.5c) and thus the

measurement uncertainty was reduced. Furthermore, the  $W$  increase facilitated the evacuation of molten and vaporised material from the channels and this could explain the  $D$  increase when BIA was higher. At the same time, as expected the tapering angles,  $\theta$ , increased progressively with the increase of BIA (see Fig. 5.5d) however this increase was much more pronounced on the beam incident side of the channels, i.e. for  $\theta_1$  that reached  $64^\circ$  when BIA was at  $40^\circ$ .

The deviations of the resulting profiles from the reference one were calculated using Eq. 5.3, again, and plotted in Fig. 5.5e. As expected, the deviations of all surface profile parameters increased with the increase of BIA.

As it was already stated the increase of  $\theta_1$  was significant and it was not surprising that the  $\theta_1$  deviation was the biggest, i.e. 150%, while the deviations for the other surface profile parameters were less than 50% for any BIA up to  $35^\circ$  (see Fig. 5.5e). Magnified views of  $\theta$ ,  $D$  and  $H$  &  $W$  deviations are provided in Fig. 5.5f-h, respectively. As it was already stressed, the BIA increase had a big impact on  $\theta_1$  and therefore, this profile parameter would be critical for obtaining surface profiles with acceptable deviations. In particular,  $\theta_1$  deviations were initially smaller for BIA up to  $5^\circ$  but then there was a steep increase to values higher than 30% at BIA of  $10^\circ$  (see Fig. 5.5f). At the same time the  $\theta_2$ , deviations increased progressively to reach maximum values of approximately 30%. Regarding  $D$ , there was no clear trend that can be explained with the high standard deviations discussed before (see Fig. 5.5g) and the values did not exceed 50%. The trends for the other profile parameters, i.e.  $H$  and  $W$ , were very similar and the deviations were less than 15% for BIA up to  $10^\circ$ , and then they increased progressively (see Fig. 5.5h).

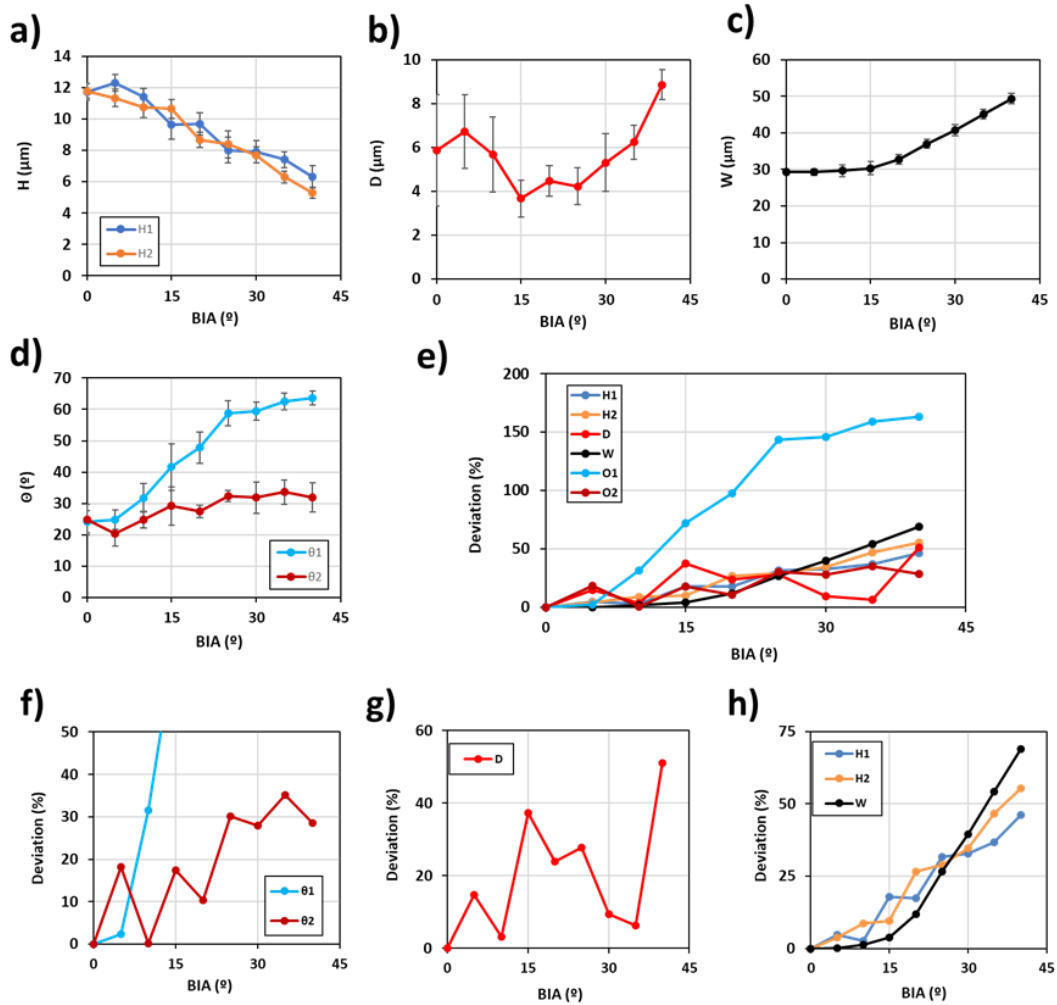


**Fig 5.5.** Surface profile parameters of samples produced with varying BIA, i.e.: a) bulges' heights ( $H$ ); b) channels' depth ( $D$ ); c) channels' width ( $W$ ), d) walls tapering angles ( $\vartheta$ ); and e-h) their deviations from the reference profile.

### 5.3.3 Effects on areal surface parameters

The effects of increasing FOD, BIA and the channel distance on areal surface parameters were analysed, i.e.  $S_a$  and  $A_r$ , were studied (see Section 2.2).

Fig. 5.6a-c plot  $A_r$  values obtained for the three sets of samples produced with the increasing channel distance, FOD and BIA. It was found that the  $A_r$  values peaked on the reference pattern ( $A_r = 1.57$ ) and then decreased progressively with the increase of

processing disturbances. As expected, the area factor decreased linearly with the increase of the channel distance as shown in Fig. 5.6a. The shift in the trend for the last two points could be explained with the bigger distance between the channels and therefore there was less channels within the microscope field of view. The evolution of  $A_r$  with the FOD increase is depicted in Fig. 5.6b. Due to the higher ablation efficiency, i.e. higher  $D$ , and the reduced material deposition, i.e. lower  $H$ , when processing out of focus, the  $A_r$  values peak in focus. Then, there is a relatively small  $A_r$  decrease with the FOD increase up to 1mm while any further increases resulted in much steeper  $A_r$  decrease (see Fig. 5.6b). The BIA increase led to a progressive  $A_r$  decrease in line with the surface profile evolution, especially the increase of profile deviations (see Fig. 5.6c).  $S_a$  is plotted in Fig. 5.6d-f, and again the  $S_a$  values peaked on the reference sample, i.e.  $S_a$  was  $5.16 \mu\text{m}$ , and then decreased for the three sets of samples progressively with the increase of all three processing disturbances.

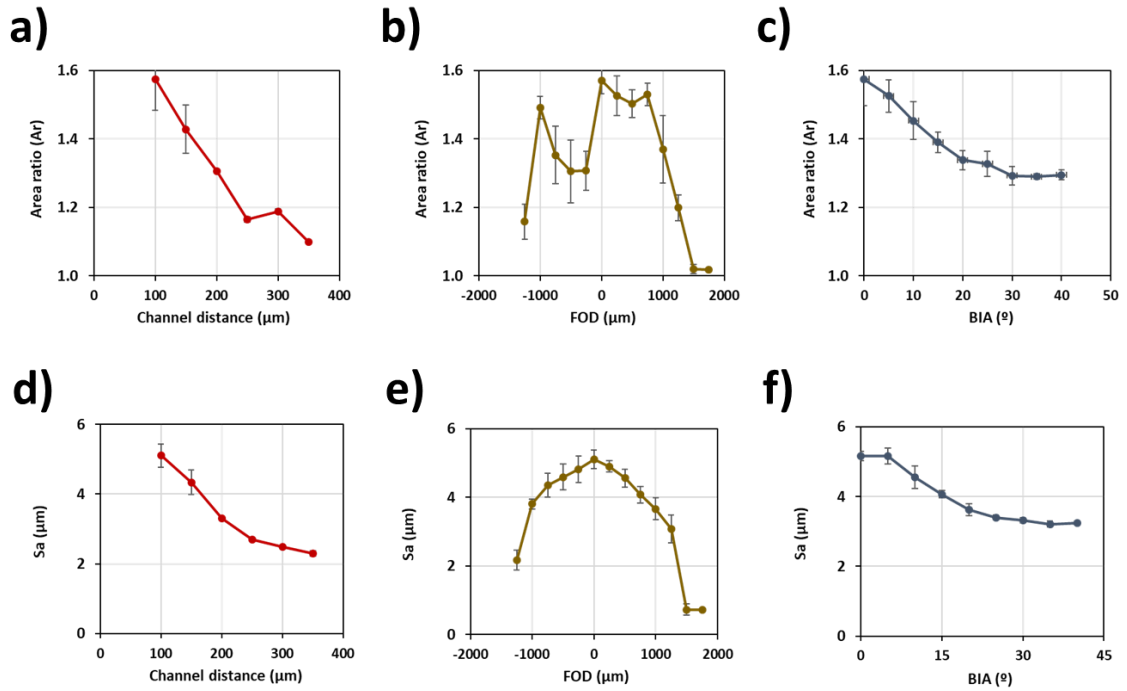


**Fig 5.6.** Areal surface parameters: a-c) area ratios, Ar; and d-f) arithmetical mean heights, Sa, for the set of samples produced with the three processing disturbances, i.e. channel distance, FOD and BIA, respectively.

### 5.3.4 Effects on functional response

The relation between the functional response, i.e. the static contact angles (CA), of surfaces produced with increasing channel distance, FOD and BIA are depicted in Fig. 5.7a-c, respectively. The surfaces with a channel distance less than 200 μm were super hydrophobic, i.e. CA higher than 150°, as shown in Fig. 5.7a and then decreased progressively due to the decreasing roughness, indicated by both Sa and Ar in Fig. 5.6a and 6d. This surface functional response can be explained with the Cassie-Baxter state where as a result of the progressive roughness decrease there is less air trapped in the channels, especially the lower roughness leads to changes in the area fraction of the

water-solid area to the projected area between the drops and the surface [182]. Furthermore, as the distance between channels increases, water drops can touch the untreated surface and spread and thus to reduce its hydrophobicity. There was a similar surface response to the FOD increase, especially the patterned surface remained super hydrophobic when FOD was less than 1mm, both above or below the focal plane, and then decreased progressively (see Fig. 5.7b). Again, this can be explained with the Cassie-Baxter state where due to the decreasing surface roughness (see Fig. 5.6b and 6e), there is less air trapped in the channels and also there is less absorption of airborne organic substances because of the smaller bulges and lesser porosity (see Fig. 5.3d) [127]. Regarding the other processing disturbance, super hydrophobicity of the patterned surface was not affected by the BIA increase and remained constant and higher than  $160^\circ$  (see Fig. 5.7c) in spite of the roughness decrease. This can be explained with the high surface porosity of the bulges (See Fig. 5.3e-f), and also the slower decrease of areal surface parameters i.e. both  $S_a$  and  $A_r$  (See Fig. 5.6c and 6f), and much lesser deviations of surface profile parameters compared with those resulting from the FOD increase. As the contact between drops and surfaces takes place onto the bulges, and the distance between the channels was maintained the same when BIA was varied, the drop-air surface did not change sufficiently to induce CA changes. Furthermore, as the BIA experiments were conducted at focus, i.e. with zero FOD, the porosity of the bulges was kept the same, and thus any CA changes in time should be attributed to the absorption of airborne organics. It is worth noting that the maximum BIA studied in this research was  $40^\circ$ , due to limitations in the laser processing setup, while the maximum tapering angle was approximately  $60^\circ$ . It could be expected that the tapering angles could increase to almost  $90^\circ$  if higher BIA than  $40^\circ$  were used and thus the contact

between drops and surfaces would increase, too, in a decrement of air trapping, and hence could lead to a CA decrease.

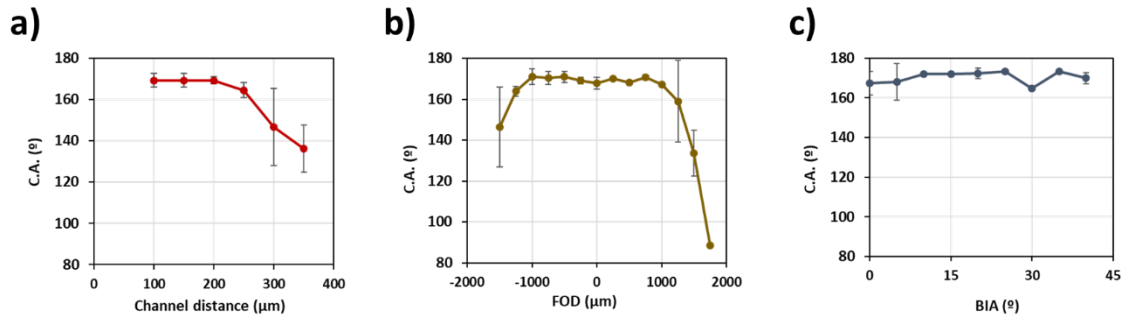


**Fig 5.7.** Contact angles, CA, for the set of samples produced with the three processing disturbances, i.e. a) channel distance, b) FOD and c) BIA, respectively.

### 5.3.5 Correlations between disturbances, areal parameters and functional response

The resulting surface patterns were very sensitive to processing disturbances, i.e. FOD and BIA, that are commonly present in laser patterning of 3-D surfaces (see Section 3.2). However, it is even more important to determine how the evolution of resulting patterns as a result of increasing FOD, BIA and the channel distance affects the functional response of surfaces and if there is any correlation to the areal surface parameters. This is important as a potential solution for monitoring the laser patterning process and thus to use such correlations for triggering routines that can keep the process in control. Therefore, Pearson correlation analysis was conducted to examine the relationship between the functional response, i.e. the surface hydrophobicity, and either processing disturbances or the two areal surface parameters, i.e. Sa and Ar,

investigated in this research, but also the correlation between the disturbances and the areal surface parameters.

The results of Pearson correlation analysis between the studied disturbances and the areal surface parameters of patterned surfaces together with their respective P-values are provided in Table 5.2. They confirm that the two parameters, i.e. Sa and Ar, considered in this research can be used to monitor whether the patterning process is in control. In particular, all Pearson correlation coefficients between disturbances and areal parameters are higher than 0.8, and very close to 1 in most of the cases, while the P-values are less than 0.05. Thus, there is a very strong correlation and Ar and Sa can be considered good indicators about the process performance. Especially, the process can be considered in control in regards to the resulting surface profiles, and thus they can be employed for inline monitoring, e.g. by integrating a focus variation sensor in laser processing setups [183].

Regarding the functional response, there is a strong correlation with two disturbances, i.e. channel distance and FOD, but it is less pronounced compared with that to areal parameters and it is statically significant only in respect to FOD. At the same time, there is no correlation between BIAs and CAs as it has been already indicated in Fig. 5.7c.

The correlation between areal parameters and disturbances is very strong and thus by knowing the interrelation between the disturbances, i.e. channel' distance, FOD and BIA, and the functionality (see Fig. 5.7), it is possible indirectly to judge what will be the functional response. In particular, when 3-D surfaces are laser patterned and thus the three processing disturbances investigated in this research are present, the process can be considered as performing acceptably or the targeting hydrophobic properties are still present if Sa and Ar are higher than 3  $\mu\text{m}$  and 1.3, respectively.

	FOD		Ch distance		BIA	
	Pearson	P-Value	Pearson	P-Value	Pearson	P-Value
<b>Disturbance vs Sa</b>	-0.93	0.0	-0.96	0.0024	-0.95	0.0001
<b>Disturbance vs Ar</b>	-0.80	0.0011	-0.96	0.0024	-0.94	0.0001
<b>Disturbance vs CA</b>	-0.70	0.0072	-0.89	0.0170	0.19	0.6285
<b>Sa vs CA</b>	0.82	0.0006	0.73	0.0973	-0.29	0.4427
<b>Ar vs CA</b>	0.73	0.0050	0.73	0.0979	-0.29	0.4546

*Table 5.2. Pearson coefficients together with P-values for the investigated correlations between disturbances, areal parameters and contact angles.*

### 5.3.6 Patterning of 3-D surfaces

The results obtained with the proposed methodology can be used to set constraints in pre-processing 3-D surfaces for follow up laser patterning and thus to maintain the desired functional response within acceptable limits while minimising the processing time. For example, the results from its pilot implementation in this research can be used to drive the partitioning/tessellation process when channel-like patterns are used for producing hydrophobic surfaces, especially by setting limits on processing disturbances. In particular, the wettability achieved on the reference surfaces was maintained only when FOD was varying within the range from -1000 to 1000  $\mu\text{m}$  and the distance between channels did not exceed 200  $\mu\text{m}$ . At the same time BIA deviations had only a marginal effect and should be constrained to  $60^\circ$  as otherwise the channel distance can exceed 200  $\mu\text{m}$  (see Section 3.4).

The proposed methodology for setting up constraints in pre-processing 3-D surfaces is generic and can be applied for producing different functional patterns and also on other materials than stainless steel. However, while the methodology is generic the produced topologies are dependent on the laser material interactions in any specific laser processing setup and also on the selected patterns for achieving a given functional response. Therefore, an empirical study as described in this research should be executed to determine what are the constraints on processing disturbances, i.e. pattern distortion, FOD and BIA deviations from normal, that should apply in pre-processing 3-D surfaces for any given functional pattern and workpiece material. And, again the functional response of three sets of samples should be investigated in order to set these constraints and thus to make sure that the desired functionality varies only within an acceptable range. All together, as it was already mentioned the results from such empirical studies can be used in proprietary software as Smartpatch and CALM to optimise the partitioning process.

## **5.4 Conclusions**

A methodology is proposed in this research to investigate the effects of three process factors, also referred to as processing disturbances, i.e. pattern distortion, FOD and BIA, that can be present in laser patterning 3-D surfaces. A pilot implementation of this methodology is reported to illustrate how the effects of these processing disturbances on topographies, profiles and areal parameters together with the respective functional responses of patterned planar surfaces can be analysed and then used to set constraints in pre-processing 3-D surfaces for follow up laser patterning. The results are analysed

in detail to show how such constraints can be set on channel-like patterns for producing surfaces with hydrophobic properties. In particular, the following conclusions can be made based on the results in this pilot implementation of the proposed methodology:

1. The analysis of the surface profile parameters has shown that the depth of the channels was the most sensitive to the FOD increase and therefore it is important process setting up parameter in determining the laser patterning window. However, it is worth noting that DOF of a given laser source could be a good indicator for maintaining the surface profile parameters within acceptable limits because the depth maximum deviations were obtained when FOD exceeded DOF.
2. The BIA increase had a big impact on the tapering angle, especially on the beam incident side of the channels, and therefore this profile parameter could be critical when processing 3-D surfaces.
3. The areal surface parameters, i.e.  $A_r$  and  $S_a$ , can be considered good indicators about the process performance. A strong correlation between disturbances and these resulting surface parameters was demonstrated. Especially, they can indicate if the process is still performing acceptably in regards to the resulting surface profiles and thus can be used for inline monitoring of the laser patterning process.
4. Two processing disturbances, i.e. channel distance and FOD, had a similar effect on functional response of patterned surfaces, i.e. their hydrophobicity. In particular, the surfaces with a channel distance less than 200  $\mu\text{m}$  were super hydrophobic and then hydrophobicity decreased progressively due to the increasing deviation from the reference patterns and decreasing roughness.

There was a similar surface response to the FOD increase, especially the patterned surface remained super hydrophobic when FOD was less than 1mm, both above or below the focal plane, and then again decreased progressively.

5. The BIA increase did not have a negative effect on functional response of patterned surfaces, i.e. their hydrophobicity. In particular, super hydrophobicity of the patterned surface was not affected by the BIA increase in spite of the roughness decrease. This was attributed to the relatively slower decrease of the surface roughness and much lesser deviations of surface profile parameters except the bulges' height compared with those resulting from the FOD increase.
6. There was a strong correlation between two disturbances, i.e. channel distance and FOD, and the functional response of the laser patterned surfaces. At the same time, there was no correlation between BIAs and hydrophobicity and thus this confirmed that the surface functional response was not sensitive to the BIA increase. So, when patterning 3-D surfaces it would be necessary to introduce constraints regarding FOD and channel distance. In addition, due to the strong correlation between FOD/channel distance and areal surface parameters it will be possible by monitoring them to judge indirectly if hydrophobic properties are still present.

## **Acknowledgements**

The research reported in this paper was carried out within the framework of European Commission H2020 ITN programme "European ESRs Network on Short Pulsed Laser Micro/Nanostructuring of Surfaces for Improved Functional Applications"

([www.laser4fun.eu](http://www.laser4fun.eu)) under the Marie Skłodowska-Curie grant agreement No. 675063.

The work was supported by two other programmes, i.e. the H2020 project “High-Impact Injection Moulding Platform for mass-production of 3D and/or large micro-structured surfaces with Antimicrobial, Self-cleaning, Anti-scratch, Anti-squeak and Aesthetic functionalities” (HIMALAIA) and the UKIERI DST project “Surface functionalisation for food, packaging, and healthcare applications”. The authors would like also to acknowledge the support and assistance of GF Machining Solution.

## **Chapter 6**

---

### **Contribution to knowledge and future research**

---

This chapter summarises the main contributions to knowledge claimed in this research. Furthermore, future steps and research directions are discussed in the chapter.

## 6.1 Contributions

The aim of this research was to study the limitations of laser-enabled surface functionalization, in particular durability of functional patterns and associated processing issues affecting the patterning of 3D parts, especially for creating hydrophobic surfaces. The durability was improved by combining plasma surface alloying and laser patterning and thus to increase the hardness and wear resistance of the base substrate before creating the hydrophobic pattern. The effects of laser interactions with plasma alloyed surfaces were investigated in **Chapter 3** while the durability of the produced hydrophobic patterns was studied in **Chapter 4**. The limitations of 3D surface patterning were analysed in **Chapter 5** where a method was proposed for investigating the effects of processing disturbances on topography and functionality of the resulting surface patterns. Also, it was discussed how the results of such systematic investigations can inform the process design and allow an “adaptive” surface partitioning when processing 3D parts.

The main objectives of the research were achieved and the contributions to knowledge claimed in this thesis are as follows:

- i) *To develop a manufacturing process that combines synergistically the capabilities of plasma surface alloying and laser patterning to fabricate wear resistant hydrophobic surfaces.*

A method for combining low temperature plasma surface alloying and nanosecond laser patterning was proposed, i.e. to increase the substrate hardness and thus the patterns durability, and its pilot application for functionalising ferritic stainless steel surfaces was investigated. In particular, the effects of the laser patterning on plasma alloyed surfaces were studied (**Chapter 3**):

- Nitrogen and oxygen based gases were used to perform low temperature plasma surface alloying of ferritic stainless steel substrates, i.e. nitriding and carburising, to increase their hardness to 1001 and 305 HV, respectively. Channel and pillar like patterns were produced on the alloyed surfaces using 15 and 220 nanosecond lasers, especially to obtain dual scale structures as a result of combined material ablation and re-solidification (recasts) in the form of bulges. The alloyed and then patterned surfaces exhibited super-hydrophobicity and small rolling angles.
- Only the patterned carburised surfaces did not show delamination and remained intact while nitrided ones had cracks. Therefore, it was concluded that nitriding was not an acceptable treatment to achieve the required synergistic effects on patterned surfaces. Nano-hardness tests of patterned carburised surfaces proved that the heat diffusion after the laser treatment did not affect the hardened layer.

ii) *To investigate the wear resistance and durability of plasma alloyed and laser patterned hydrophobic surfaces.*

Mechanical and functional durability of surface topographies with hydrophobic properties fabricated by direct laser patterning was studied on both, ferritic stainless steel and low temperature plasma alloyed surfaces (**Chapter 4**):

- Channel-like patterns were fabricated using a conventional nanosecond laser source with 15 and 220 nanosecond pulses, on plasma carburised surfaces. The resulting topographies showed static contact angles around  $170^\circ$ , with small rolling angles.
- Abrasion test were carried out on the produced samples by adapting a standardised method to test the durability of functional paints and varnishes. 100, 200 and 300 abrasion cycles were performed and the functional response and resulting topographies were analysed.
- Patterns produced with 220 ns laser pulses were more wear resistant in regards of their functionality, as the volumes of the recast, especially the bulges formed on along the channel-like patterns, were larger. Furthermore, the carburised surfaces exhibited higher wear resistance, especially regarding their mechanical durability. In particular, the patterns produced with 220 and 15 ns laser pulses on carburised surfaces showed durability improvements of 28% and 59%, respectively, compared with results obtained on untreated stainless steel.
- The direction of the abrasion cycles had a significant impact on patterns' mechanical durability. Especially, the wear resistance of channel-like patterns was higher when the abrasion movements were parallel to the channels. However, when the abrasion was perpendicular to them, the

functionality was retained for longer, due to the mechanical protection offered by the bulges. In particular, the bulges acted as a shield absorbing the abrasion and maintained intact the surface chemistry inside the channels.

- XPS analysis of laser patterned as-received and carburised surfaces revealed changes in their oxide and carbon peaks. Results suggested that the absorption of airborne carbon-based molecules was the reason for the high hydrophobicity of the substrates.
- The combination of surface hardening, laser patterning and surface coating resulted in a higher retention of hydrophobicity after the wear cycles, compared with the laser patterned and coated stainless steel substrate. The enhanced mechanical properties of the carburised substrates led to a higher wear resistance of the patterns, especially the bulges formed along the channel-like patterns acted as a protection shield for the coating.

*iii) To investigate the effects of key processing disturbances present in laser patterning of 3D surfaces and study their impact on the resulting surface topographies and functionality.*

The effect of processing disturbances in patterning 3D surfaces was studied, i.e. focal offset distance (FOD) and beam incident angle (BIA) deviations together with patterns' distortions. A method for investigating their impact on topography and functionality of the resulting surface patterns was proposed. It was discussed how the outcomes of such systematic studies could inform the

process design and at the same time enable “adaptive” partitioning of 3D surfaces for follow up laser patterning. In particular, a pilot implementation of this methodology on channel-like patterns with hydrophobic properties revealed

**(Chapter 5):**

- The depth of the channels was found to be the most sensitive surface profile parameter to any FOD deviations, and therefore should be monitored closely when processing 3D surfaces.
- The tapering angle of the channels was highly affected by any BIA deviations and therefore should be considered a critical parameter when patterning 3D surfaces.
- Ar and Sa surface parameters were found to be highly informative about the process performance, as there was a strong correlation between them and the considered processing disturbances. They can be used to monitor inline the laser patterning processes, especially when processing 3D surfaces.
- Pattern distortions and FOD deviations affected the functional response, i.e. the hydrophobicity of patterned surfaces, whereas the BIA deviations did not affect their functional response.
- A strong correlation was found between two of investigated disturbances, i.e. the channel distance and FOD deviations, and the functional response. In addition, it was shown that it would be possible to use areal surface parameters to predict and thus to judge about the functional response of produced patterns, indirectly, because of their strong correlation to these two disturbances.

## 6.2 Future research

The carried out research led to some ideas for future research directions, in particular:

- *Nitriding after laser patterning.* Thick hardened layers with high hardness and tension on the surface were obtained after the plasma nitriding process. When the alloyed substrates were laser patterned, this stress was released and led to cracks and delamination. Therefore, the reported research was focused only on the carburising option, however, another feasible solution could be to perform the plasma nitriding after the laser patterning. In this way, the cracking due to the laser processing of hardened layers could be avoided. However, there could be some side effects that should be considered, i.e.: i) the diffusion of nitrogen through the oxides present in the bulges would be highly reduced; ii) the bulges would expand due to the diffusion into the material, resulting in bulkier patterns totally different to those investigated in this research; iii) the absorption of airborne elements from air due to the surface activation after the laser processing would be cancelled, and therefore a chemical treatment would be necessary. Such a solution requires further investigation, especially the durability of the patterned surfaces should be studied together with the stability of the resulting hardened layer.
- *The wear resistance of different patterns.* It was shown that the abrasion direction was an important factor affecting both, the mechanical durability and the surface functionality. Therefore, other surface patterns, e.g. pillar-like, sharklets, etc., can be investigated, too, to see how their durability would be affected on both, untreated and plasma hardened surfaces. Furthermore, it

would be important to identify patterns that could resist heterogeneous wear cycles.

- *Tests on functional components.* The combination of surface hardening and laser patterning was shown to be a good method to increase lifespan of the functional surfaces. In combination with a chemical coating, wear resistant functional surfaces were produced. Furthermore, a method was proposed to identify the processing constraints in patterning 3D surfaces. Thus, the next step should be to apply both methods and thus to manufacture 3D functional components with hardened and laser patterned surfaces and then to investigate their durability in given application area.
- *Other functionalities and materials.* The method presented on Chapter 5 was tested on ferritic stainless steel, and one functional response, i.e. hydrophobicity, was studied. The laser patterning as a method to functionalise surfaces can be applied on other materials, including non-metallic ones, and different functional responses can be investigated, e.g. anti-bacterial or friction reduction properties.
- *The corrosion resistance of plasma hardened and laser patterned surfaces.* It is known that low temperature plasma alloyed surfaces exhibit good corrosion resistance. However, the corrosion resistance may not be maintained if carbide precipitation occurs. At the same time, laser patterned surfaces exhibit good corrosion resistance, as the recasts, i.e. bulges formed after nanosecond laser patterning, are composed mainly of oxides. Thus, it is important to investigate the corrosion resistance of surfaces produced by combining these two processes and compare it with that obtained on untreated stainless steel.

## List of references

- [1] A. Garcia-Giron, J.M. Romano, A. Batal, A. Michałek, P. Penchev, S.S. Dimov, Experimental investigation of processing disturbances in laser surface patterning, *Opt. Lasers Eng.* 126 (2020). doi:10.1016/j.optlaseng.2019.105900.
- [2] T.D. Ngo, *Biomimetic Technologies - Principles and Applications*, 2015.
- [3] K. Liu, J. Du, J. Wu, L. Jiang, Superhydrophobic gecko feet with high adhesive forces towards water and their bio-inspired materials, *Nanoscale*. 4 (2012) 768–772. doi:10.1039/c1nr11369k.
- [4] G.S. Watson, D.W. Green, L. Schwarzkopf, X. Li, B.W. Cribb, S. Myhra, J.A. Watson, A gecko skin micro/nano structure - A low adhesion, superhydrophobic, anti-wetting, self-cleaning, biocompatible, antibacterial surface, *Acta Biomater.* 21 (2015) 109–122. doi:10.1016/j.actbio.2015.03.007.
- [5] B. Bhushan, Adhesion of multi-level hierarchical attachment systems in gecko feet, *J. Adhes. Sci. Technol.* 21 (2007) 1213–1258. doi:10.1163/156856107782328353.
- [6] R. Hensel, C. Neinhuis, C. Werner, The springtail cuticle as a blueprint for omniphobic surfaces, *Chem. Soc. Rev.* 45 (2016) 323–341. doi:10.1039/C5CS00438A.
- [7] K. Koch, B. Bhushan, W. Barthlott, Multifunctional surface structures of plants: An inspiration for biomimetics, *Prog. Mater. Sci.* 54 (2009) 137–178. doi:10.1016/j.pmatsci.2008.07.003.
- [8] W. Barthlott, C. Neinhuis, Purity of the sacred lotus, or escape from contamination in biological surfaces, *Planta*. 202 (1996) 1–8. <https://link->

springer-

com.ezproxyd.bham.ac.uk/content/pdf/10.1007%2Fs004250050096.pdf

(accessed August 7, 2019).

- [9] B.D. Wilts, A. Matsushita, K. Arikawa, D.G. Stavenga, Spectrally tuned structural and pigmentary coloration of birdwing butterfly wing scales, *J. R. Soc. Interface.* 12 (2015) 20150717. doi:10.1098/rsif.2015.0717.
- [10] Y. Luo, L. Yuan, J. Li, J. Wang, Boundary layer drag reduction research hypotheses derived from bio-inspired surface and recent advanced applications, *Micron.* 79 (2015) 59–73. doi:10.1016/j.micron.2015.07.006.
- [11] A.T. Abdulhussein, G.K. Kannarpady, A.B. Wright, A. Ghosh, A.S. Biris, Current trend in fabrication of complex morphologically tunable superhydrophobic nano scale surfaces, *Appl. Surf. Sci.* 384 (2016) 311–332. doi:10.1016/j.apsusc.2016.04.186.
- [12] K. Glinel, P. Thebault, V. Humblot, C.M. Pradier, T. Jouenne, Antibacterial surfaces developed from bio-inspired approaches, *Acta Biomater.* 8 (2012) 1670–1684. doi:10.1016/j.actbio.2012.01.011.
- [13] M. Wakuda, Y. Yamauchi, S. Kanzaki, Y. Yasuda, Effect of surface texturing on friction reduction between ceramic and steel materials under lubricated sliding contact, *Wear.* 254 (2003) 356–363. doi:10.1016/S0043-1648(03)00004-8.
- [14] R. Liao, Z. Zuo, C. Guo, A. Zhuang, X. Zhao, Y. Yuan, Anti-icing performance in glaze ice of nanostructured film prepared by RF magnetron sputtering, *Appl. Surf. Sci.* 356 (2015) 539–545. doi:10.1016/j.apsusc.2015.08.103.
- [15] L.B. Boinovich, A.M. Emelyanenko, The behaviour of fluoro- and hydrocarbon surfactants used for fabrication of superhydrophobic coatings at solid/water

- interface, *Colloids Surfaces A Physicochem. Eng. Asp.* 481 (2015) 167–175.  
doi:10.1016/j.colsurfa.2015.05.003.
- [16] J. Bico, C. Tordeux, D. Quéré, Rough wetting, *Europhys. Lett.* 55 (2001) 214–220.  
doi:10.1209/epl/i2001-00402-x.
- [17] A. Batal, R. Sammons, S. Dimov, Response of Saos-2 osteoblast-like cells to laser surface texturing, sandblasting and hydroxyapatite coating on CoCrMo alloy surfaces, *Mater. Sci. Eng. C.* 98 (2019) 1005–1013.  
doi:10.1016/j.msec.2019.01.067.
- [18] B. Bhushan, Y.C. Jung, Natural and biomimetic artificial surfaces for superhydrophobicity, self-cleaning, low adhesion, and drag reduction, *Prog. Mater. Sci.* 56 (2011) 1–108. doi:10.1016/j.pmatsci.2010.04.003.
- [19] P. Wang, T. Yao, B. Sun, T. Ci, X. Fan, H. Han, Fabrication of mechanically robust superhydrophobic steel surface with corrosion resistance property, *RSC Adv.* 7 (2017) 39699–39703. doi:10.1039/c7ra06836k.
- [20] S. Suzuki, A. Nakajima, K. Tanaka, M. Sakai, A. Hashimoto, N. Yoshida, Y. Kameshima, K. Okada, Sliding behavior of water droplets on line-patterned hydrophobic surfaces, *Appl. Surf. Sci.* 254 (2008) 1797–1805.  
doi:10.1016/j.apsusc.2007.07.171.
- [21] L. Cao, H.-H. Hu, D. Gao, Design and Fabrication of Micro-textures for Inducing a Superhydrophobic Behavior on Hydrophilic Materials, (2007).  
doi:10.1021/la063572r.
- [22] X. Li, J. Shao, Y. Ding, H. Tian, Microbowl-arrayed surface generated by EBL of negative-tone SU-8 for highly adhesive hydrophobicity, *Appl. Surf. Sci.* 307 (2014) 365–371. doi:10.1016/j.apsusc.2014.04.039.

- [23] S. Beckford, N. Langston, M. Zou, R. Wei, Fabrication of durable hydrophobic surfaces through surface texturing, *Appl. Surf. Sci.* 257 (2011) 5688–5693. doi:10.1016/j.apsusc.2011.01.074.
- [24] J.-M. Romano, M. Gulcur, A. Garcia-Giron, E. Martinez-Solanas, B.R. Whiteside, S.S. Dimov, Mechanical durability of hydrophobic surfaces fabricated by injection moulding of laser-induced textures, *Appl. Surf. Sci.* 476 (2019) 850–860. doi:10.1016/j.apsusc.2019.01.162.
- [25] T. Young, An Essay on the Cohesion of Fluids, *Philos. Trans. R. Soc. London.* 95 (1805) 65–87. <https://about.jstor.org/terms> (accessed August 15, 2019).
- [26] J.D. Bernardin, I. Mudawar, C.B. Walsh, E.I. Franses, Contact angle temperature dependence for water droplets on practical aluminum surfaces, *Int. J. Heat Mass Transf.* 40 (1997) 1017–1033. doi:10.1016/0017-9310(96)00184-6.
- [27] J. Bico, U. Thiele, D. Quéré, Wetting of textured surfaces, *Colloids Surfaces A Physicochem. Eng. Asp.* 206 (2002) 41–46. doi:10.1016/S0927-7757(02)00061-4.
- [28] A.M. Kietzig, S.G. Hatzikiriakos, P. Englezos, Patterned superhydrophobic metallic surfaces, *Langmuir.* 25 (2009) 4821–4827. doi:10.1021/la8037582.
- [29] E. Bormashenko, Historical perspective Progress in understanding wetting transitions on rough surfaces, *Adv. Colloid Interface Sci.* 222 (2015) 92–103. doi:10.1016/j.cis.2014.02.009.
- [30] R.N. Wenzel, Resistance of solid surfaces to wetting by water, *Ind. Eng. Chem.* 28 (1936) 988–994. doi:10.1021/ie50320a024.
- [31] A.B.D. Cassie, S. Baxter, Wettability of porous surfaces, *Trans. Faraday Soc.* 40 (1944) 546. doi:10.1039/tf94444000546.
- [32] D. Quéré, Rough ideas on wetting, *Phys. A Stat. Mech. Its Appl.* 313 (2002) 32–

46. doi:10.1016/S0378-4371(02)01033-6.
- [33] Z. Wang, M. Elimelech, S. Lin, Environmental Applications of Interfacial Materials with Special Wettability, *Environ. Sci. Technol.* 50 (2016) 2132–2150. doi:10.1021/acs.est.5b04351.
- [34] E. Bertrand, T.D. Blake, J. De Coninck, Influence of solid–liquid interactions on dynamic wetting: a molecular dynamics study, *J. Phys. Condens. Matter.* 21 (2009) 464124. doi:10.1088/0953-8984/21/46/464124.
- [35] C.E. Cansoy, The effect of drop size on contact angle measurements of superhydrophobic surfaces, *RSC Adv.* 4 (2014) 1197–1203. doi:10.1039/C3RA45947K.
- [36] A. Marmur, Soft contact: measurement and interpretation of contact angles, *Soft Matter.* 2 (2006) 12–17. doi:10.1039/B514811C.
- [37] H.-Y. Kim, H.J. Lee, B.H. Kang, Sliding of Liquid Drops Down an Inclined Solid Surface, *J. Colloid Interface Sci.* 247 (2002) 372–380. doi:10.1006/jcis.2001.8156.
- [38] E. Pierce, F. Carmona, A. Amirfazli, Understanding of sliding and contact angle results in tilted plate experiments, *Physicochem. Eng. Asp.* 323 (2008) 73–82. doi:10.1016/j.colsurfa.2007.09.032.
- [39] Y. Qin, X. Wang, R. Chen, X. Shangguan, Water Transport and Removal in PEMFC Gas Flow Channel with Various Water Droplet Locations and Channel Surface Wettability, (2018). doi:10.3390/en11040880.
- [40] A. Einstein, Strahlungs-Emission und -Absorption nach der Quantentheorie, *Dtsch. Phys. Gesellschaft, Verhandlungen.* 18 (1916) 318–323.
- [41] T.H. Maiman, Stimulated Optical Radiation in Ruby, *Nature.* 187 (1960) 493–

494. doi:10.1038/187493a0.
- [42] J. Dutta Majumdar, I. Manna, Laser material processing, *Int. Mater. Rev.* 56 (2011) 341–388. doi:10.1179/1743280411Y.0000000003.
- [43] D. Bäuerle, Laser processing and chemistry, 4th ed., Springer London, London, 2011.
- [44] W.M. Steen, J. Mazumder, Laser material processing, 4th ed., Springer London, London, 2010.
- [45] R. Paschotta, Field guide to laser pulse generation, SPIE, 2008.  
<https://spie.org/Publications/Book/800629> (accessed August 27, 2019).
- [46] K.H. Leitz, B. Redlingshofer, Y. Reg, A. Otto, M. Schmidt, Metal ablation with short and ultrashort laser pulses, *Phys. Procedia.* 12 (2011) 230–238.  
doi:10.1016/j.phpro.2011.03.128.
- [47] W.M. Steen, J. Mazumder, Laser Material Processing, Springer London, London, 2010. doi:10.1007/978-1-84996-062-5.
- [48] P. Penchev, S. Dimov, D. Bhaduri, Experimental investigation of 3D scanheads for laser micro-processing, *Opt. Laser Technol. J.* 81 (2016) 55–59.  
doi:10.1016/j.optlastec.2016.01.035.
- [49] R. Jagdheesh, M. Diaz, J.L. Ocaña, Bio inspired self-cleaning ultrahydrophobic aluminium surface by laser processing, *RSC Adv.* 6 (2016) 72933–72941.  
doi:10.1039/C6RA12236A.
- [50] A.Y. Vorobyev, C. Guo, Direct femtosecond laser surface nano/microstructuring and its applications, *Laser Photonics Rev.* 7 (2013) 385–407.  
doi:10.1002/lpor.201200017.
- [51] K. Wagner, S. Friedrich, C. Stang, T. Bley, N. Schilling, M. Bieda, A. Lasagni, E.

- Boschke, Initial phases of microbial biofilm formation on opaque, innovative anti-adhesive surfaces using a modular microfluidic system, *Eng. Life Sci.* 14 (2014) 76–84. doi:10.1002/elsc.201200035.
- [52] J.-M. Romano, A. Garcia-Giron, P. Penchev, S. Dimov, Triangular laser-induced submicron textures for functionalising stainless steel surfaces, *Appl. Surf. Sci.* 440 (2018). doi:10.1016/j.apsusc.2018.01.086.
- [53] A. Chebolu, B. Laha, M. Ghosh, Engineering of Micro Patterned Surface Topographies – Correlating Pattern Geometry and Bacterial Resistance, (2014) 1–6.
- [54] J.L. Ocaña, R. Jagdheesh, J.J. Garcia-Ballesteros, Direct generation of superhydrophobic microstructures in metals by UV laser sources in the nanosecond regime, *Adv. Opt. Technol.* 5 (2016) 87–93. doi:10.1515/aot-2016-0002.
- [55] H. He, N. Qu, Y. Zeng, Lotus-leaf-like microstructures on tungsten surface induced by one-step nanosecond laser irradiation, *Surf. Coat. Technol.* 307 (2016) 898–907. doi:10.1016/j.surfcoat.2016.10.033.
- [56] T. Jwad, S. Deng, H. Butt, S. Dimov, Laser induced single spot oxidation of titanium, *Appl. Surf. Sci.* 387 (2016) 617–624. doi:10.1016/j.apsusc.2016.06.136.
- [57] D. Bhaduri, P. Penchev, A. Batal, S. Dimov, S.L. Soo, S. Sten, U. Harrysson, Z. Zhang, H. Dong, Laser polishing of 3D printed mesoscale components, *Appl. Surf. Sci.* 405 (2017) 29–46. doi:10.1016/j.apsusc.2017.01.211.
- [58] I. Etsion, Improving tribological performance of mechanical components by laser surface texturing, *Tribol. Lett.* 17 (2004) 733–737. doi:10.1007/s11249-004-8081-1.

- [59] M. Martínez-Calderon, A. Rodríguez, A. Dias-Ponte, M.C. Morant-Miñana, M. Gómez-Aranzadi, S.M. Olaizola, Femtosecond laser fabrication of highly hydrophobic stainless steel surface with hierarchical structures fabricated by combining ordered microstructures and LIPSS, *Appl. Surf. Sci.* 374 (2016) 81–89. doi:10.1016/J.APSUSC.2015.09.261.
- [60] J. Long, P. Fan, D. Gong, D. Jiang, H. Zhang, L. Li, M. Zhong, Superhydrophobic surfaces fabricated by femtosecond laser with tunable water adhesion: From lotus leaf to rose petal, *ACS Appl. Mater. Interfaces.* 7 (2015) 9858–9865. doi:10.1021/acsami.5b01870.
- [61] A.M. Emelyanenko, F.M. Shagieva, A.G. Domantovsky, L.B. Boinovich, Nanosecond laser micro- and nanotexturing for the design of a superhydrophobic coating robust against long-term contact with water, cavitation, and abrasion, *Appl. Surf. Sci.* 332 (2015) 513–517. doi:10.1016/j.apsusc.2015.01.202.
- [62] M. Kagerer, F. Irlinger, T.C. Lueth, Laser source independent basic parameters - Focus position, pulse overlap, track overlap in laser micro milling using as rapid manufacturing process, *IEEE/ASME Int. Conf. Adv. Intell. Mechatronics, AIM.* (2012) 135–140. doi:10.1109/AIM.2012.6265899.
- [63] D.C. Emmony, R.P. Howson, L.J. Willis, Laser mirror damage in germanium at 10.6  $\mu\text{m}$ , *Appl. Phys. Lett.* 23 (1973) 598–600. doi:10.1063/1.1654761.
- [64] J.E. Sipe, J.F. Young, J.S. Preston, H.M. van Driel, Laser-induced periodic surface structure. I. Theory, *Phys. Rev. B.* 27 (1983) 1141–1154. doi:10.1103/PhysRevB.27.1141.
- [65] F. Keilmann, Y.H. Bai, Periodic surface structures frozen into CO<sub>2</sub> laser-melted

- quartz, *Appl. Phys. A Solids Surfaces*. 29 (1982) 9–18. doi:10.1007/BF00618110.
- [66] F. Fraggelakis, G. Mincuzzi, J. Lopez, I. Manek-Hönniger, R. Kling, Controlling 2D laser nano structuring over large area with double femtosecond pulses, *Appl. Surf. Sci.* 470 (2019) 677–686. doi:10.1016/J.APSUSC.2018.11.106.
- [67] B.K. Nayak, M.C. Gupta, Self-organized micro/nano structures in metal surfaces by ultrafast laser irradiation, *Opt. Lasers Eng.* 48 (2010) 940–949. doi:10.1016/j.optlaseng.2010.04.010.
- [68] S. Moradi, S. Kamal, P. Englezos, S.G. Hatzikiriakos, Femtosecond laser irradiation of metallic surfaces: effects of laser parameters on superhydrophobicity, *Nanotechnology*. 24 (2013) 415302. doi:10.1088/0957-4484/24/41/415302.
- [69] A. Rosenkranz, M. Hans, C. Gachot, A. Thome, S. Bonk, F. Mücklich, Direct Laser Interference Patterning: Tailoring of Contact Area for Frictional and Antibacterial Properties, *Lubricants*. 4 (2016) 2. doi:10.3390/lubricants4010002.
- [70] J. Valle, S. Burgui, D. Langheinrich, C. Gil, C. Solano, A. Toledo-Arana, R. Helbig, A. Lasagni, I. Lasa, Evaluation of Surface Microtopography Engineered by Direct Laser Interference for Bacterial Anti-Biofouling, *Macromol. Biosci.* 15 (2015) 1060–1069. doi:10.1002/mabi.201500107.
- [71] A.I. Aguilar-Morales, S. Alamri, B. Voisiat, T. Kunze, A.F. Lasagni, The Role of the Surface Nano-Roughness on the Wettability Performance of Microstructured Metallic Surface Using Direct Laser Interference Patterning, *Materials (Basel)*. 12 (2019) 2737. doi:10.3390/ma12172737.
- [72] A. Lasagni, S. Alamri, A. Aguilar-Morales, F. Rößler, B. Voisiat, T. Kunze, A.F. Lasagni, S. Alamri, A.I. Aguilar-Morales, F. Rößler, B. Voisiat, T. Kunze,

- Biomimetic Surface Structuring Using Laser Based Interferometric Methods, *Appl. Sci.* 8 (2018) 1260. doi:10.3390/app8081260.
- [73] C. Harris, K.D. Dean, P. Penchev, S.S. Dimov, Investigation of air entrapment and weld line defects in micro injection moulded thermoplastic elastomer micro rings, *4M/Iccom 2015*. (2015) 978–981. doi:10.3850/978-981-09-4609-8.
- [74] L. Overmeyer, J.F. Duesing, O. Suttmann, U. Stute, Laser patterning of thin film sensors on 3-D surfaces, *CIRP Ann. - Manuf. Technol.* 61 (2012) 215–218. doi:10.1016/j.cirp.2012.03.087.
- [75] D. Sola, A. Escartín, R. Cases, J.I. Peña, Laser ablation of advanced ceramics and glass-ceramic materials: Reference position dependence, *Appl. Surf. Sci.* 257 (2011) 5413–5419. doi:10.1016/J.APSUSC.2010.09.089.
- [76] X. Wang, J. Duan, M. Jiang, S. Ke, B. Wu, X. Zeng, Study of laser precision ablating texture patterns on large-scale freeform surface, *Int J Adv Manuf Technol.* 92 (2017) 4571–4581. doi:10.1007/s00170-017-0413-z.
- [77] J. Diaci, D. Bračun, A. Gorkič, J. Možina, Rapid and flexible laser marking and engraving of tilted and curved surfaces, *Appl. Surf. Sci.* 49 (2011) 195–199. doi:10.1016/j.optlaseng.2010.09.003.
- [78] G. Cuccolini, L. Orazi, A. Fortunato, 5 Axes computer aided laser milling, *Opt. Lasers Eng.* 51 (2013) 749–760. doi:10.1016/j.optlaseng.2013.01.015.
- [79] M. Jiang, X. Wang, S. Ke, F. Zhang, X. Zeng, Large scale layering laser surface texturing system based on high speed optical scanners and gantry machine tool, *Robot. Comput. Integr. Manuf.* 48 (2018) 113–120. doi:10.1016/j.rcim.2017.03.005.
- [80] L. Mishchenko, B. Hatton, V. Bahadur, J.A. Taylor, T. Krupenkin, J. Aizenberg,

- Design of Ice-free Nanostructured Surfaces Based on Repulsion of Impacting Water Droplets, (2010). doi:10.1021/nn102557p.
- [81] G.-W. Römer, D. Arnaldo Del Cerro, R.C.J. Siphema, M.N.W. Groenendijk, A.J. Huis In 't Veld, Ultra short pulse laser generated surface textures for anti-ice applications in aviation, Proc. ICALEO 2009 (Laser Inst. Am. Orlando, United States). (2009) 30–37. <https://core.ac.uk/download/pdf/11485820.pdf> (accessed August 29, 2019).
- [82] M.J. Kreder, J. Alvarenga, P. Kim, J. Aizenberg, Design of anti-icing surfaces: smooth, textured or slippery?, *Nat. Rev. Mater.* 1 (2016) 15003. doi:10.1038/natrevmats.2015.3.
- [83] V. Vercillo, J.T. Cardoso, D. Huerta-Murillo, S. Tonnichia, A. Laroche, J.A. Mayén Guillén, J.L. Ocaña, A.F. Lasagni, E. Bonaccorso, Durability of superhydrophobic laser-treated metal surfaces under icing conditions, *Mater. Lett. X.* 3 (2019) 100021. doi:10.1016/J.MLBLUX.2019.100021.
- [84] D. Perera-costa, J.M. Bruque, Studying the Influence of Surface Topography on Bacterial Adhesion using Spatially Organized Microtopographic Surface Patterns, (2014).
- [85] J.T. Decker, C.M. Kirschner, C.J. Long, J.A. Finlay, M.E. Callow, J.A. Callow, A.B. Brennan, Engineered antifouling microtopographies: An energetic model that predicts cell attachment, *Langmuir.* 29 (2013) 13023–13030. doi:10.1021/la402952u.
- [86] J.F. Schumacher, M.L. Carman, T.G. Estes, A.W. Feinberg, L.H. Wilson, M.E. Callow, J.A. Callow, J.A. Finlay, A.B. Brennan, Engineered antifouling microtopographies – effect of feature size, geometry, and roughness on

- settlement of zoospores of the green alga *Ulva*, *Biofouling*. 23 (2007) 55–62.  
doi:10.1080/08927010601136957.
- [87] B. Laha, M. Ghosh, A. Chebolu, Nagahanumaiah, Investigation on bacterial adhesion and colonisation resistance over laser-machined micro patterned surfaces, *Micro Nano Lett.* 8 (2013) 280–283. doi:10.1049/mnl.2013.0109.
- [88] Alexandre Cunha, Anne-Marie Elie, Laurent Plawinski, Ana Paula Serro, Ana Maria Botelho do Rego, Amélia Almeida, Maria C. Urdaci, Marie-Christine Durrieu, Rui Vilar, Femtosecond laser surface texturing of titanium as a method to reduce the adhesion of *Staphylococcus aureus* and biofilm formation, *Appl. Surf. Sci.* 360 (2016) 485–493. <https://pdf.sciencedirectassets.com/271533/1-s2.0-S0169433215X00389/1-s2.0-S0169433215025210/main.pdf?X-Amz-Security-Token=AgoJb3JpZ2luX2VjEDlaCXVzLWVhc3QtMSJIMEYCIQCOZS%2FeW8DFsVQHZhXUX1UPDf%2FxtFKkGunlfYZgsPCUAQlhAJOc74PWJlcNTgjEW3cZzd4MXYLZCcGsbgOZYcVh> (accessed September 12, 2019).
- [89] S. Perni, P. Prokopovich, Micropatterning with conical features can control bacterial adhesion on silicone, *Soft Matter*. 9 (2013) 1844–1851.  
doi:10.1039/C2SM26828K.
- [90] J.-M. Romano, R. Ahmed, A. Garcia-Giron, P. Penchev, H. Butt, O. Delléa, M. Sikosana, R. Helbig, C. Werner, S. Dimov, Subwavelength Direct Laser Nanopatterning Via Microparticle Arrays for Functionalizing Metallic Surfaces, *J. Micro Nano-Manufacturing*. 7 (2019). doi:10.1115/1.4042964.
- [91] L. Ploux, K. Anselme, A. Dirani, A. Ponche, O. Soppera, V. Roucoules, Opposite responses of cells and bacteria to micro/nanopatterned surfaces prepared by

- pulsed plasma polymerization and UV-irradiation, *Langmuir*. 25 (2009) 8161–8169. doi:10.1021/la900457f.
- [92] Esther Rebollar, Irene Frischauf, Michael Olbrich, Thomas Peterbauer, Steffen Hering, Johannes Preiner, Peter Hinterdorfer, Christoph Romanin, Johannes Heitz, Proliferation of aligned mammalian cells on laser-nanostructured polystyrene, *Biomaterials*. 29 (2007) 1796–1806.  
<https://pdf.sciencedirectassets.com/271870/1-s2.0-S0142961208X00043/1-s2.0-S0142961207010642/main.pdf?X-Amz-Security-Token=AgoJb3JpZ2luX2VjEDEaCXVzLWVhc3QtMSJHMEUCIQDDUYBHPe0qTDyfHIQOOzO%2BwtYuPi0Ato4r%2Bg7hMwZG4gIgLStzftHkxRA6UrggrO2VPBOICeu2el5OZZhTpGKz> (accessed September 12, 2019).
- [93] E. Rebollar, M. Castillejo, T.A. Ezquerro, Laser induced periodic surface structures on polymer films: From fundamentals to applications, *Eur. Polym. J.* 73 (2015) 162–174. doi:10.1016/j.eurpolymj.2015.10.012.
- [94] E. Fadeeva, S. Schlie, J. Koch, B.N. Chichkov, Selective Cell Control by Surface Structuring for Orthopedic Applications, *J. Adhes. Sci. Technol.* 24 (2010) 2257–2270. doi:10.1163/016942410X508000.
- [95] A. Pérez Del Pino, P. Serra, J.L. Morenza, Coloring of titanium by pulsed laser processing in air, *Thin Solid Films*. 415 (2002) 201–205. doi:10.1016/S0040-6090(02)00632-6.
- [96] J.-M. Romano, R. Helbig, F. Fraggelakis, A. Garcia-Giron, C. Werner, R. Kling, S. Dimov, Springtail-Inspired Triangular Laser-Induced Surface Textures on Metals Using MHz Ultrashort Pulses, *J. Micro Nano-Manufacturing*. 7 (2019). doi:10.1115/1.4043417.

- [97] M. Faucon, A. Laffitte, J. Lopez, R. Kling, Surface blackening by laser texturing with high repetition rate femtosecond laser up to 1MHz, in: A. Heisterkamp, P.R. Herman, M. Meunier, S. Nolte (Eds.), International Society for Optics and Photonics, 2014: p. 89721M. doi:10.1117/12.2039469.
- [98] S. Storm, S. Alamri, M. Soldera, T. Kunze, A.F. Lasagni, How to Tailor Structural Colors for Extended Visibility and White Light Generation Employing Direct Laser Interference Patterning, *Macromol. Chem. Phys.* 220 (2019) 1900205. doi:10.1002/macp.201900205.
- [99] T. Jwad, P. Penchev, V. Nasrollahi, S. Dimov, Laser induced ripples' gratings with angular periodicity for fabrication of diffraction holograms, *Appl. Surf. Sci.* 453 (2018) 449–456. doi:10.1016/J.APSUSC.2018.04.277.
- [100] R. Ahmed, A.K. Yetisen, S.H. Yun, H. Butt, Color-selective holographic retroreflector array for sensing applications, *Light Sci. Appl.* 6 (2017) e16214–e16214. doi:10.1038/lssa.2016.214.
- [101] S. Deng, T. Jwad, C. Li, D. Benton, A.K. Yetisen, K. Jiang, Q. Dai, H. Butt, Carbon Nanotube Array Based Binary Gabor Zone Plate Lenses, *Sci. Rep.* 7 (2017) 15256. doi:10.1038/s41598-017-15472-9.
- [102] I. Etsion, G. Halperin, A Laser Surface Textured Hydrostatic Mechanical Seal, *Tribol. Trans.* 45 (2002) 430–434. doi:10.1080/10402000208982570.
- [103] I. Etsion, Y. Kligerman, G. Halperin, Analytical and Experimental Investigation of Laser-Textured Mechanical Seal Faces, *Tribol. Trans.* 42 (1999) 511–516. doi:10.1080/10402009908982248.
- [104] G. Ryk, Y. Kligerman, I. Etsion, A. Shinkarenko, Experimental Investigation of Partial Laser Surface Texturing for Piston-Ring Friction Reduction, *Tribol. Trans.*

- 48 (2005) 583–588. doi:10.1080/05698190500313544.
- [105] H. Yu, X. Wang, F. Zhou, Geometric shape effects of surface texture on the generation of hydrodynamic pressure between conformal contacting surfaces, *Tribol. Lett.* 37 (2010) 123–130. doi:10.1007/s11249-009-9497-4.
- [106] T. Ibatan, M.S. Uddin, M.A.K. Chowdhury, Recent development on surface texturing in enhancing tribological performance of bearing sliders, *Surf. Coatings Technol.* 272 (2015) 102–120. doi:10.1016/j.surfcoat.2015.04.017.
- [107] S. Schreck, K.H. Zum Gahr, Laser-assisted structuring of ceramic and steel surfaces for improving tribological properties, *Appl. Surf. Sci.* 247 (2005) 616–622. doi:10.1016/j.apsusc.2005.01.173.
- [108] A. Kovalchenko, O. Ajayi, A. Erdemir, G. Fenske, I. Etsion, The effect of laser surface texturing on transitions in lubrication regimes during unidirectional sliding contact, *Tribol. Int.* 38 (2005) 219–225.  
doi:10.1016/j.triboint.2004.08.004.
- [109] P. Andersson, J. Koskinen, S. Varjus, Y. Gerbig, H. Haefke, S. Georgiou, B. Zhmud, W. Buss, Microlubrication effect by laser-textured steel surfaces, *Wear.* 262 (2007) 369–379. doi:10.1016/j.wear.2006.06.003.
- [110] T. Stark, S. Alamri, A.I. Aguilar-Morales, T. Kiedrowski, A.F. Lasagni, Positive Effect of Laser Structured Surfaces on Tribological Performance, *JLMN-Journal of Laser Micro/Nanoengineering.* 14 (2019) 13–18.  
doi:10.2961/jlmn.2019.01.0003.
- [111] J. Bonse, R. Koter, M. Hartelt, D. Spaltmann, S. Pentzien, S. Höhm, A. Rosenfeld, J. Krüger, Tribological performance of femtosecond laser-induced periodic surface structures on titanium and a high toughness bearing steel, *Appl. Surf.*

- Sci. 336 (2015) 21–27. doi:10.1016/j.apsusc.2014.08.111.
- [112] M. Varenberg, G. Halperin, I. Etsion, Different aspects of the role of wear debris in fretting wear, *Wear*. 252 (2002) 902–910. doi:10.1016/S0043-1648(02)00044-3.
- [113] A.M. Emelyanenko, F.M. Shagieva, A.G. Domantovsky, L.B. Boinovich, Nanosecond laser micro- and nanotexturing for the design of a superhydrophobic coating robust against long-term contact with water, cavitation, and abrasion, *Appl. Surf. Sci.* 332 (2015) 513–517. doi:10.1016/j.apsusc.2015.01.202.
- [114] L.B. Boinovich, A.M. Emelyanenko, A.D. Modestov, A.G. Domantovsky, K.A. Emelyanenko, Synergistic Effect of Superhydrophobicity and Oxidized Layers on Corrosion Resistance of Aluminum Alloy Surface Textured by Nanosecond Laser Treatment, *ACS Appl. Mater. Interfaces*. 7 (2015) 19500–19508. doi:10.1021/acsami.5b06217.
- [115] Y. Liu, J. Liu, S. Li, H. Zhiwu, S. Yu, L. Ren, Fabrication of biomimetic superhydrophobic surface on aluminum alloy, *J. Mater. Sci.* 49 (2014) 1624–1629. doi:10.1007/s10853-013-7845-0.
- [116] Y. Zhang, G. Zou, L. Liu, Y. Zhao, Q. Liang, A. Wu, Y.N. Zhou, Time-dependent wettability of nano-patterned surfaces fabricated by femtosecond laser with high efficiency, *Appl. Surf. Sci.* 389 (2016) 554–559. doi:10.1016/j.apsusc.2016.07.089.
- [117] S. Alamri, A.I. Aguilar-Morales, A.F. Lasagni, Controlling the wettability of polycarbonate substrates by producing hierarchical structures using Direct Laser Interference Patterning, *Eur. Polym. J.* 99 (2018) 27–37.

doi:10.1016/j.eurpolymj.2017.12.001.

- [118] P. Bizi-Bandoki, S. Valette, E. Audouard, S. Benayoun, Time dependency of the hydrophilicity and hydrophobicity of metallic alloys subjected to femtosecond laser irradiations, *Appl. Surf. Sci.* 273 (2013) 399–407.  
doi:10.1016/j.apsusc.2013.02.054.
- [119] J. Long, M. Zhong, H. Zhang, P. Fan, Superhydrophilicity to superhydrophobicity transition of picosecond laser microstructured aluminum in ambient air, *J. Colloid Interface Sci.* 441 (2015) 1–9. doi:10.1016/j.jcis.2014.11.015.
- [120] J. Long, M. Zhong, P. Fan, D. Gong, H. Zhang, Wettability conversion of ultrafast laser structured copper surface, *J. Laser Appl.* 27 (2015) S29107.  
doi:10.2351/1.4906477.
- [121] M.C. Sharp, A.P. Rosowski, P.W. French, Nanosecond laser texturing of aluminium for control of wettability, *Proc. SPIE.* 9657 (2015) 96570J.  
doi:10.1117/12.2179929.
- [122] R. Jagdheesh, J.J. Garcia-Ballesteros, J.L. Ocaña, One-step fabrication of near superhydrophobic aluminum surface by nanosecond laser ablation, *Appl. Surf. Sci.* 374 (2016) 2–11. doi:10.1016/j.apsusc.2015.06.104.
- [123] J.T. Cardoso, A. Garcia-Girón, J.M. Romano, D. Huerta-Murillo, R. Jagdheesh, M. Walker, S.S. Dimov, J.L. Ocaña, Influence of ambient conditions on the evolution of wettability properties of an IR-, ns-laser textured aluminium alloy, *RSC Adv.* 7 (2017). doi:10.1039/c7ra07421b.
- [124] V.D. Ta, A. Dunn, T.J. Wasley, J. Li, R.W. Kay, J. Stringer, P.J. Smith, E. Esenturk, C. Connaughton, J.D. Shephard, Laser textured superhydrophobic surfaces and their applications for homogeneous spot deposition, *Appl. Surf. Sci.* 365 (2016)

- 153–159. doi:10.1016/j.apsusc.2016.01.019.
- [125] D. V Ta, A. Dunn, T.J. Wasley, R.W. Kay, J. Stringer, P.J. Smith, C. Connaughton, J.D. Shephard, Nanosecond laser textured superhydrophobic metallic surfaces and their chemical sensing applications, 357 (2015) 248–254.
- [126] L.B. Boinovich, A.M. Emelyanenko, K.A. Emelyanenko, A.G. Domantovsky, A.A. Shiryayev, Comment on “Nanosecond laser textured superhydrophobic metallic surfaces and their chemical sensing applications” by Duong V. Ta, Andrew Dunn, Thomas J. Wasley, Robert W. Kay, Jonathan Stringer, Patrick J. Smith, Colm Connaughton, Jonathan D. Shephard (Ap, Appl. Surf. Sci. 379 (2016) 111–113. doi:10.1016/j.apsusc.2016.04.056.
- [127] D. Huerta-Murillo, A. García-Girón, J.M. Romano, J.T. Cardoso, F. Cordovilla, M. Walker, S.S. Dimov, J.L. Ocaña, Wettability modification of laser-fabricated hierarchical surface structures in Ti-6Al-4V titanium alloy, Appl. Surf. Sci. 463 (2019) 838–846. doi:10.1016/j.apsusc.2018.09.012.
- [128] Y.C. Guan, F.F. Luo, G.C. Lim, M.H. Hong, H.Y. Zheng, B. Qi, Fabrication of metallic surfaces with long-term superhydrophilic property using one-stop laser method, Mater. Des. 78 (2015) 19–24.
- [129] S.P. Mishra, A.A. Polycarpou, Tribological studies of unpolished laser surface textures under starved lubrication conditions for use in air-conditioning and refrigeration compressors, Tribology Int. 44 (2011) 1890–1901. doi:10.1016/j.triboint.2011.08.005.
- [130] D. Bhaduri, A. Batal, S.S. Dimov, Z. Zhang, H. Dong, M. Fallqvist, R. M’saoubi, On design and tribological behaviour of laser textured surfaces, Procedia CIRP. 60 (2017) 20–25. doi:10.1016/j.procir.2017.02.050.

- [131] L.R.J. Scarratt, U. Steiner, C. Neto, A review on the mechanical and thermodynamic robustness of superhydrophobic surfaces, *Adv. Colloid Interface Sci.* 246 (2017) 133–152. doi:10.1016/j.cis.2017.05.018.
- [132] J. Han, M. Cai, Y. Lin, W. Liu, X. Luo, H. Zhang, K. Wang, M. Zhong, Comprehensively durable superhydrophobic metallic hierarchical surfaces via tunable micro- cone design to protect functional nanostructures, *RSC Adv.* 8 (2018) 6733–6744. doi:10.1039/c7ra13496g.
- [133] M.-K. Tang, X.-J. Huang, Z. Guo, J.-G. Yu, X.-W. Li, Q.-X. Zhang, Fabrication of robust and stable superhydrophobic surface by a convenient, low-cost and efficient laser marking approach, *Colloids Surfaces A Physicochem. Eng. Asp.* 484 (2015) 449–456. doi:10.1016/J.COLSURFA.2015.08.029.
- [134] T. Verho, C. Bower, P. Andrew, S. Franssila, O. Ikkala, R.H.A. Ras, Mechanically Durable Superhydrophobic Surfaces, *Adv. Mater.* 23 (2011) 673–678. doi:10.1002/adma.201003129.
- [135] L.B. Boinovich, K.A. Emelyanenko, A.G. Domantovsky, A.M. Emelyanenko, Laser Tailoring the Surface Chemistry and Morphology for Wear, Scale and Corrosion Resistant Superhydrophobic Coatings, *Langmuir.* 34 (2018) 14. doi:10.1021/acs.langmuir.8b01317.
- [136] A. Milionis, E. Loth, I.S. Bayer, Recent advances in the mechanical durability of superhydrophobic materials, *Adv. Colloid Interface Sci.* 229 (2016) 57–79. doi:10.1016/J.CIS.2015.12.007.
- [137] H. Dong, S-phase surface engineering of Fe-Cr, Co-Cr and Ni-Cr alloys, *Int. Mater. Rev.* 55 (2010) 65–98. doi:10.1179/095066009X12572530170589.
- [138] J. Chen, X.Y. Li, T. Bell, H. Dong, Improving the wear properties of Stellite 21

- alloy by plasma surface alloying with carbon and nitrogen, *Wear*. 264 (2008) 157–165. doi:10.1016/j.wear.2006.12.012.
- [139] H. Dong, *Tribological properties of titanium-based alloys*, Woodhead Publishing Limited, 2010. doi:10.1533/9781845699451.1.58.
- [140] S. Corujeira Gallo, H. Dong, Study of active screen plasma processing conditions for carburising and nitriding austenitic stainless steel, *Surf. Coatings Technol.* 203 (2009) 3669–3675. doi:10.1016/j.surfcoat.2009.05.045.
- [141] B. Larisch, U. Brusky, H.-J. Spies, Plasma nitriding of stainless steels at low temperatures, *Surf. Coatings Technol.* 116–119 (1999) 205–211. doi:10.1016/S0257-8972(99)00084-5.
- [142] Z. Zhang, X. Li, H. Dong, Plasma-nitriding and characterization of FeAl40 iron aluminide, *Acta Mater.* 86 (2015) 341–351. doi:10.1016/j.actamat.2014.11.044.
- [143] A. Garcia-Giron, J.M. Romano, Y. Liang, B. Dashtbozorg, H. Dong, P. Penchev, S.S. Dimov, Combined surface hardening and laser patterning approach for functionalising stainless steel surfaces, *Appl. Surf. Sci.* 439 (2018) 516–524. doi:10.1016/J.APSUSC.2018.01.012.
- [144] R. Wu, S. Liang, A. Pan, Z. Yuan, Y. Tang, X. Tan, D. Guan, Y. Yu, Fabrication of nano-structured super-hydrophobic film on aluminum by controllable immersing method, *Appl. Surf. Sci.* 258 (2012) 5933–5937. doi:10.1016/j.apsusc.2011.10.029.
- [145] M. Zupančič, M. Može, P. Gregorčič, I. Golobič, Nanosecond laser texturing of uniformly and non-uniformly wettable micro structured metal surfaces for enhanced boiling heat transfer, *Appl. Surf. Sci.* 399 (2017) 480–490. doi:10.1016/j.apsusc.2016.12.120.

- [146] K. Li, Z. Yao, Y. Hu, W. Gu, Friction and wear performance of laser peen textured surface under starved lubrication, *Tribol. Int.* 77 (2014) 97–105.  
doi:10.1016/j.triboint.2014.04.017.
- [147] A.-M. Kietzig, M.N. Mirvakili, S. Kamal, P. Englezos, S.G. Hatzikiriakos, Nanopatterned Metallic Surfaces: Their Wettability and Impact on Ice Friction, *J. Adhes. Sci. Technol.* 25 (2011) 1293–1303. doi:10.1163/016942411X555872.
- [148] K.M. Tanvir Ahmmed, A.-M. Kietzig, Drag reduction on laser-patterned hierarchical superhydrophobic surfaces, *Soft Matter*. 12 (2016) 4912–4922.  
doi:10.1039/c6sm00436a.
- [149] E. Bormashenko, Progress in understanding wetting transitions on rough surfaces, *Adv. Colloid Interface Sci.* 222 (2015) 92–103.  
doi:10.1016/j.cis.2014.02.009.
- [150] L. Mishchenko, B. Hatton, V. Bahadur, J.A. Taylor, T. Krupenkin, J. Aizenberg, Design of ice-free nanostructured surfaces based on repulsion of impacting water droplets, *ACS Nano*. 4 (2010) 7699–7707. doi:10.1021/nn102557p.
- [151] A. Malijevsky, Does surface roughness amplify wetting?, *J. Chem. Phys.* 141 (2014). doi:10.1063/1.4901128.
- [152] B.H. Luo, P.W. Shum, Z.F. Zhou, K.Y. Li, Surface geometrical model modification and contact angle prediction for the laser patterned steel surface, *Surf. Coatings Technol.* 205 (2010) 2597–2604. doi:10.1016/j.surfcoat.2010.10.003.
- [153] Y. Wu, Y. Wang, H. Liu, Y. Liu, L. Guo, D. Jia, J. Ouyang, Y. Zhou, The fabrication and hydrophobic property of micro-nano patterned surface on magnesium alloy using combined sparking sculpture and etching route, *Appl. Surf. Sci.* 389 (2016) 80–87. doi:10.1016/j.apsusc.2016.07.060.

- [154] R.G. Joshi, A. Goel, V.M. Mannari, J.A. Finlay, M.E. Callow, J.A. Callow, Evaluating fouling-resistance and fouling-release performance of smart polyurethane surfaces: An outlook for efficient and environmentally benign marine coatings, *J. Appl. Polym. Sci.* 114 (2009) 3693–3703. doi:10.1002/app.30899.
- [155] C. Lee, S. Baik, Vertically-aligned carbon nano-tube membrane filters with superhydrophobicity and superoleophilicity, *Carbon*. 48 (2010) 2192–2197. doi:10.1016/j.carbon.2010.02.020.
- [156] A.-M. Kietzig, S.G. Hatzikiriakos, P. Englezos, Patterned Superhydrophobic Metallic Surfaces, *Langmuir*. 25 (2009) 4821–4827. doi:10.1021/la8037582.
- [157] J.T. Cardoso, A. Garcia-Girón, J.M. Romano, D. Huerta-Murillo, R. Jagdheesh, M. Walker, S.S. Dimov, J.L. Ocaña, Influence of ambient conditions on the evolution of wettability properties of an IR-, ns-laser textured aluminium alloy, *RSC Adv.* 7 (2017) 39617–39627. doi:10.1039/C7RA07421B.
- [158] V.D. Ta, A. Dunn, T.J. Wasley, J. Li, R.W. Kay, J. Stringer, P.J. Smith, E. Esenturk, C. Connaughton, J.D. Shephard, Laser textured superhydrophobic surfaces and their applications for homogeneous spot deposition, *Appl. Surf. Sci.* 365 (2016) 153–159. doi:10.1016/j.apsusc.2016.01.019.
- [159] D. V. Ta, A. Dunn, T.J. Wasley, R.W. Kay, J. Stringer, P.J. Smith, C. Connaughton, J.D. Shephard, Nanosecond laser textured superhydrophobic metallic surfaces and their chemical sensing applications, *Appl. Surf. Sci.* 357 (2015) 248–254. doi:10.1016/j.apsusc.2015.09.027.
- [160] S.P. Mishra, A.A. Polycarpou, Tribological studies of unpolished laser surface textures under starved lubrication conditions for use in air-conditioning and refrigeration compressors, *Tribol. Int.* 44 (2011) 1890–1901.

doi:10.1016/j.triboint.2011.08.005.

- [161] J.M. Liu, Simple technique for measurements of pulsed Gaussian-beam spot sizes, *Opt. Lett.* 7 (1982) 196. doi:10.1364/OL.7.000196.
- [162] J. Long, M. Zhong, H. Zhang, P. Fan, Superhydrophilicity to superhydrophobicity transition of picosecond laser microstructured aluminum in ambient air, *J. Colloid Interface Sci.* 441 (2015) 1–9. doi:10.1016/j.jcis.2014.11.015.
- [163] A. Garcia-Giron, J.M. Romano, A. Batal, B. Dashtbozorg, H. Dong, E. Martinez Solanas, D. Urrutia, M. Walker, P. Penchev, S.S. Dimov, Durability and Wear Resistance of Laser-Textured Hardened Stainless Steel Surfaces with Hydrophobic Properties, *Langmuir.* 35 (2019) 5353–5363. doi:10.1021/acs.langmuir.9b00398.
- [164] D. Campoccia, L. Montanaro, C.R. Arciola, A review of the biomaterials technologies for infection-resistant surfaces, *Biomaterials.* 34 (2013) 8533–8554. doi:10.1016/j.biomaterials.2013.07.089.
- [165] D.I. Yu, S.W. Doh, H.J. Kwak, H.C. Kang, H.S. Ahn, H.S. Park, M. Kiyofumi, M.H. Kim, Wetting state on hydrophilic and hydrophobic micro-textured surfaces: Thermodynamic analysis and X-ray visualization, *Appl. Phys. Lett.* 106 (2015). doi:10.1063/1.4919136.
- [166] X. Yao, Y. Song, L. Jiang, Applications of bio-inspired special wettable surfaces, *Adv. Mater.* 23 (2011) 719–734. doi:10.1002/adma.201002689.
- [167] G. Bracco, B. Holst, *Surface science techniques*, 2013. doi:10.1007/978-3-642-34243-1.
- [168] I.S. Bayer, On the Durability and Wear Resistance of Transparent Superhydrophobic Coatings, (n.d.). doi:10.3390/coatings7010012.

- [169] N. Cohen, A. Dotan, H. Dodiuk, S. Kenig, *Materials and Manufacturing Processes Superhydrophobic Coatings and Their Durability Superhydrophobic Coatings and Their Durability*, (2016). doi:10.1080/10426914.2015.1090600.
- [170] P. Wang, T. Yao, B. Sun, T. Ci, X. Fan, H. Han, *Fabrication of mechanically robust superhydrophobic steel surface with corrosion resistance property*, (n.d.). doi:10.1039/c7ra06836k.
- [171] N. Wang, D. Xiong, Y. Deng, Y. Shi, K. Wang, *Mechanically Robust Superhydrophobic Steel Surface with Anti- Icing, UV-Durability, and Corrosion Resistance Properties*, (n.d.). doi:10.1021/acsami.5b00558.
- [172] F. Su, K. Yao, *Facile Fabrication of Superhydrophobic Surface with Excellent Mechanical Abrasion and Corrosion Resistance on Copper Substrate by a Novel Method*, *ACS Appl. Mater. Interfaces*. 6 (2014) 8762–8770. doi:10.1021/am501539b.
- [173] Z. She, Q. Li, Z. Wang, L. Li, F. Chen, J. Zhou, *Researching the fabrication of anticorrosion superhydrophobic surface on magnesium alloy and its mechanical stability and durability*, *Chem. Eng. J.* 228 (2013) 415–424. doi:10.1016/J.CEJ.2013.05.017.
- [174] I. Standard, *ISO 11998:2006 “Paints and varnishes – Determination of wet-scrub resistance and cleanability of samples,”* 1998 (1998).
- [175] D. Bhaduri, P. Penchev, S. Dimov, S.L. Soo, *An investigation of accuracy, repeatability and reproducibility of laser micromachining systems*, *Measurement*. 88 (2016) 248–261. doi:10.1016/J.MEASUREMENT.2016.03.033.
- [176] P. Penchev, S. Dimov, D. Bhaduri, S.L. Soo, *Generic integration tools for reconfigurable laser micromachining systems*, *J. Manuf. Syst.* 38 (2016) 27–45.

doi:10.1016/j.jmsy.2015.10.006.

- [177] S. Alamri, M. El-Khoury, A.I. Aguilar-Morales, S. Storm, T. Kunze, A.F. Lasagni, Fabrication of inclined non-symmetrical periodic micro-structures using Direct Laser Interference Patterning, *Sci. Rep.* 9 (2019) 5455. doi:10.1038/s41598-019-41902-x.
- [178] D. Sola, J. Peña, D. Sola, J.I. Peña, Study of the Wavelength Dependence in Laser Ablation of Advanced Ceramics and Glass-Ceramic Materials in the Nanosecond Range, *Materials (Basel)*. 6 (2013) 5302–5313. doi:10.3390/ma6115302.
- [179] Z. Zhang, Q. Gu, W. Jiang, H. Zhu, K. Xu, Y. Ren, C. Xu, Achieving of bionic super-hydrophobicity by electrodepositing nano-Ni-pyramids on the picosecond laser-ablated micro-Cu-cone surface, *Surf. Coatings Technol.* 363 (2019) 170–178. doi:10.1016/j.surfcoat.2019.02.037.
- [180] A. Rodrigues, Technical article GF Machining Solutions ' latest -generation GF Laser Workstation Software revolutionizes Laser texturing by guaranteeing both quality and productivity, *GF Mach. Solut.* (2017).
- [181] Fraunhofer IPT, CALM - Computer Aided Laser Manufacturing, Fraunhofer-Institut Für Produktionstechnologie IPT. (n.d.).
- [182] A. Garcia-Giron, J.M. Romano, Y. Liang, B. Dashtbozorg, H. Dong, P. Penchev, S.S. Dimov, Combined surface hardening and laser patterning approach for functionalising stainless steel surfaces, *Appl. Surf. Sci.* 439 (2018) 516–524. doi:10.1016/j.apsusc.2018.01.012.
- [183] V. Nasrollahi, P. Penchev, S. Dimov, L. Korner, R. Leach, K. Kim, Two-Side Laser Processing Method for Producing High Aspect Ratio Microholes, *J. Micro Nano-Manufacturing*. 5 (2017) 041006. doi:10.1115/1.4037645.

